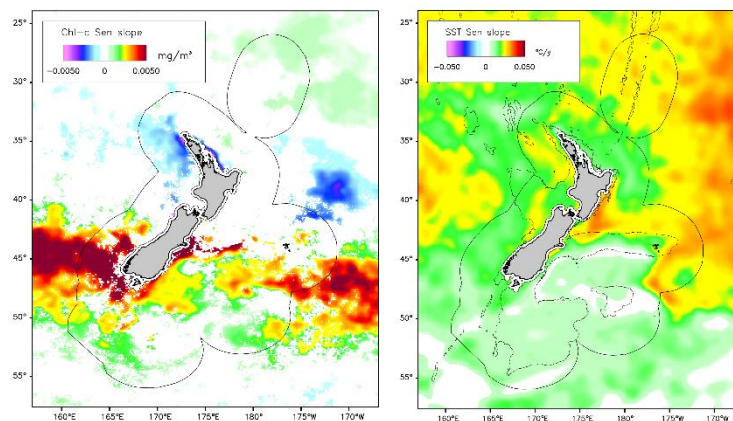


Satellite indicators of phytoplankton and ocean surface temperature for New Zealand

Prepared for Ministry for the Environment

June 2019



Long-term trends in phytoplankton abundance (1997-2018) and ocean surface temperature (1981-2018) from satellite observations

Prepared by:

Matt Pinkerton
Philip Sutton
Simon Wood



For any information regarding this report please contact:

Matt Pinkerton
Principal Scientist
Wellington
+64-4-386 0369
m.pinkerton@niwa.co.nz

National Institute of Water & Atmospheric Research Ltd
Private Bag 14901
Kilbirnie
Wellington 6241

Phone +64 4 386 0300

NIWA CLIENT REPORT No: 2018180WN rev 1
Report date: June 2019
NIWA Project: MFE19304

Quality Assurance Statement		
	Reviewed by:	Dr Stephen Chiswell
	Formatting checked by:	P Allen
	Approved for release by:	Dr Alison MacDiarmid

© All rights reserved. This publication may not be reproduced or copied in any form without the permission of the copyright owner(s). Such permission is only to be given in accordance with the terms of the client's contract with NIWA. This copyright extends to all forms of copying and any storage of material in any kind of information retrieval system.

Whilst NIWA has used all reasonable endeavours to ensure that the information contained in this document is accurate, NIWA does not give any express or implied warranty as to the completeness of the information contained herein, or that it will be suitable for any purpose(s) other than those specifically contemplated during the Project or agreed by NIWA and the Client.

Contents

Executive summary	6
1 Introduction	8
1.1 Surface ocean temperature	8
1.2 Remote sensing of phytoplankton.....	8
1.3 Phytoplankton and ocean primary productivity.....	8
2 Methods.....	9
2.1 Overview of satellite data	9
2.2 Ocean chlorophyll-a concentration	10
2.3 Coastal chlorophyll-a concentration.....	12
2.4 Sea-surface temperature	14
2.5 Anomalies	16
2.6 Descriptive regions	17
2.7 Trend analysis	19
2.8 Correlation analysis	20
3 Results	20
3.1 Ocean analyses	20
3.2 Coastal analyses.....	46
3.3 New Zealand’s 2017 “marine heat wave”	68
4 Discussion and conclusions	69
4.1 Chlorophyll-a and primary productivity.....	69
4.2 Accuracy of satellite estimates of chl-a	70
4.3 Oceanic variations in chl-a and SST	72
4.4 Coastal variations in chl-a and SST	75
4.5 Recommendations.....	76
5 Acknowledgements	78
6 Glossary of abbreviations and terms	79
7 References.....	80
Appendix A Descriptive sub-regions	87

Tables

Table 2-1:	Satellite data files used in this study.	10
Table 2-2:	Comparison of satellite estimates of chlorophyll-a concentration (chl-a).	13
Table 3-1:	Trend analysis for oceanic chl-a and sea surface temperature (SST).	44
Table 3-2:	Coastal region trend analysis for sea surface temperature (SST).	48
Table 3-3:	Trend analysis for coastal region chlorophyll-a concentration (chl-a).	54
Table B-1:	Co-ordinates defining descriptive regions.	87

Figures

Figure 2-1:	Comparison between in situ and satellite estimates of chlorophyll-a concentration (chl-a).	14
Figure 2-2:	Comparison between OISST (Optimum Interpolation Sea Surface Temperature, SST) at 1/4° resolution with the 1 km SST product of MODIS-Aqua for the New Zealand territorial seas.	15
Figure 2-3:	Oceanic descriptive ocean regions for which summary data were extracted.	18
Figure 2-4:	Coastal descriptive regions for which summary data were extracted.	19
Figure 3-1:	Oceanic: Long-term mean a: chl-a (1997–2018) and b: sea-surface temperature (1981–2018) for the New Zealand oceanographic area	20
Figure 3-2:	Oceanic: Mean annual chl-a by year from the merged dataset of SeaWiFS and MODIS-Aqua.	21
Figure 3-3:	Oceanic: Annual mean chl-a and sea-surface temperature (SST) annual anomalies by year.	26
Figure 3-4:	Oceanic: Monthly mean chl-a concentrations between 1997 and 2018 for descriptive New Zealand regions.	36
Figure 3-5:	Oceanic: Monthly chl-a anomalies between 1997 and 2018 for descriptive New Zealand regions.	38
Figure 3-6:	Oceanic: Monthly SST anomalies between 1981 and 2018 for descriptive New Zealand regions.	40
Figure 3-7:	Oceanic: Spatial trends in monthly anomalies of SST from AVHRR (1981-2018).	42
Figure 3-7:	Oceanic: Spatial trends in monthly anomalies of surface chl-a (1997-2018).	43
Figure 3-8:	Oceanic: the linear Pearson correlation coefficient between monthly anomalies of chl-a and SST (1997–2018).	45
Figure 3-9:	Comparison between OISST (Optimum Interpolation Sea Surface Temperature, SST) at 1/4° resolution with the results from NIWA 1 km SST product (Uddstrom & Oien, 1999) as used in 2016 State of the Environment reporting.	46
Figure 3-10:	Coastal: Long-term mean a: chl-a and b: sea-surface temperature for the New Zealand territorial seas.	47
Figure 3-11:	Coastal sea-surface temperature (SST) anomalies by month for coastal descriptive regions.	49
Figure 3-12:	Coastal mean chlorophyll-a (chl-a) by month for coastal descriptive regions.	55

Figure 3-13:	Coastal chlorophyll-a (chl-a) anomalies by month for coastal descriptive regions.	60
Figure 3-14:	Coastal: Spatial trends in monthly anomalies of SST from MODIS-Aqua, 2002-2018.	65
Figure 3-15:	Coastal: Spatial trends in monthly anomalies of surface chl-a from MODIS-Aqua, 2002-2018.	66
Figure 3-16:	Coastal: the linear Pearson correlation coefficient (R) between monthly anomalies of chl-a and SST from MODIS-Aqua (2002–2018).	67
Figure 3-17:	Monthly anomalies in chl-a and SST for December 2017 (oceanic) and January 2018 (coastal).	69
Figure 4-1:	Anomalies in sea-surface temperature (SST): global average and New Zealand EEZ.	73

Executive summary

Satellite measurement of the near-surface concentration of chlorophyll-a (“chl-a”, which is an indicator of phytoplankton biomass) and sea-surface temperature (SST) are powerful and cost-effective ways of monitoring ocean properties over large areas and long periods. Ocean temperature affects climate patterns and ocean mixing, which in turn, affects ocean primary productivity and hence chl-a. Because phytoplankton are the base of offshore marine food-webs, these measurements can provide information relevant to fisheries, seabirds and marine mammals.

This report updates the analysis presented in Our Marine Environment 2016 and adds a coastal (territorial sea) analysis to the previous ocean (EEZ) analysis. Updates to the ocean analysis include: (1) lengthening the time series of chl-a by 28 months (1997-2018); (2) using new versions of SeaWiFS (R2018.0) and MODIS-Aqua (R2018.0) satellite data; (3) analysing trends in SST based on global “optimum Interpolated” data (1981-2018); (4) correlation analysis between monthly anomalies in SST and chl-a to investigate reasons for changes to ocean productivity.

The new coastal analysis provides information on trends in SST and chl-a within New Zealand’s territorial seas (within 12 nautical miles of the coast) over periods of 1981-2018 (SST) and 2002-2018 (chl-a). Trends were summarised at the scale of Regional Council jurisdictions.

Key results were as follows:

- **Oceanic SST:** Significant positive trends 1981-2018 in SST at the EEZ scale, and in four descriptive regions (Chatham Rise, Tasman Sea, Subtropical Water, Subantarctic Water), with average trends of 0.1–0.2°C per decade which is similar to the global average rate of ocean warming.
- **Coastal SST:** New Zealand territorial waters all warmed significantly over the period 1981–2018, with average rates of warming between +0.12 and +0.28°C per decade (mean of +0.20°C per decade). Most coastal regions showed a period of cooling between 1990–1994, a rapid temperature rise 1994–2000, and then evidence of gradual warming 2010–2018.
- **Oceanic chl-a:** Patterns of variation in chl-a seen in the EEZ and oceanic regions are similar to those reported previously with a mixture of increasing and decreasing trends. Chl-a was generally below the long-term mean around the start and end of the period (1997–2003 and 2012–2018) and above average in the middle period (2003–2012). The highest trends in chl-a were positive (indicative of increasing ocean productivity of +2% per year) and found in the Subtropical Front (west of Fiordland and over the Chatham Rise). Smaller positive trends in chl-a (1997-2002) were found in Subantarctic Waters. Small negative trends in chl-a (indicative of decreasing productivity) were found in Subtropical waters, especially around Northland and the northeast New Zealand continental slope. Changes in chl-a in non-frontal areas were related to upper ocean warming a way that is consistent with our understanding of the factors controlling ocean productivity in these regions. The period of satellite observation of chl-a in oceanic waters (21 years, 1997–2018) is shorter than for oceanic SST which limits our ability to assess the statistical significance of these changes.
- **Coastal chl-a:** Decreasing trends in coastal chl-a between 2002-2018 (likely indicative of decreasing coastal productivity) were found: (1) around Northland and the north-east shelf offshore of Auckland and the Coromandel where changes closely followed trends in offshore productivity suggesting large-scale oceanic forcing; and (2) around the top and west coast of South Island (Tasman, Nelson, West coast) where there were no significant offshore trends in

productivity suggesting that smaller-scale factors and/or coastal processes were responsible. Positive trends in chl-a between 2002-2018 (likely indicative of increasing coastal productivity) were found in the Firth of Thames (Hauraki Gulf), along the west coast of North Island (between Kaipara and New Plymouth), in Hawke's Bay, on north-east coast of South Island (around Kaikoura), along the Oamaru coast, and around Stewart Island. The period of satellite observation of chl-a in territorial waters (16 years, 2002–2018) is much shorter than for oceanic SST which limits our ability to assess the statistical significance of changes.

- **Marine heat wave:** There was an unprecedented (in the satellite data record since 1981) warming event in the Tasman Sea and south of Chatham Rise around December 2017 and January 2018. This heat wave had corresponding strong negative anomalies in chl-a along the west coast of the South Island (especially around Westport and south of Fiordland) and elevated chl-a offshore south of the Snares Islands and over Chatham Rise.

1 Introduction

The physical conditions in New Zealand’s coastal and oceanic waters vary in response to local climate and weather on a range of space and time scales. Changes in the physical conditions affect primary production - the growth of phytoplankton in the upper layers of the ocean. In this report, for the purposes of monitoring and reporting on the state of the New Zealand marine environment, we use satellite data to observe changes in the average monthly temperature of near-surface waters (sea surface temperature) around New Zealand between 1981 and 2018. We use different satellite data to observe the changes in the concentrations of surface phytoplankton in the ocean between 1997 and 2018 and relate these to changes in productivity to changes in sea surface temperature.

This report updates the analysis used for Environment Aotearoa 2015 (Pinkerton, 2015; MfE & Statistics NZ, 2015), for Our Marine Environment 2016 (Pinkerton, 2016; MfE & Statistics NZ, 2016) and in 2018 (Pinkerton, 2018). The time series are lengthened to cover the period up to September 2018.

1.1 Surface ocean temperature

The temperature of the uppermost layers of the ocean (surface few metres) is called sea surface temperature (SST). This temperature is determined by the balance between radiative solar heating (i.e. incoming solar radiation absorbed in the upper ocean), evaporation from the ocean surface, sensible (conductive) heat flux from the air to the sea, and mixing of deeper water with surface waters (convective energy transfer). SST is a useful indicator of the state of the well-mixed upper ocean layer (called the “mixed layer”), which varies between about 20 m and 200 m in depth. This upper ocean mixed layer is important because most oceanic primary production takes place within it and also because it is the part of the ocean in contact with the atmosphere and so affects exchange of gases between the atmosphere and ocean.

1.2 Remote sensing of phytoplankton

Phytoplankton are microscopic algae which are kept in suspension in the upper parts of the ocean by the movement of the water. Variability in phytoplankton biomass is characterised by a wide range of scales, both temporal (1 day–decadal) and spatial (1–10⁴ km), and so cannot be adequately monitored across a region as big as the New Zealand Exclusive Economic Zone (EEZ) by in situ sampling (e.g. from research vessels, moorings or autonomous instrumentation). Instead, satellite measurements of ocean colour have proved to be a powerful and cost-effective way of monitoring near-surface phytoplankton abundance and distribution over large areas (Hooker et al., 1992; Murphy et al., 2001). Because it is ubiquitous in phytoplankton, the concentration of chlorophyll-a (chl-a) is often used as a proxy for phytoplankton biomass (Gordon et al., 1988; Hooker et al., 1992; O’Reilly et al., 1998). Except where sub-surface chlorophyll maxima occur, a near surface measurement of chl-a is typically indicative of water-column integrated phytoplankton abundance and, at broad time and space scales, ocean productivity (Campbell et al., 2002; Aiken et al., 2004; see also Section 4.1 in this report).

1.3 Phytoplankton and ocean primary productivity

Phytoplankton grow by the process of photosynthesis, whereby energy from the sun is captured by coloured compounds (pigments) in the algal cells and used to create organic matter. This “phytoplankton biomass” can be consumed by microscopic animals (zooplankton) or broken down by bacteria. The grazers of phytoplankton and consumers of breakdown products are themselves

consumed by larger animals in the marine food-web. Through these processes, the growth of phytoplankton in the upper layers of the ocean ultimately supports virtually¹ all marine organisms including squid, fish, mammals, seabirds and benthic biota like corals and sponges.

On large time and space scales (multi-year, basin-scales), higher phytoplankton biomass is an indicator of higher ocean productivity across all trophic levels, though the relationship between phytoplankton biomass and primary productivity is complex (Parsons et al., 1977; Friedland et al., 2012). Monitoring changes in the magnitude and patterns of phytoplankton biomass is hence likely to provide valuable context for understanding changes in fisheries, marine biogeochemistry, and climate-related changes to ocean productivity (Murphy et al., 2001; Aiken et al., 2004; IOCCG, 2008).

2 Methods

2.1 Overview of satellite data

We primarily used data from two ocean colour satellite sensors for chl-a (SeaWiFS, MODIS-Aqua) and from one series of ocean temperature sensors (AVHRR) – see Table 2-1.

SeaWiFS: The Sea Viewing Wide Field-of-view Sensor (SeaWiFS, Hooker et al., 1992) was operated by Orbimage and NASA, and was operational between September 1997 and December 2010.

MODIS-Aqua: The NASA Moderate Resolution Imaging Spectroradiometer (MODIS-Aqua²), providing data from July 2002 to the present

AVHRR: The Advanced Very High Resolution Radiometer series of satellite sensors have been operated by NOAA (National Oceanic and Atmospheric Administration of the USA) since 1978 and have provided continuous data since 1981.

Data from the European Space Agency (ESA) Medium Resolution Imaging Spectroradiometer (MERIS, Rast & Bezy, 1990) were used as independent validation for the period April 2002 to April 2012. Specifics of the datasets used are given below in sections 2.2.1, 2.2.2 and 2.2.4. Earlier measurements of ocean colour (e.g. the Coastal Zone Color Scanner, 1979-1986; MODIS-Terra sensor, operational from 2000) are not used because they are of lower quality (Gordon et al., 1983). Observations from SeaWiFS and MODIS-Aqua were merged (method described in Section 2.2.3) to provide a consistent time-series of satellite measurements of ocean colour covering more than 18 years (September 1997 – March 2018).

Because ocean colour data and AVHRR data are only obtained when there are no clouds, a challenge in achieving long-term monitoring is eliminating cloud contamination. Satellite data are typically composited in time and space to provide nearly clear images. We used monthly composite images for analysis. In the New Zealand region, SeaWiFS data have a base spatial resolution of 4 km and MODIS-Aqua and AVHRR data have a base resolution of 1 km. Composite (time-averaged) ocean colour data with a spatial resolution of 9 km were used here as this scale is appropriate for monitoring changes in ocean productivity in large offshore regions like the New Zealand EEZ. The SST analysis uses Optimum Interpolation Sea Surface Temperature (OISST), version 2 (Reynolds et al., 2002).

¹ Some animals around deep-sea thermal vents obtain their energy from chemosynthetic processes rather than from phytoplankton.

² <http://modis.gsfc.nasa.gov/about/>

Table 2-1: Satellite data files used in this study. Version numbers are given in square brackets. Dark shading indicates the sensor was not operational. Satellites become less reliable towards the end of their lifetimes and the data record becomes intermittent - this is shown as light shading (SeaWiFS 2008–2010; MERIS in 2012). The main overlap period for the ocean colour satellite data (i.e. between SeaWiFS and MODIS-Aqua) was 2003 to 2007 (inclusive, highlighted yellow). Satellite sea-surface temperature data were from NOAA (National Oceanic and Atmospheric Administration, US) Optimum Interpolation (OI) Sea Surface Temperature (SST) product based on AVHRR (Advanced Very High Resolution Radiometer) satellite data.

	SeaWiFS [R2018.0]	MODIS-Aqua [R2018.0]	Merged SeaWiFS and MODIS-Aqua	MERIS [R2012.1]	AVHRR OI-SST [v2]
Year	Monthly	Monthly	Monthly	Monthly	Monthly
1981	0	0	0	0	3
1982-1996	0	0	0	0	180
1997	4	0	4	0	12
1998	12	0	12	0	12
1999	12	0	12	0	12
2000	12	0	12	0	12
2001	12	0	12	0	12
2002	12	6	12	9	12
2003	12	12	12	12	12
2004	12	12	12	12	12
2005	12	12	12	12	12
2006	12	12	12	12	12
2007	12	12	12	12	12
2008	8	12	12	12	12
2009	11	12	12	12	12
2010	12	12	12	12	12
2011	0	12	12	12	12
2012	0	12	12	4	12
2013	0	12	12	0	12
2014	0	12	12	0	12
2015	0	12	12	0	12
2016	0	12	12	0	12
2017	0	12	12	0	12
2018	0	9	9	0	9
All	155	195	253	121	444

2.2 Ocean chlorophyll-a concentration

2.2.1 SeaWiFS R2018.0

We used the most recent processing of SeaWiFS ocean colour data available at the time of writing, namely SeaWiFS version R2018.0. These data were updated from SeaWiFS version 2014.0 (June 2015) which was used in Our Marine Environment 2016 (Pinkerton, 2016). The reprocessing of SeaWiFS ocean colour data was part of a multi-mission effort to update the instrument calibrations

and vicarious calibration³ (NASA et al., 2018a). Briefly, the SeaWiFS R2018.0 reprocessing included new vicarious methods but the instrument calibration was unchanged. The Level 2 processing (science algorithms) were unchanged from those employed in the R2014.0 SeaWiFS processing. SeaWiFS data were only used for oceanic chl-a because at 4 km they have insufficient spatial resolution to be useful for measuring phytoplankton in the coastal zone which is highly heterogenous.

2.2.2 MODIS-Aqua R2018.0

We used MODIS-Aqua data version R2018.0 which is the most recent processing of MODIS-Aqua ocean colour data available at the time of writing. These data were updated from MODIS-Aqua version 2014.0 (June 2015) which was used in Our Marine Environment 2016 (Pinkerton, 2016). The reprocessing of MODIS-Aqua ocean colour data was part of a multi-mission effort by NASA to update the instrument calibrations and vicarious calibration (NASA et al., 2018b). The MODIS-Aqua R2018.0 reprocessing was a result of a major end-to-end re-analysis of the MODIS-Aqua instrument calibration as derived from on-board calibration sources (solar/lunar) and vicarious methods. The Level 2 processing (science algorithms) were identical to those employed in the R2014.0 MODIS-Aqua processing.

2.2.3 Merging SeaWiFS and MODIS-Aqua ocean data

There are discrepancies between measurements of oceanic chl-a made by different satellite sensors. These arise from reasons including: (1) differing times of day for overpasses; (2) different sensor designs and performance (Brewin et al., 2014); (3) different spectral bands and processing algorithms (both in-water and atmospheric, (Pinkerton et al., 2005; Gordon, 1997); and (4) different sensor degradation rates over time (Barnes et al., 2001; Eplee et al., 2001). Much effort by international research teams for example at NASA is made to minimise the effects of these variations and provide consistent, long-term datasets for climate-related monitoring and research.

We used the same process of blending chl-a measurements from SeaWiFS and MODIS-Aqua into a consistent time series for the New Zealand ocean as previously (Pinkerton, 2016; Pinkerton, 2018). Over all months and all years, MODIS-Aqua tended to give slightly higher chl-a values than SeaWiFS but the differences were very small (median difference in chl-a of $-0.0023 \text{ mg m}^{-3}$). We found that differences tended not to vary with chl-a and there was no indication of a long-term (interannual) variation in the differences between SeaWiFS and MODIS-Aqua measurements (Pinkerton, 2016; Pinkerton, 2018).

2.2.4 MERIS R2012.1

As an independent check of the blended ocean chl-a time-series, we used MERIS data from the European Space Agency. We used the most recent MERIS data version available at the time of writing: version R2012.1 (Melin et al 2011; NASA et al., 2016c). This version of MERIS data is unchanged from previous similar work (Pinkerton, 2016; Pinkerton, 2018). MERIS data were only used for validation of the ocean chlorophyll products, though it is possible that these could be used in the future in the coastal zone as they have 300 m spatial resolution.

³ "Vicarious calibration" refers to techniques that make use of natural or artificial sites on the surface of the Earth for the post-launch calibration of sensors

2.3 Coastal chlorophyll-a concentration

MODIS Aqua data alone were used to observe coastal chl-a round New Zealand. Processing of ocean colour satellite data for chl-a in the coastal zone where resuspended sediment and coloured dissolved organic matter (CDOM) substance are intermittently present remains scientifically challenging and is still an area of active research (Siegel et al., 2000; Babin et al., 2003b; Pinkerton et al., 2005, 2018).

2.3.1 Coastal atmospheric correction

The normal atmospheric correction process for ocean colour data (“dark pixel method”) does not apply to turbid waters but alternatives have been developed (Ruddick et al., 2000; Lavender et al., 2005; Wang & Shi, 2007). We investigated two atmospheric correction methods appropriate for turbid coastal New Zealand waters. (1) The NIR-short-wave infrared radiation (SWIR) switching algorithm (Wang & Shi, 2007). In this approach, near infra-red (NIR) wavelengths are used to estimate reflectance by atmospheric aerosols over clear waters, and short-wave infra-red (SWIR) wavelengths are used over turbid waters. (2) The MUMM model with the default MUMM alpha for MODIS of 1.945 (Ruddick et al., 2000), which has been implemented in later versions of SeaDAS and is based on the spatial homogeneity of the water-leaving radiances and aerosols ratios between NIR bands (748 and 869 nm for MODIS sensors). In a comparison in European coastal waters, it was found that the NIR-SWIR and MUMM methods performed similarly, but that “the MUMM algorithm gives a better quality product” (Ody et al., 2016). The performances of these different atmospheric correction approaches in the New Zealand region have not previously been intercompared.

2.3.2 Coastal in-water inversion algorithms

Simple empirical methods (e.g. O’Reilly et al. 1998) can robustly estimate chl-a in ocean waters but typically perform poorly coastally (IOCGG 2000; Pinkerton et al. 2006; Zeldis et al. 2015). Two main types of semi-analytical in-water algorithms were tested here. (1) The Quasi-Analytical Algorithm (QAA) algorithm (Lee et al. 2002; Lee et al. 2009) estimates particulate backscatter at 555 nm [$b_{bp}(555)$] and phytoplankton absorption at 488 [$a_{ph}(488)$]. (2) The Garver-Siegel-Maritorena (GSM) algorithm (Garver & Siegel 1997; updated processing⁴). Phytoplankton absorption was converted to an estimate of chl-a using the chl-specific absorption coefficient, $a_{ph}^*(488)$. The value of $a_{ph}^*(488)$ can vary seasonally and spatially, related to different phytoplankton species (varying cell physiology and pigments), different phytoplankton cell sizes, and the light environment (phytoplankton in more turbid waters may increase light harvesting pigments) (Kirk, 2011). Here, we used an average of values found for oceanic phytoplankton (Bricaud et al. 1995; Bissett et al. 1997), and measurements in the lower reaches of New Zealand rivers and estuaries (Pinkerton, 2017). The latter measurements were made as part of the National River Water Quality Network (NRWQN) project (Mark Gall, NIWA – unpublished data). MODIS data were interpolated to 500 m using paired bands where necessary (Franz et al. 2006). We did not blend the coastal chl-a and the open-ocean chl-a (e.g. Pinkerton et al., 2018) because more work is needed on the appropriate scaling of $b_{bp}(555)$ to use for this blending.

2.3.3 Validation of coastal chl-a data

Measurements of chl-a in the New Zealand coastal zone were compared with in situ measurements to explore data quality. In situ measurements of coastal water quality have been carried out by Regional Councils since 2002. We used 15,588 measurements of chl-a that were recently brought together for State of the Environment reporting (Dudley et al., 2017; Dudley & Jones-Todd, 2018).

⁴ www.icess.ucsb.edu/OCisD/

We matched these in situ measurements to satellite data collected within 1 day of the in situ sampling, and used a mean of the nearest 9 satellite pixels around the point of sampling. Results are shown in Table 2-2 and Figure 2-1. As expected, the case 1 (band ratio) algorithm leads to a positive bias in chl-a because it mis-identifies suspended sediment as chl-a. This bias (overestimate of chl-a) is reduced by using the semi-analytical algorithms (QAA and GSM). The GSM algorithm performs more poorly than the QAA algorithm (lower R^2 and higher fail rate). The satellite estimates of chl-a based on data processed with the MUMM atmospheric correction algorithm agree with the in situ measurements slightly better than those using the NIR-SWIR algorithm. Based on this analysis, we used the MUMM atmospheric correction and QAA algorithm, as this processing chain had good robustness (high number of samples), the highest R^2 , lowest RMS difference, and was closest to 1:1 agreement with the in situ measurements (i.e. offset close to zero and slope close to unity).

Table 2-2: Comparison of satellite estimates of chlorophyll-a concentration (chl-a). We tested two atmospheric correction (AC) methods: (1) near infra-red short-wave infra-red switching (NIR-SWIR, Wang & Shi, 2007); (2) MUMM method (Ruddick et al., 2000). We tested three in water algorithms: (1) band-ratio (O'Reilly et al. 1998); (2) Quasi-analytical algorithm (QAA v5, Lee et al. 2009); (3) Garver-Siegel-Maritorena algorithm (GSM, Garver & Siegel 1997). Metrics used were: (1) the number of valid pixels for comparison (N) which is indicative of the stability of the processing chain; (2) the coefficient of determination between the in situ and satellite estimates of chl-a (R^2); (3) the root-mean-square difference between the in situ and satellite estimate of chl-a (RMS); (4) the offset and (5) slope of the reduced major axis least squares regression line. The best performing processing is shown in bold for each metric.

AC method	In water algorithm	N	R^2	RMS	offset	slope	Figure 2-1
NIR-SWIR	Band-ratio	1131	0.22	0.38	0.39	0.86	a
NIR-SWIR	QAA	887	0.20	0.06	-0.01	1.15	c
NIR-SWIR	GSM	724	0.14	0.49	-0.45	2.03	e
MUMM	Band-ratio	1199	0.20	0.35	0.36	0.80	b
MUMM	QAA	1022	0.23	0.01	0.00	1.04	d
MUMM	GSM	882	0.15	0.48	-0.46	1.81	f

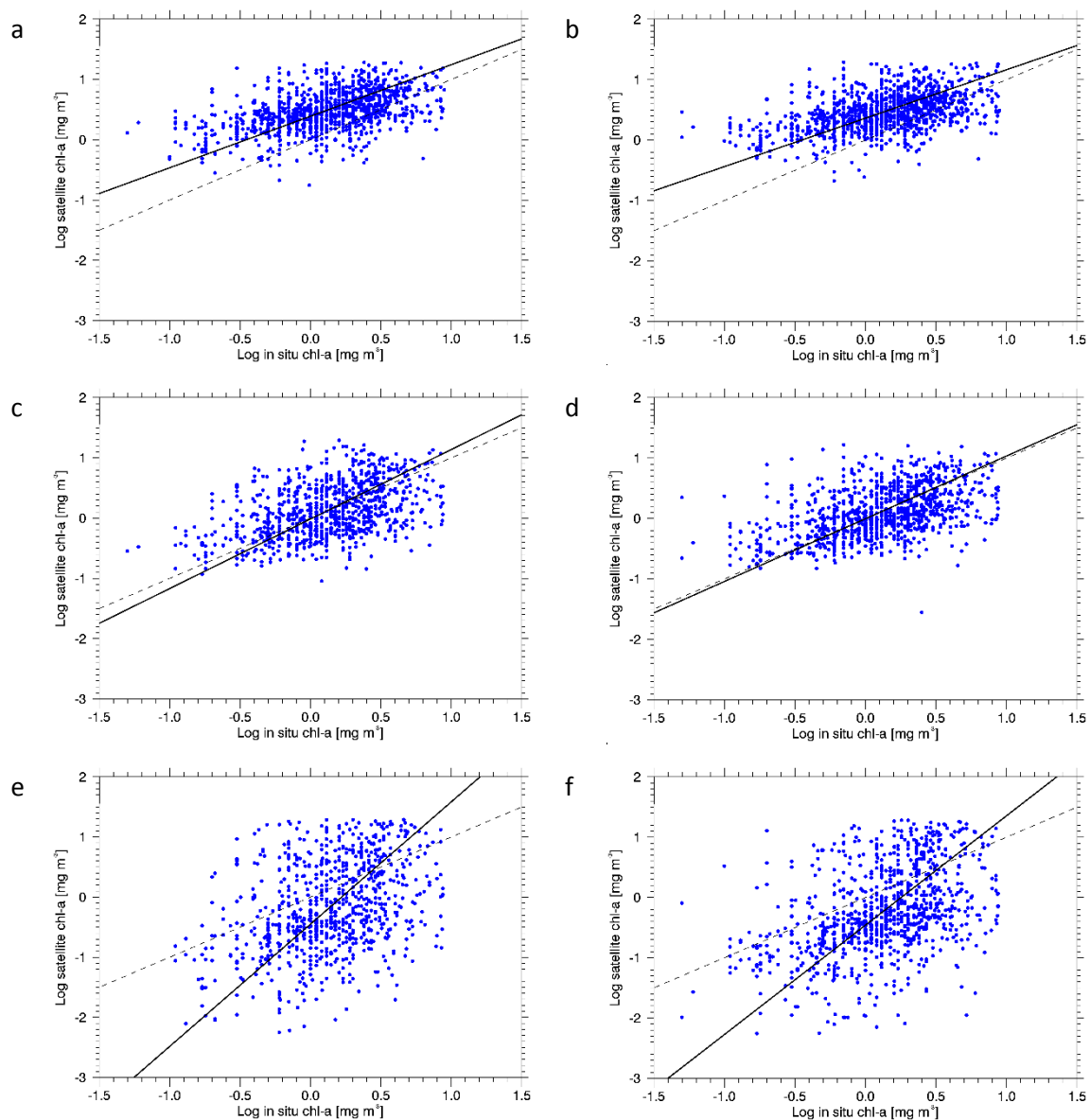


Figure 2-1: Comparison between in situ and satellite estimates of chlorophyll-a concentration (chl-a). Different processing methods are shown: a: NIR-SWIR, band-ratio; b: MUMM, band-ratio; c: NIR-SWIR, QAA; d: MUMM, QAA; e: NIR-SWIR, GSM; f: MUMM, GSM. See Table 2-2 and text for acronyms (and Glossary).

2.4 Sea-surface temperature

2.4.1 Satellite data source

We used the AVHRR processed product called “OISST-AVHRR only” which is a $1/4^\circ$ daily SST estimate derived by Optimum Interpolation Sea Surface Temperature, version 2 (Reynolds et al., 2002). OISST data were interpolated by bilinear interpolation to the 9 km New Zealand grid to enable pixel-by-pixel intercomparison of trends in SST monthly anomalies and chl-a monthly anomalies.

This source of SST data is different to that used in previous SST indicators in New Zealand (MfE & Statistics NZ 2015; 2016). These previous versions used the same raw AVHRR data, but these were processed locally in New Zealand using different cloud-clearing, processing and compositing methods

(Uddstrom & Oien, 1999). A comparison between the previous and present results and discussion is given in Section 3.1.6.

2.4.2 Coastal SST comparison with MODIS-Aqua SST

Although the $1/4^\circ$ resolution OISST data is appropriate for oceanic analysis, it is relatively coarse for coastal investigations. Higher-resolution SST datasets are available, for example 1 km data from MODIS, but these are of much shorter duration (2000–2018). In order to confirm that the OISST data are appropriate for investigating long-term trends in SST in New Zealand’s territorial waters, we compared the coarse-scale OISST data with the fine-scale MODIS SST data in the territorial waters. In the New Zealand coastal zone we found that the OISST data agreed closely with the MODIS-Aqua 1 km measurements between 2002 and 2018 (Figure 2-2). Our first comparison (Figure 2-2a) matched each monthly-composited OISST pixel in the New Zealand territorial seas (less than 12 nautical miles from the coast) with the median of the corresponding MODIS-Aqua pixels from the same month. The regression line is not significantly different from unity and more than 97% of the variance in the MODIS-Aqua measurements was described by the OISST measurements. The small differences between OISST and MODIS-Aqua SST result from small-scale variations in SST with area, the effects of spatial averaging, and differences between the satellite sensors and processing methods. The second comparison compared mean SST monthly anomalies for the coastal descriptive regions (Figure 2-2b). The agreement was very good ($R^2=0.79$), with an intercept not significantly different from zero, and a slope close to unity (0.91). For the purpose of this study, we conclude that the OISST data are suitable to track long term change in New Zealand territorial waters.

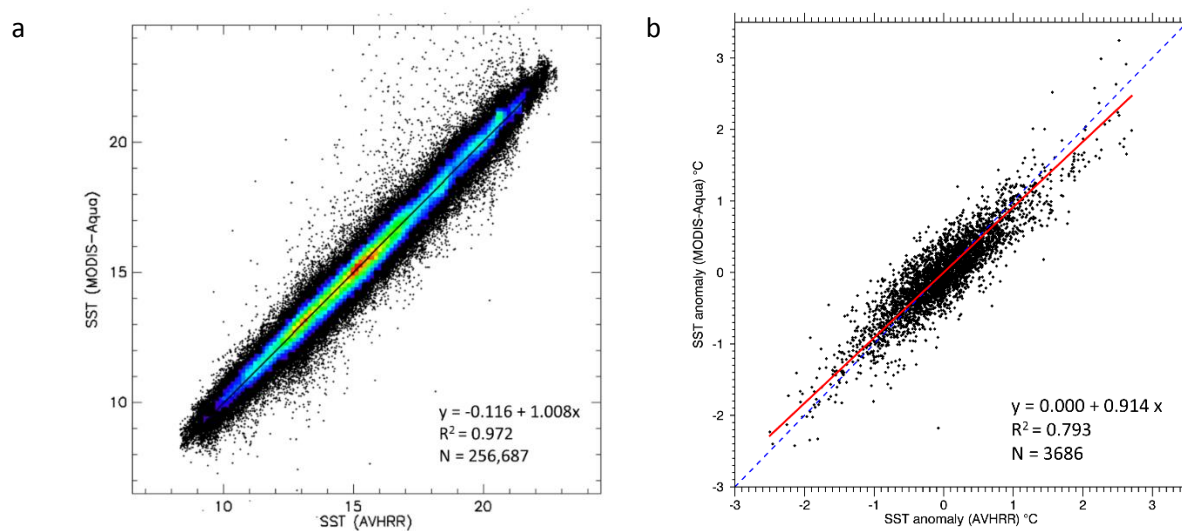


Figure 2-2: Comparison between OISST (Optimum Interpolation Sea Surface Temperature, SST) at $1/4^\circ$ resolution with the 1 km SST product of MODIS-Aqua for the New Zealand territorial seas. a: Comparisons between SST ($^\circ\text{C}$) for each pixel. Colours show densities of points (red=higher densities; blue=lower densities), with less than 100 points per pixel shown as separate black points. b: Comparison of mean SST monthly anomalies at the scale of coastal descriptive regions (see Section 2.7.2). All comparisons based on month resolution, between 2002 and 2018. The least-squares regression lines, coefficients of determination (R^2) and number of points (N) are also shown.

2.5 Anomalies

2.5.1 Annual anomalies

Annual anomalies were calculated as the mean value for a given year minus the long-term mean (Equation 1). For example, the 2000 chl-a anomaly is the mean value of chl-a for 2000 at a given pixel minus the long-term mean chl-a value for the same pixel. In Equation 1, δ_y is the annual anomaly for year y , N_y is the total number of years of data, N_m is the total number of months of data per year, and $C_{y,m}$ is the chl-a or SST value for year y and month m . Annual anomalies were only calculated for years where there were potentially observations in all months. This means that, for example, we do not calculate annual means or anomalies of chl-a for 1997 (SeaWiFS observation started in September 1997) or 2018 (observation ceased in September 2018).

$$\delta_y = \frac{1}{N_m} \sum_m C_{y,m} - \frac{1}{N_y N_m} \sum_y \sum_m C_{y,m} \quad [\text{Equation 1}]$$

2.5.2 Monthly anomalies

Monthly anomalies were calculated as the average value for each month minus the long-term monthly mean (Equation 2). For example, the monthly anomaly for January 2000 was calculated as the mean of January 2000 minus the long-term mean of all Januarys. Symbols in Equation 2 are the same as in Equation 1.

$$\delta_m = C_{y,m} - \frac{1}{N_m} \sum_m C_{y,m} \quad [\text{Equation 2}]$$

2.5.3 Effect of missing data

We note that annual anomalies calculated in this way will tend to be biased in areas where observations are missing in some months. The OISST analysis means that this does not occur for SST: data are present in all months. But, chl-a observations can be absent in some months, for example, because of persistent clouds or low solar elevation (especially in Subantarctic Waters in winter).

By using monthly composites rather than 8-day or shorter composites, the problem of persistent cloud is minimised. The effect on systematic missing chl-a data in the winter in Subantarctic Water is likely to be relatively small for two reasons. First, chl-a values do not show a strong seasonal pattern in this area over the winter (unlike SST). Second, the lack of chl-a data in Subantarctic Water in winter is relatively consistent from year to year so that there is consistency between the months used to calculate the long-term average and to calculate the annual averages. However, because of the remaining potential for bias due to missing chl-a data in the winter, we caution that maps of annual chl-a and annual chl-a anomalies should be considered indicative, especially in Subantarctic Water. Finally, we note that the main analyses in this report are based on monthly anomalies which do not suffer from this problem.

2.5.4 Reference period

Because we are calculating the anomalies based on the whole reference period, each time the analysis is updated by adding recent measurements, the reference (“baseline”) changes, and hence the historical anomalies also change. Some time series analysis elsewhere in the world are based on

a fixed reference period so this does not happen; the time series can be updated without effecting the historical anomalies. The choice of reference period is somewhat subjective however, and can be problematic if different reference periods are used for different data. This is discussed further in Section 4.5 where we recommend that future updates of SST and chl-a indicators should consider whether a fixed reference period should be adopted for these data in New Zealand's environmental reporting system.

2.6 Descriptive regions

2.6.1 Oceanic regions

Monthly anomalies of chl-a and SST were extracted for the EEZ and four descriptive oceanic regions (Figure 2-3; Appendix A). These regions were chosen to include productive regions and particular water masses: the Chatham Rise (Subtropical Front east of New Zealand); the Tasman Sea (including the Subtropical Front west of New Zealand); Subtropical Water (STW); and Subantarctic Water (SAW). All descriptive regions, including the EEZ region, do not include chl-a data in New Zealand territorial waters. Given that our analyses show important differences in chl-a between the Subtropical Front west of New Zealand and the Tasman Sea proper, it may be sensible to separate these for future analyses (see also recommendations in Section 4.5).

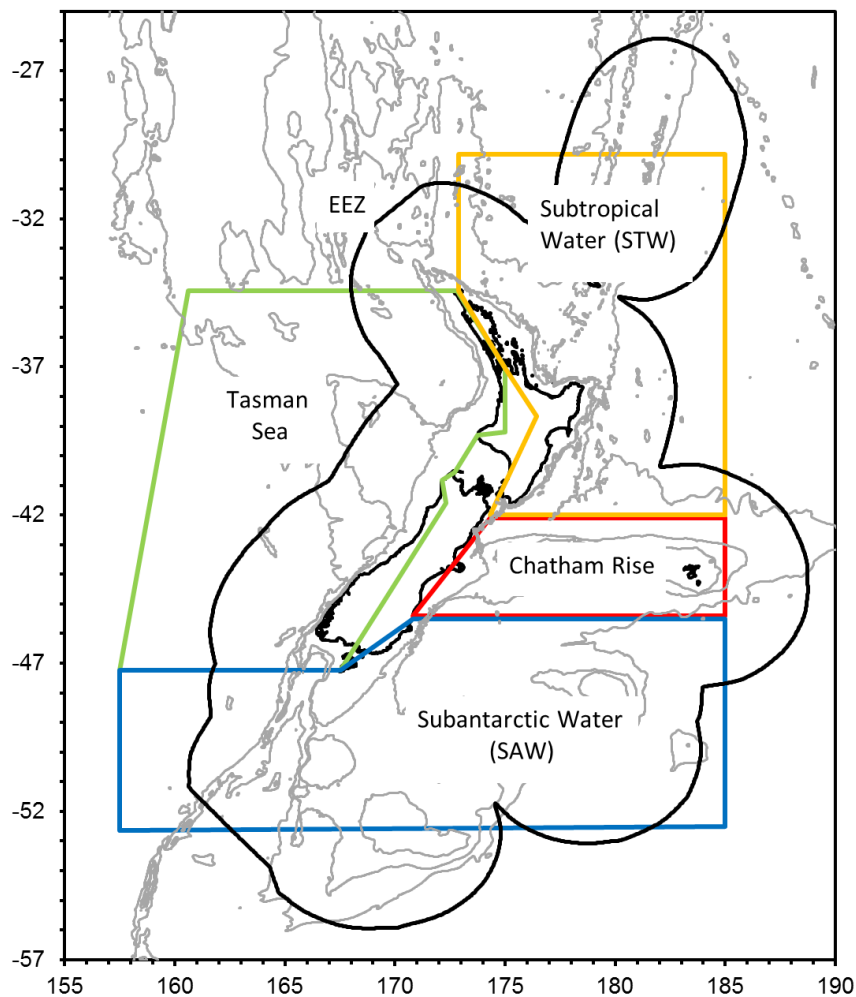


Figure 2-3: Oceanic descriptive ocean regions for which summary data were extracted. Depth contours are shown in grey at 500 m, 1000 m and 3000 m depths.

2.6.2 Coastal regions

Information on trends in chl-a and SST in coastal regions were summarised based on Regional Council boundaries and extended to the territorial limit of 12 nautical miles offshore (Figure 2-4). Coastal areas were split if different non-contiguous parts of the Regional Council's marine areas occurred on different sides of the country. For example, the Auckland Region was split into "Auckland_east" and "Auckland_west". This was also done for the Manawatu-Wanganui and Waikato regions.



Figure 2-4: Coastal descriptive regions for which summary data were extracted. Boundaries are based on Regional Council boundaries.

2.7 Trend analysis

For the oceanic areas, temporal trends in monthly anomalies (chl-a and SST) for each pixel were determined using Mann-Kendall test (Mann, 1945; Kendall, 1975) and the estimation of the Sen slope (Sen, 1968). Statistical significance was assessed using unadjusted Mann-Kendall P values; trends were identified as significant when the P-value is less than 5% and the Sen slope not equal to zero. A statistically significant Kendall test with an annual trend of more than 1% of the median value is often considered meaningful (Hipel & McLeod, 1994; Scarsbrook, 2006).

The Mann-Kendall trend test assesses significance (or lack) of a trend by looking at whether the distribution of “increases” versus “decreases” between pairs of points in the time series is different from that expected with random variations and no trend (Mann, 1945; Kendall, 1975). The Mann-Kendall test is preferred over linear regression analysis because it is non parametric (distribution free) and does not require an assumption that the data are normally distributed. The insensitivity of the Sen slope to outliers means that it is generally the preferred non-parametric method for estimating a linear trend (Hipel & McLeod, 1994).

We note that the null hypothesis in the Mann-Kendall test assumes that the data are independent and randomly ordered (Mann, 1945; Kendall, 1975). The existence of positive autocorrelation in the data increases the probability of detecting trends when actually none exist, and vice versa (Hamed &

Rao, 1997). A number of correction methods for autocorrelation in the Mann-Kendall test exist and we used the method of Yue & Wang (2004). This correction method reduces the effective number of degrees of freedom if positive autocorrelation occurs and hence tends to reduce the risk of type 1 errors (false positives). This correction also reduces our statistical power to correctly identify significant trends so increases the risk of type 2 error (false negatives).

2.8 Correlation analysis

For the oceanic areas, the linear Pearson correlation coefficient between monthly anomalies in chl-a and SST were determined for each pixel separately, using the 247-month overlap period between 1997 and 2018. This correlation analysis investigates to what extent changes in chl-a may be related to changes in ocean surface temperature.

3 Results

3.1 Ocean analyses

3.1.1 Long-term mean chl-a and SST

The long-term average chl-a (2002–2018) and SST (1981–2018) for the New Zealand oceanic region based on complete years of observation only are shown in Figure 3-2. Higher oceanic chl-a is associated with the Subtropical front (which extends across the New Zealand domain at about 45°S), especially over Chatham Rise. Annual average surface water temperatures vary with latitude principally, from about 25°C in northern Subtropical Water to 7°C in southern Subantarctic Water.

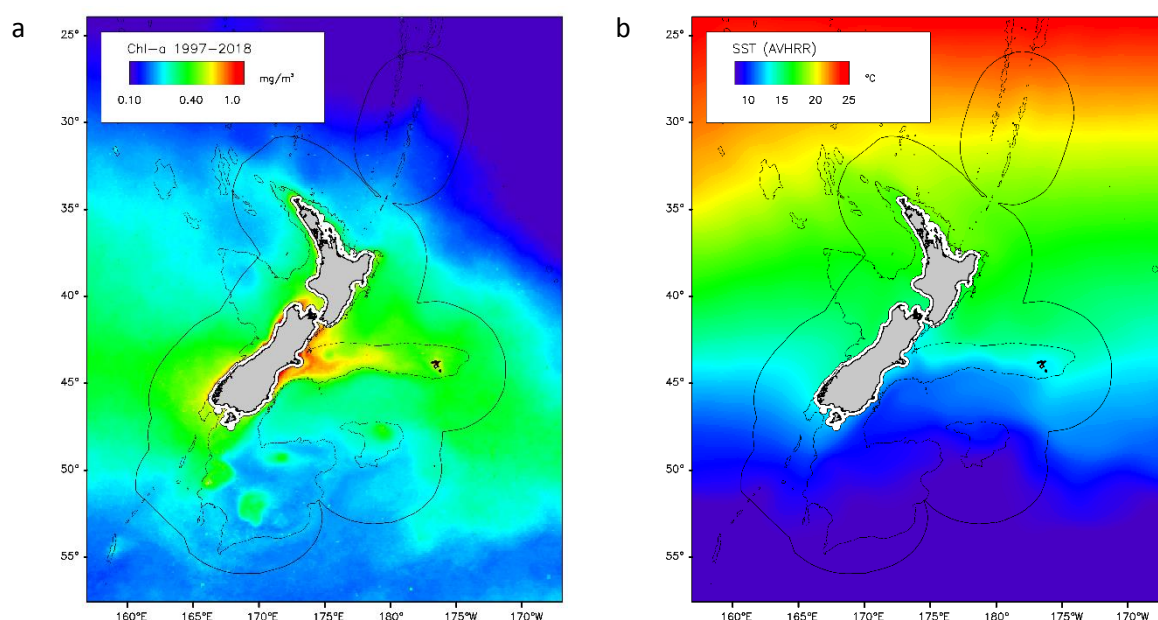


Figure 3-1: Oceanic: Long-term mean a: chl-a (1997–2018) and b: sea-surface temperature (1981–2018) for the New Zealand oceanographic area The boundary of the New Zealand EEZ is also shown. Analyses are based on complete years of observation only so that partial years do not seasonally bias the average.

3.1.2 Annual chl-a and SST anomalies

The mean chl-a values for each year based on the merged SeaWiFS and MODIS-Aqua dataset are shown in Figure 3-2. Annual chl-a and SST anomalies are shown in Figure 3-3.

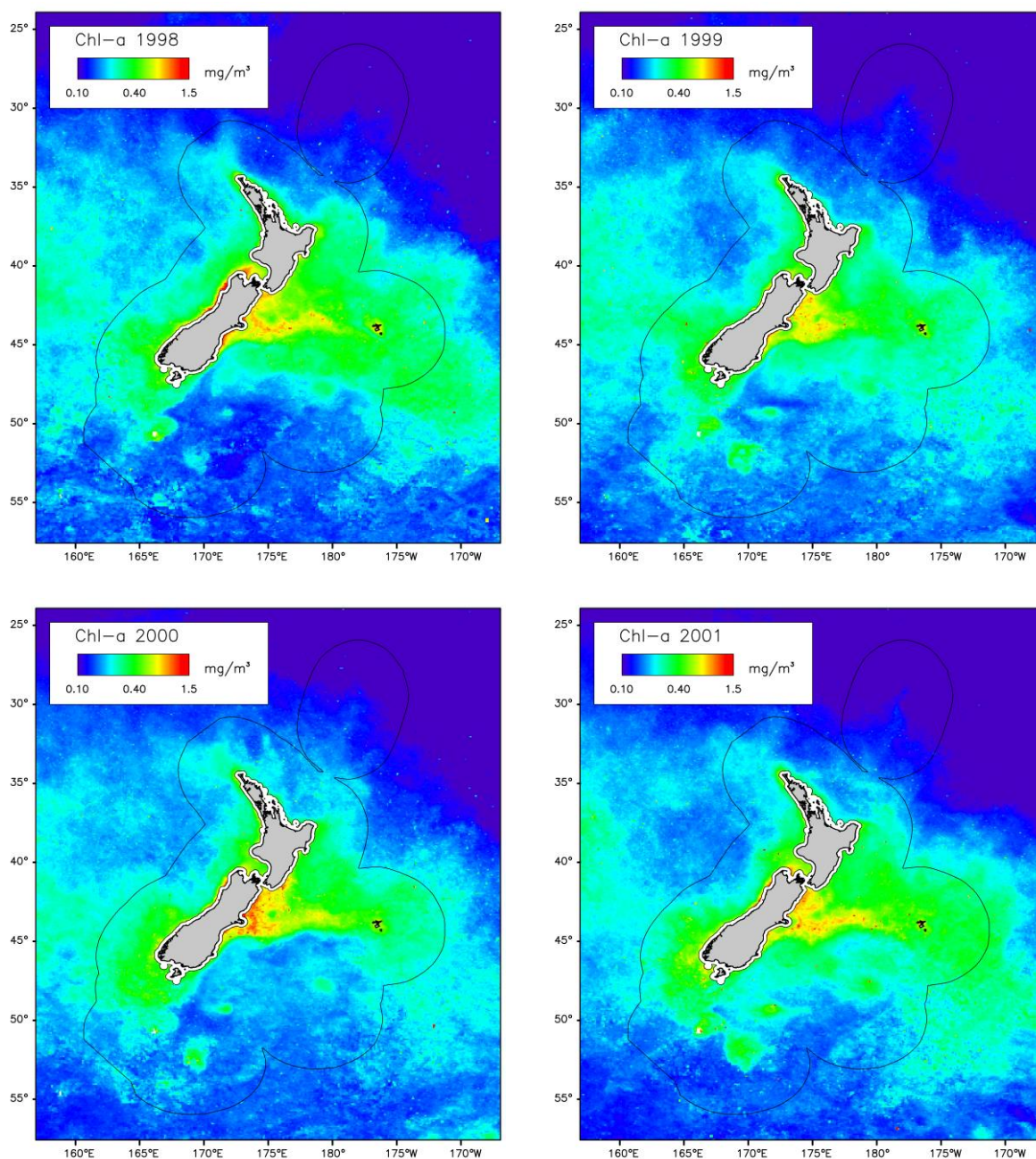


Figure 3-2: Oceanic: Mean annual chl-a by year from the merged dataset of SeaWiFS and MODIS-Aqua. The boundary of the New Zealand EEZ is also shown.

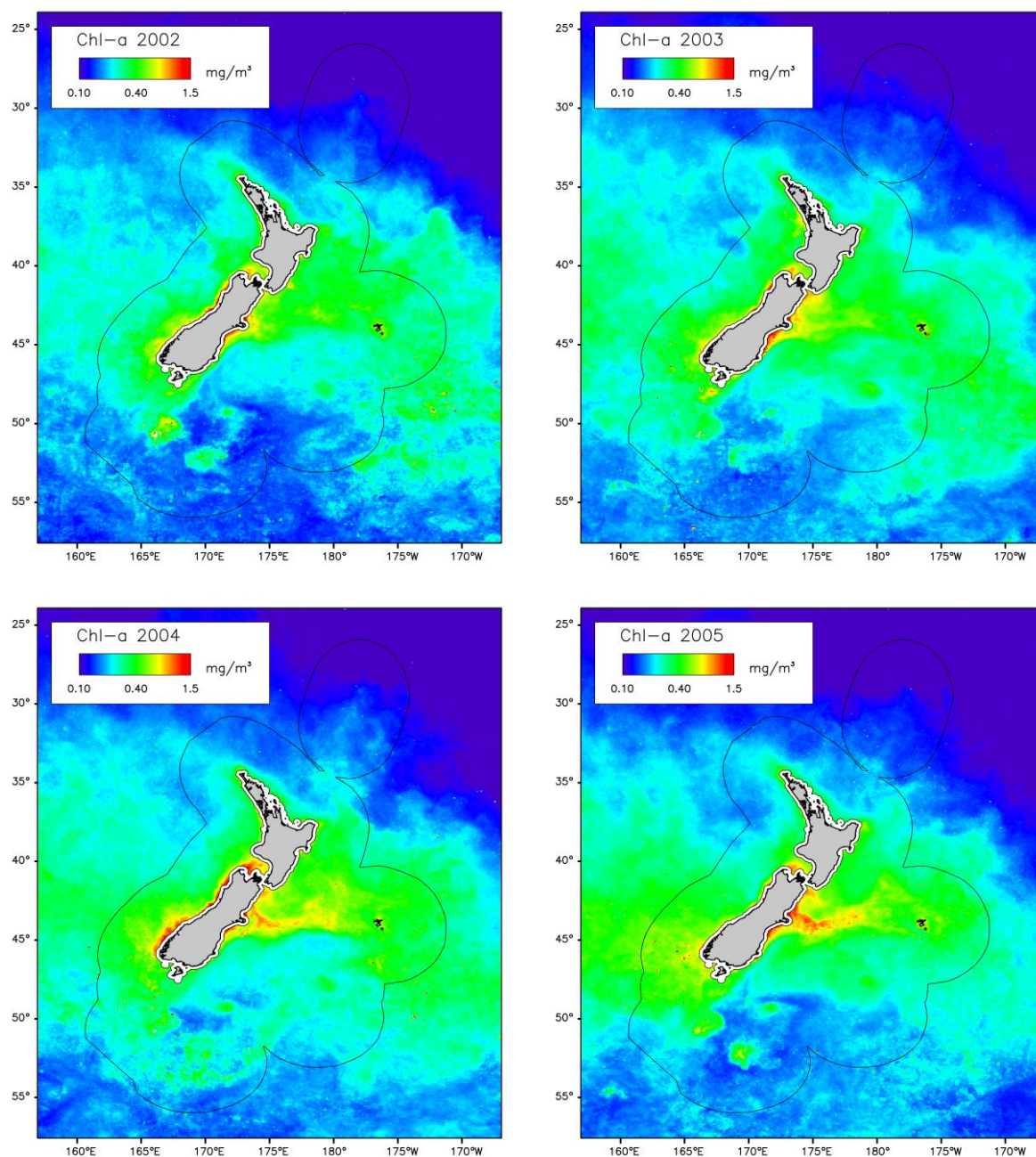


Figure 3-2: Oceanic: Mean annual chl-a by year from the merged dataset of SeaWiFS and MODIS-Aqua. (Continued)

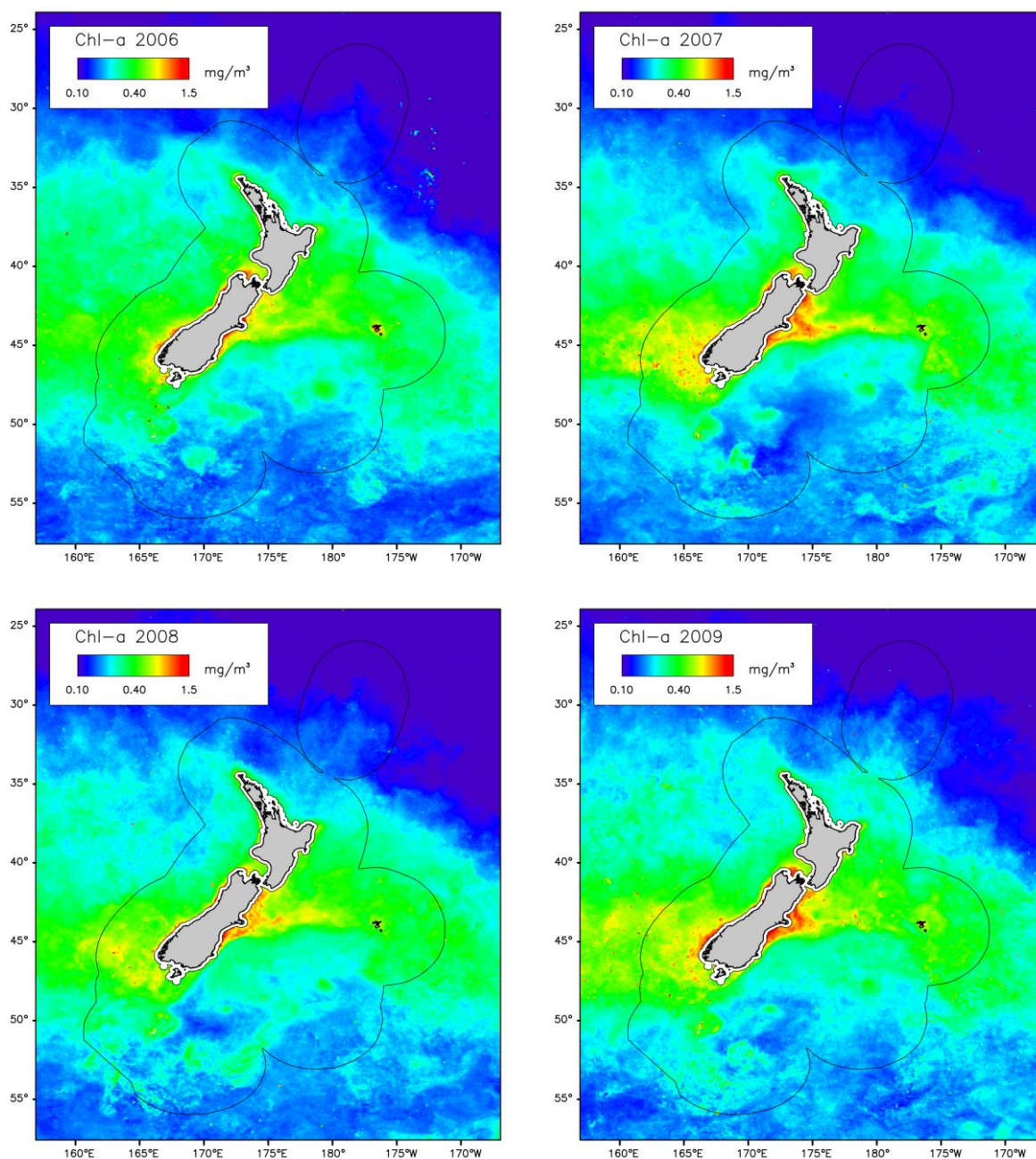


Figure 3-2: Oceanic: Mean annual chl-a by year from the merged dataset of SeaWiFS and MODIS-Aqua. (Continued)

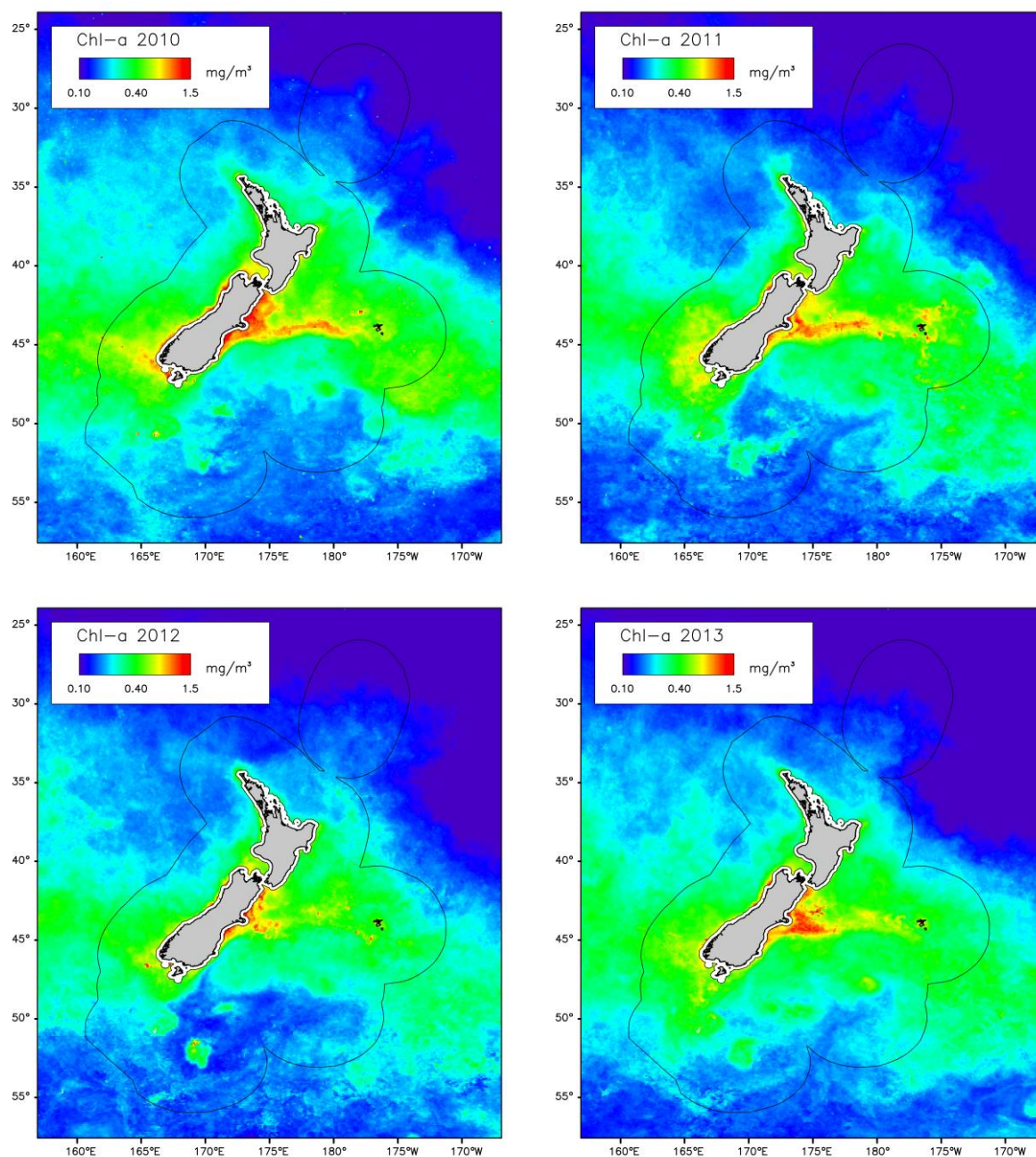


Figure 3-2: Oceanic: Mean annual chl-a by year from the merged dataset of SeaWiFS and MODIS-Aqua. (Continued)

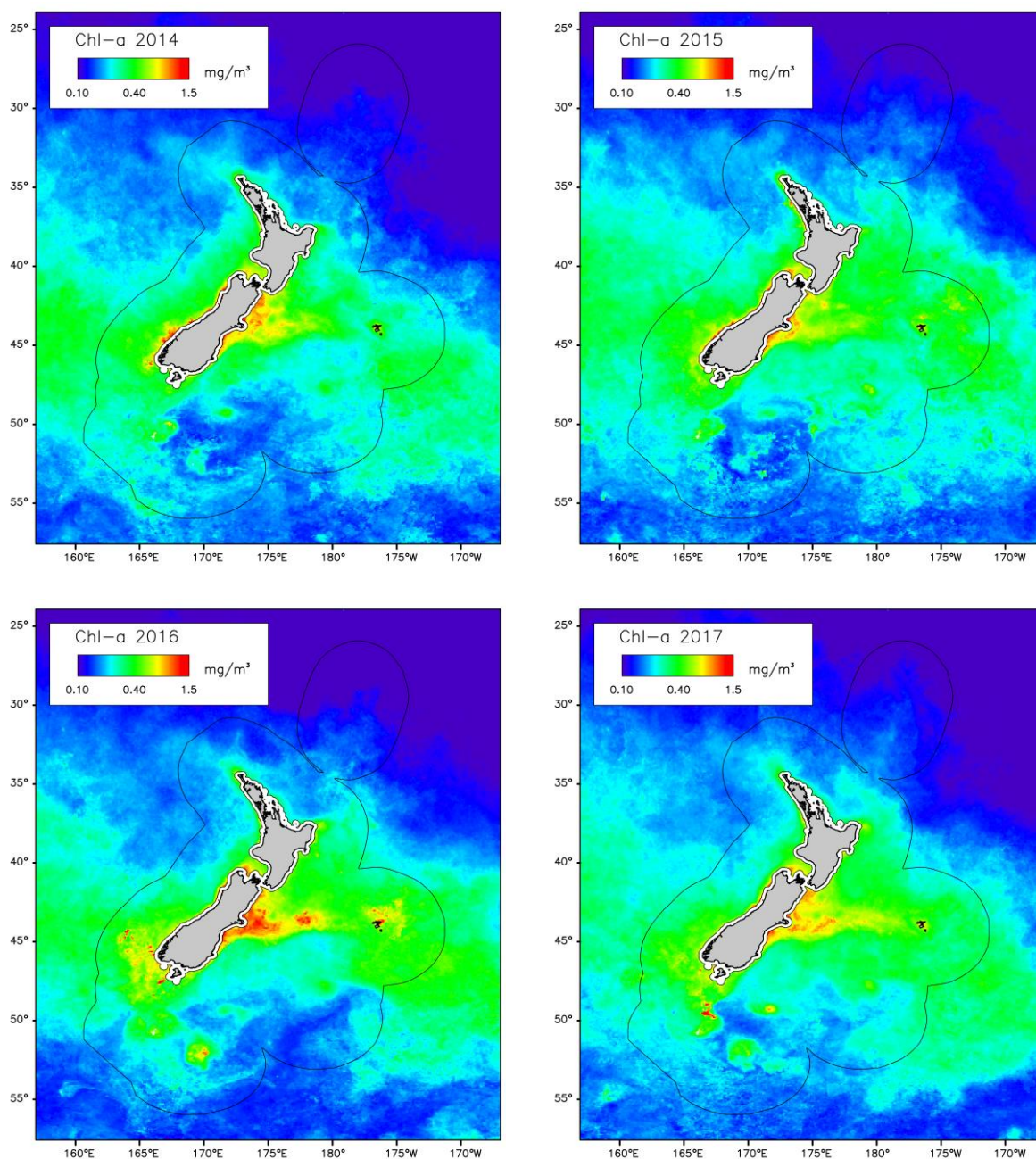


Figure 3-2: Oceanic: Mean annual chl-a by year from the merged dataset of SeaWiFS and MODIS-Aqua. (Continued and concluded)

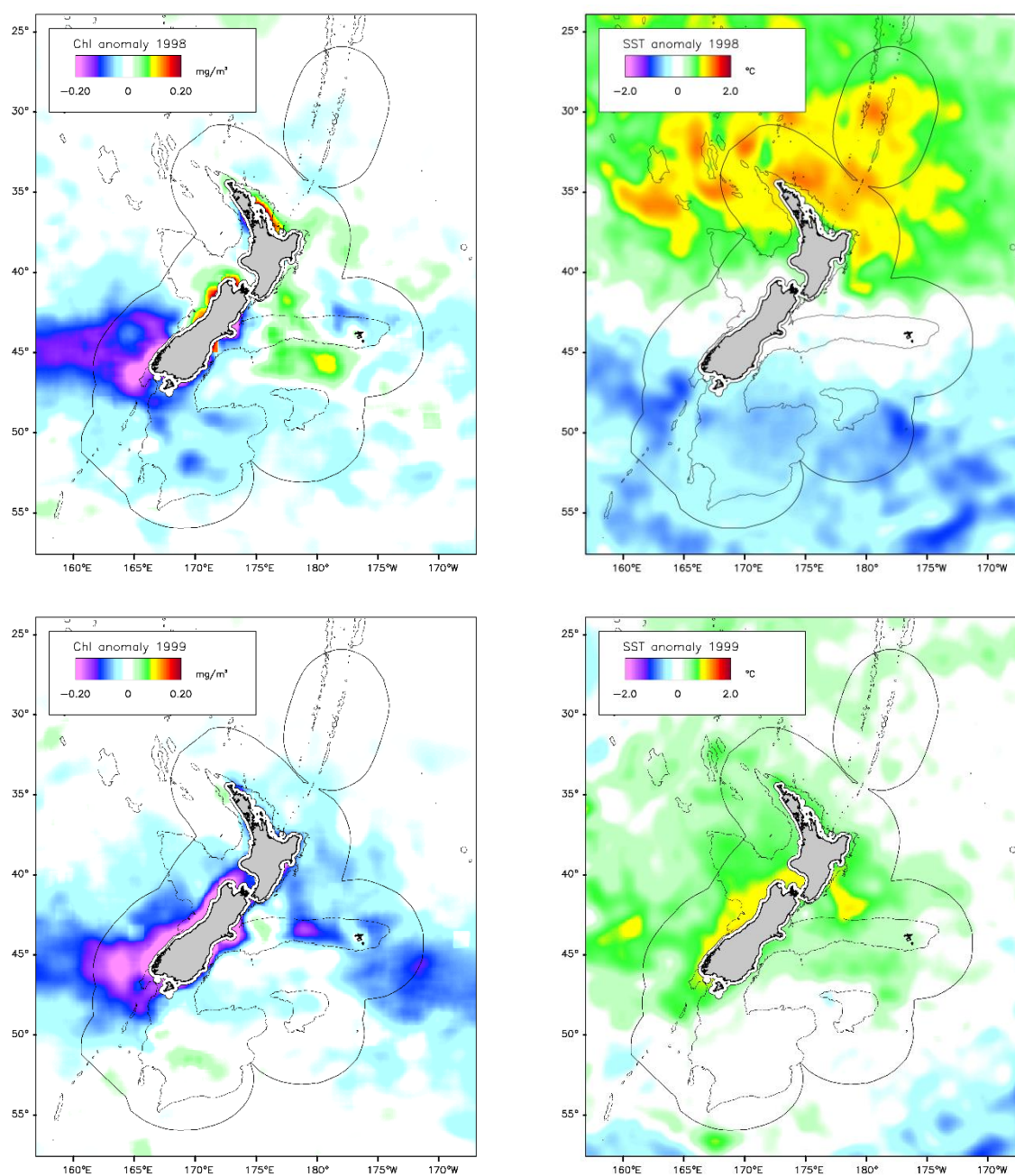


Figure 3-3: Oceanic: Annual mean chl-a and sea-surface temperature (SST) annual anomalies by year. Left: chl-a annual anomalies from the merged dataset of SeaWiFS and MODIS-Aqua (1997–2018), spatially smoothed. Right: SST annual anomalies from AVHRR satellite data (1981–2018). “Annual anomalies” are the annual mean over each pixel minus the long-term mean. The boundary of the New Zealand EEZ is also shown.

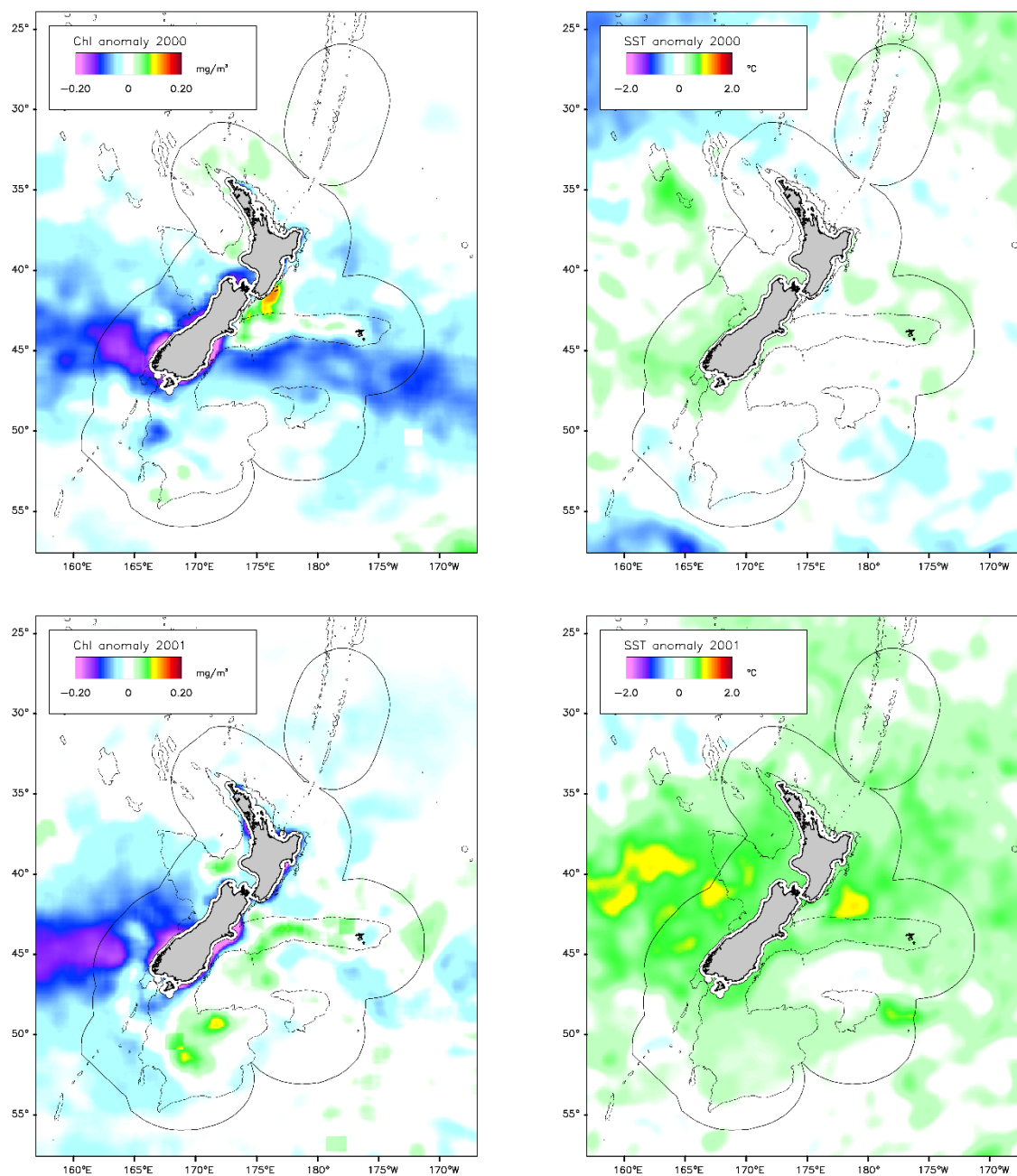


Figure 3-3: Oceanic: Annual mean chl-a and sea-surface temperature (SST) annual anomalies by year. (Continued)

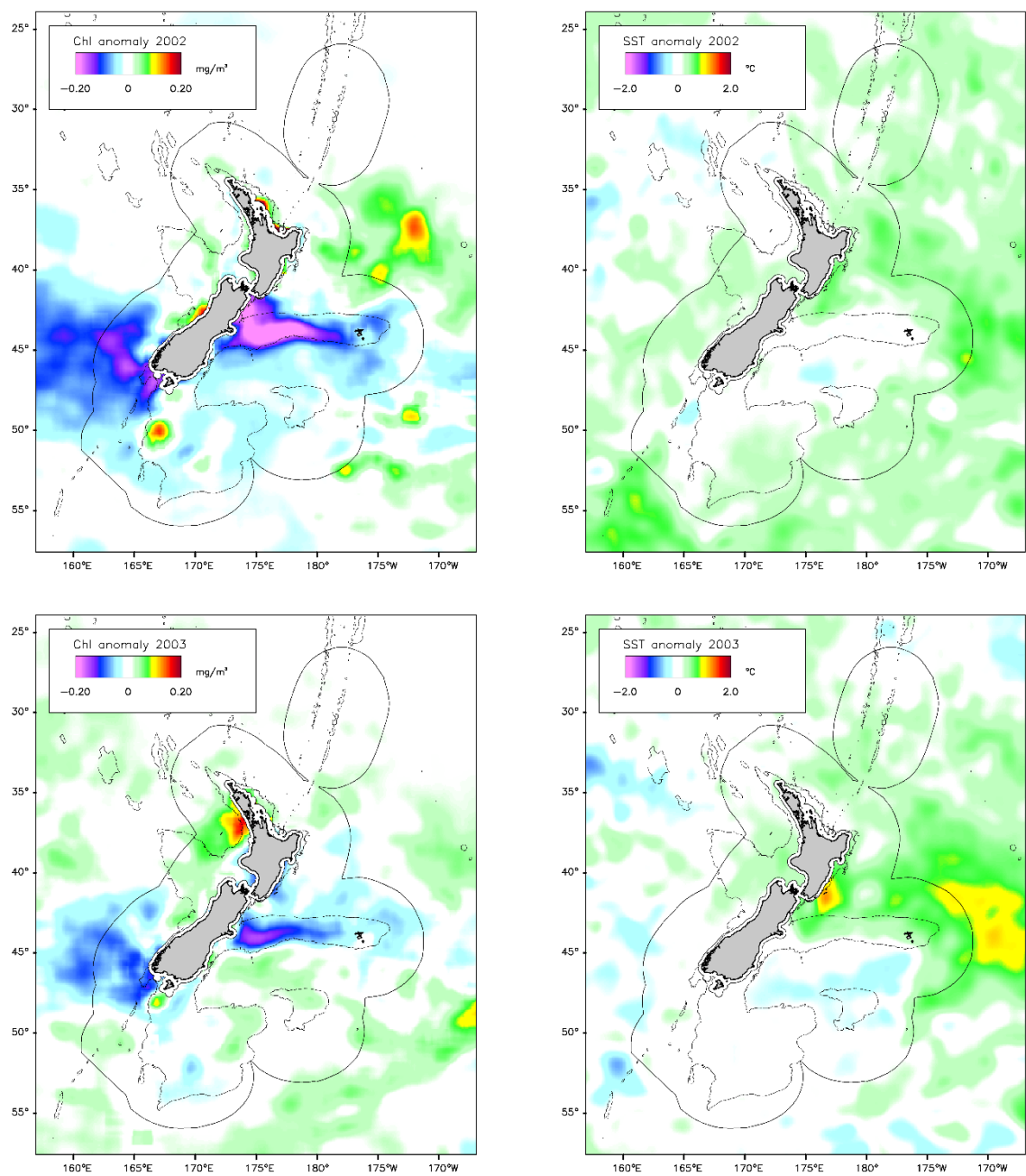


Figure 3-3: Oceanic: Annual mean chl-a and sea-surface temperature (SST) annual anomalies by year. (Continued)

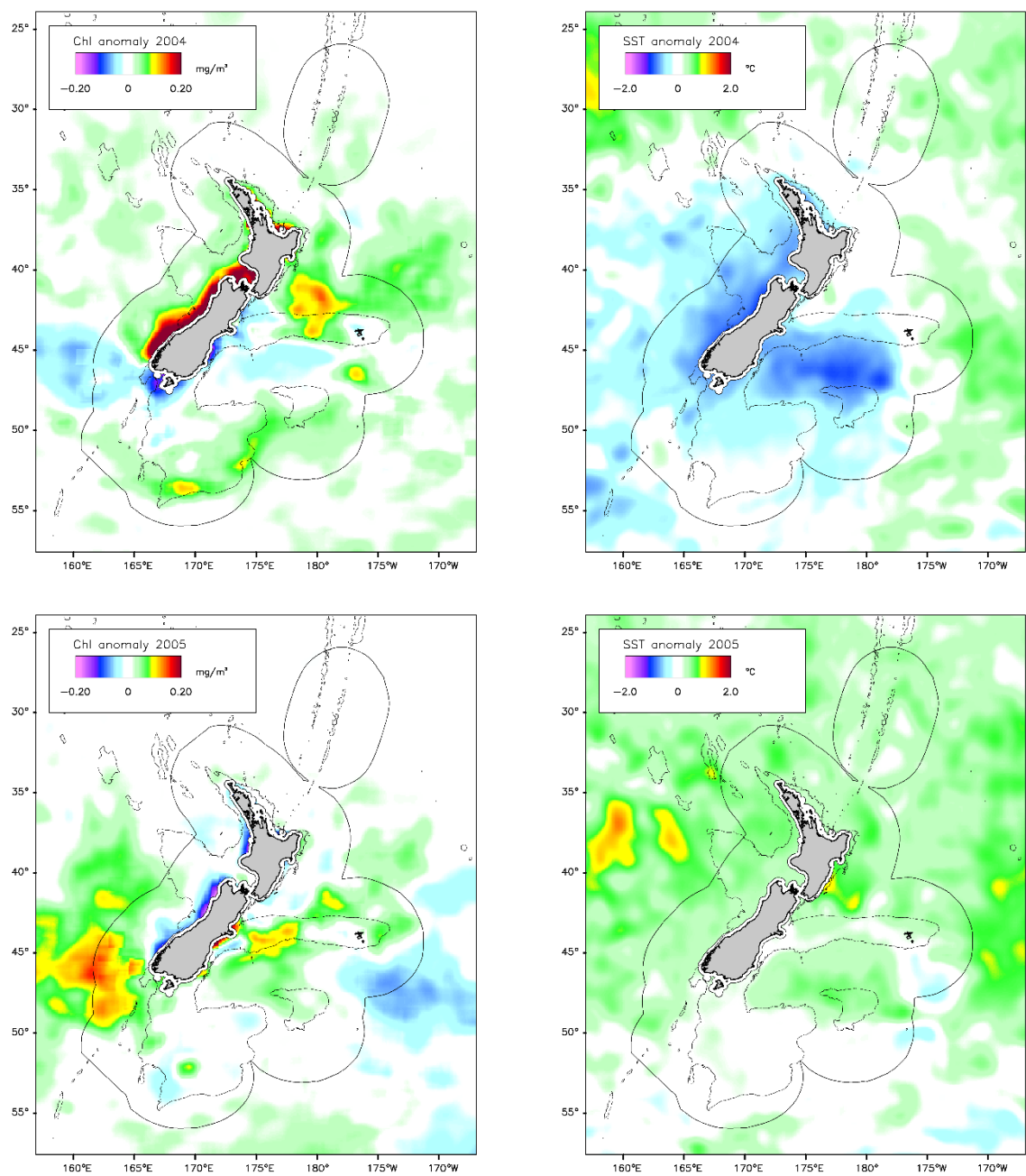


Figure 3-3: Oceanic: Annual mean chl-a and sea-surface temperature (SST) annual anomalies by year. (Continued)

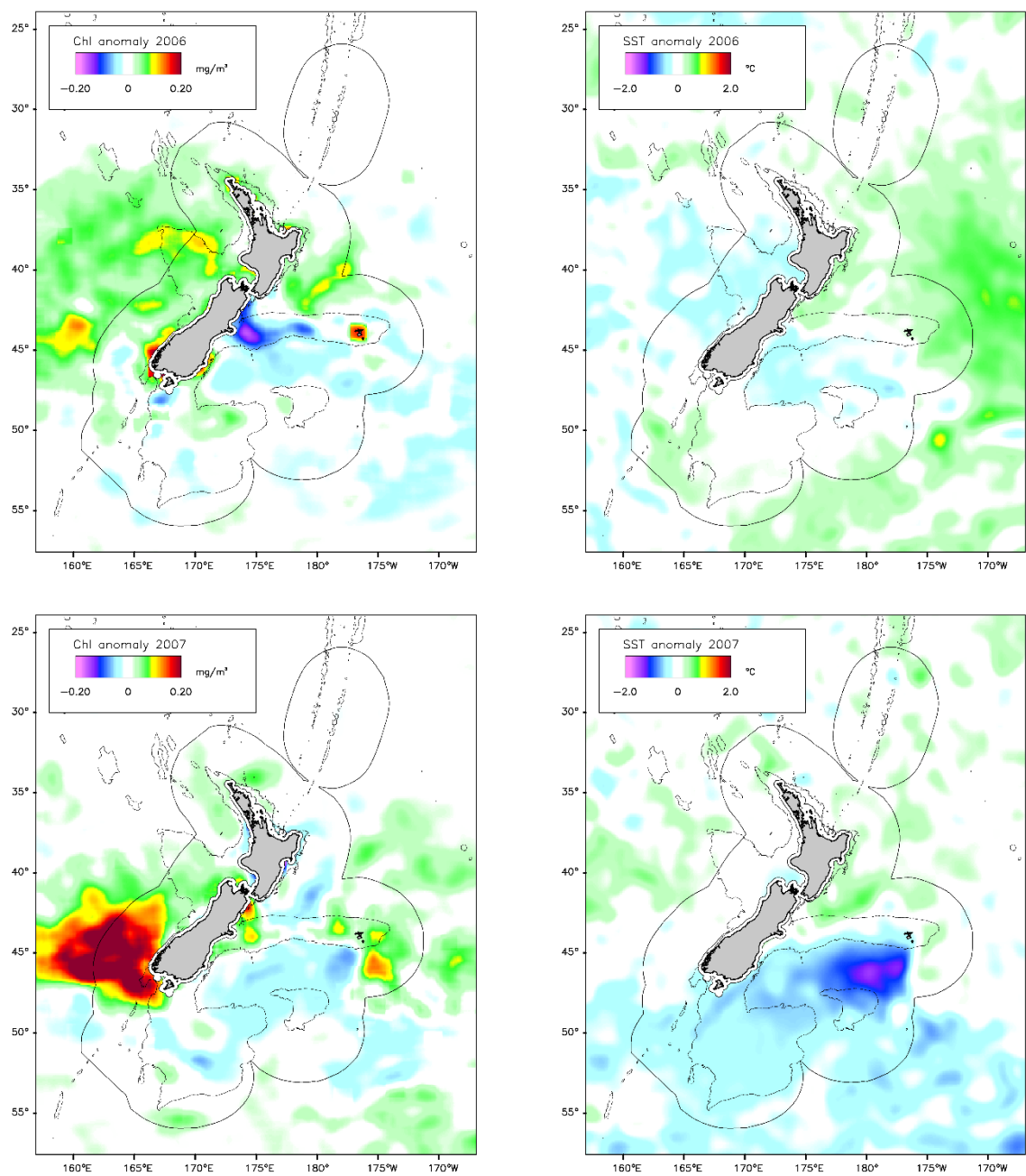


Figure 3-3: Oceanic: Annual mean chl-a and sea-surface temperature (SST) annual anomalies by year. (Continued)

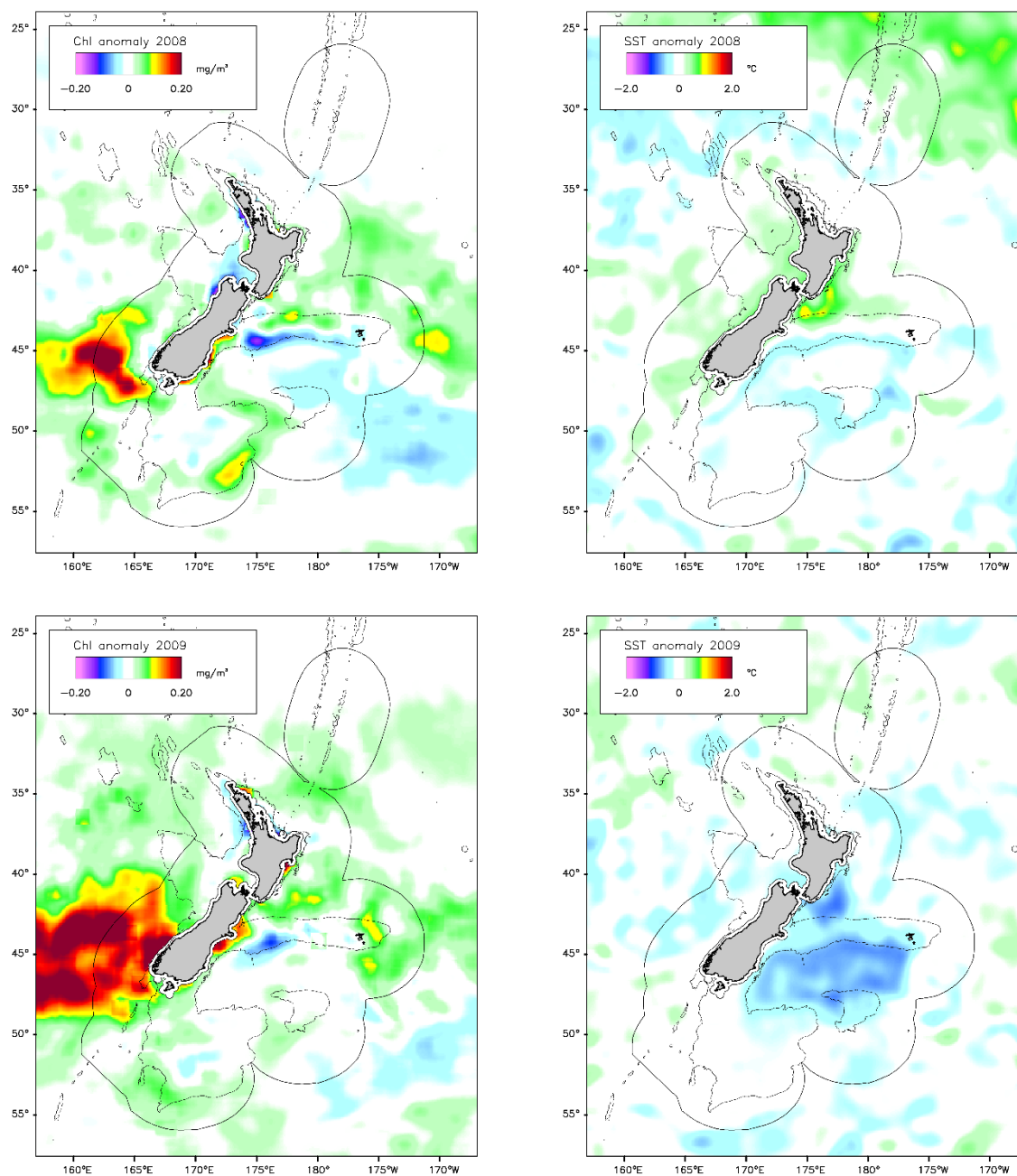


Figure 3-3: Oceanic: Annual mean chl-a and sea-surface temperature (SST) annual anomalies by year. (Continued)

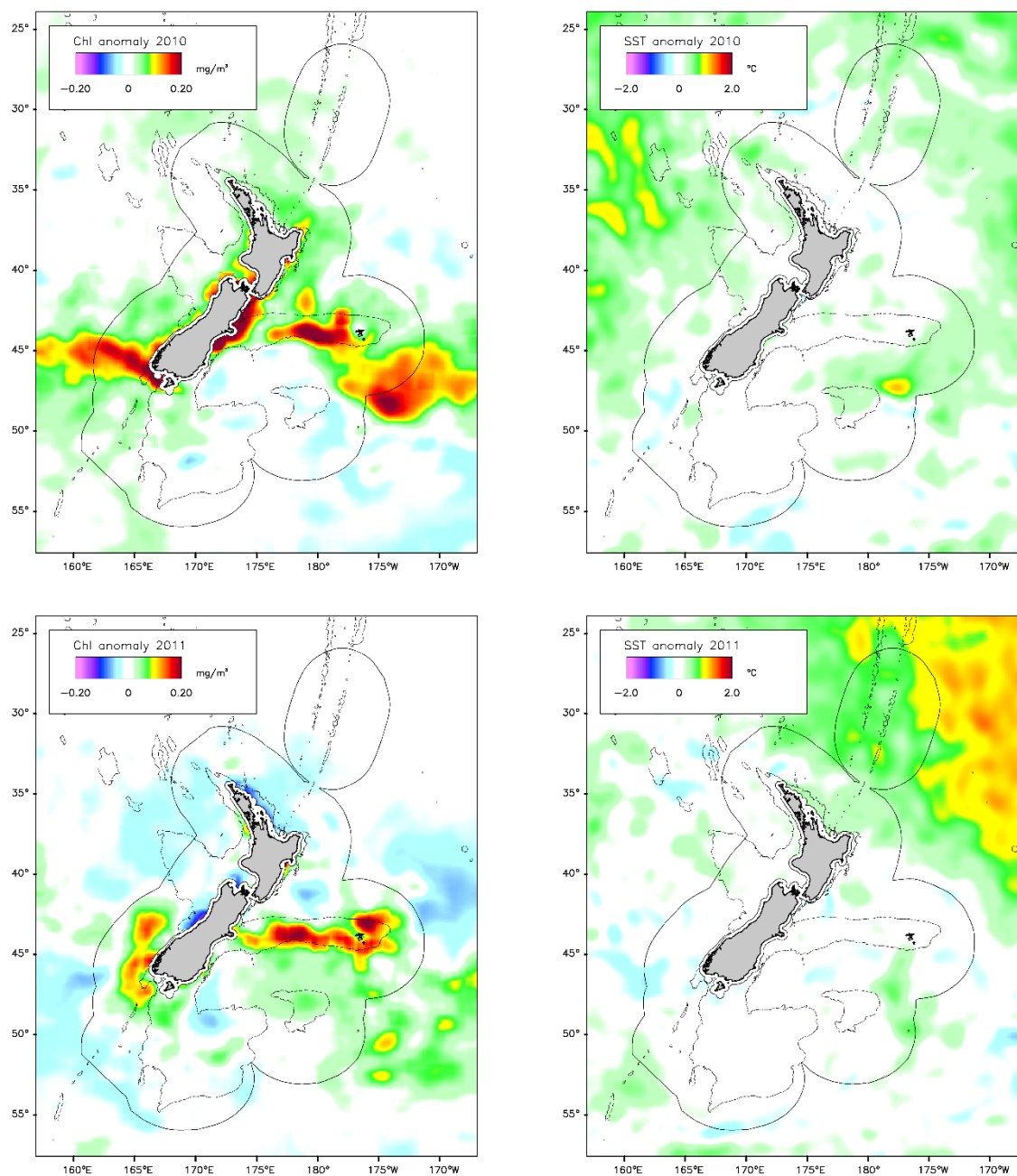


Figure 3-3: Oceanic: Annual mean chl-a and sea-surface temperature (SST) annual anomalies by year. (Continued)

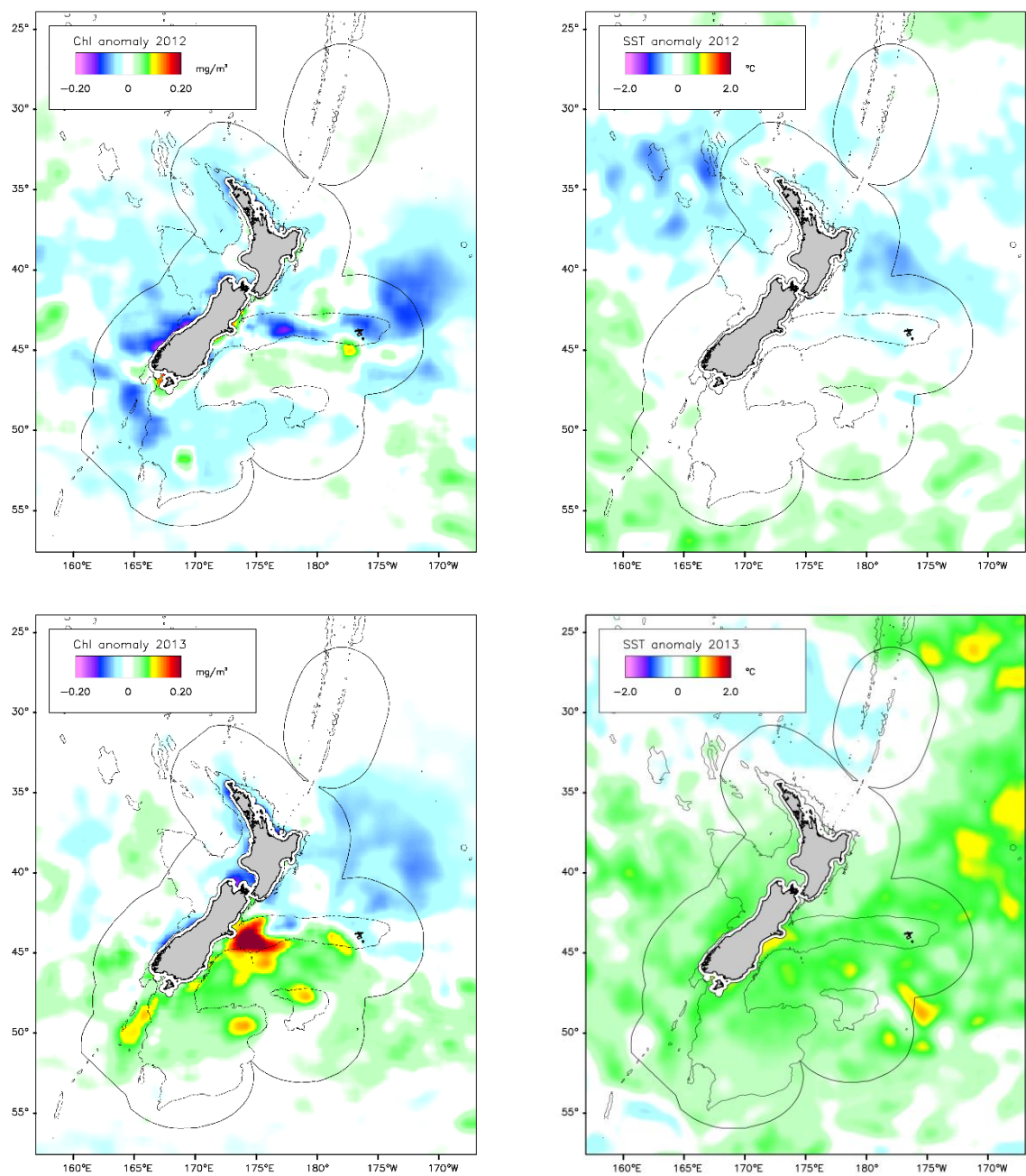


Figure 3-3: Oceanic: Annual mean chl-a and sea-surface temperature (SST) annual anomalies by year. (Continued)

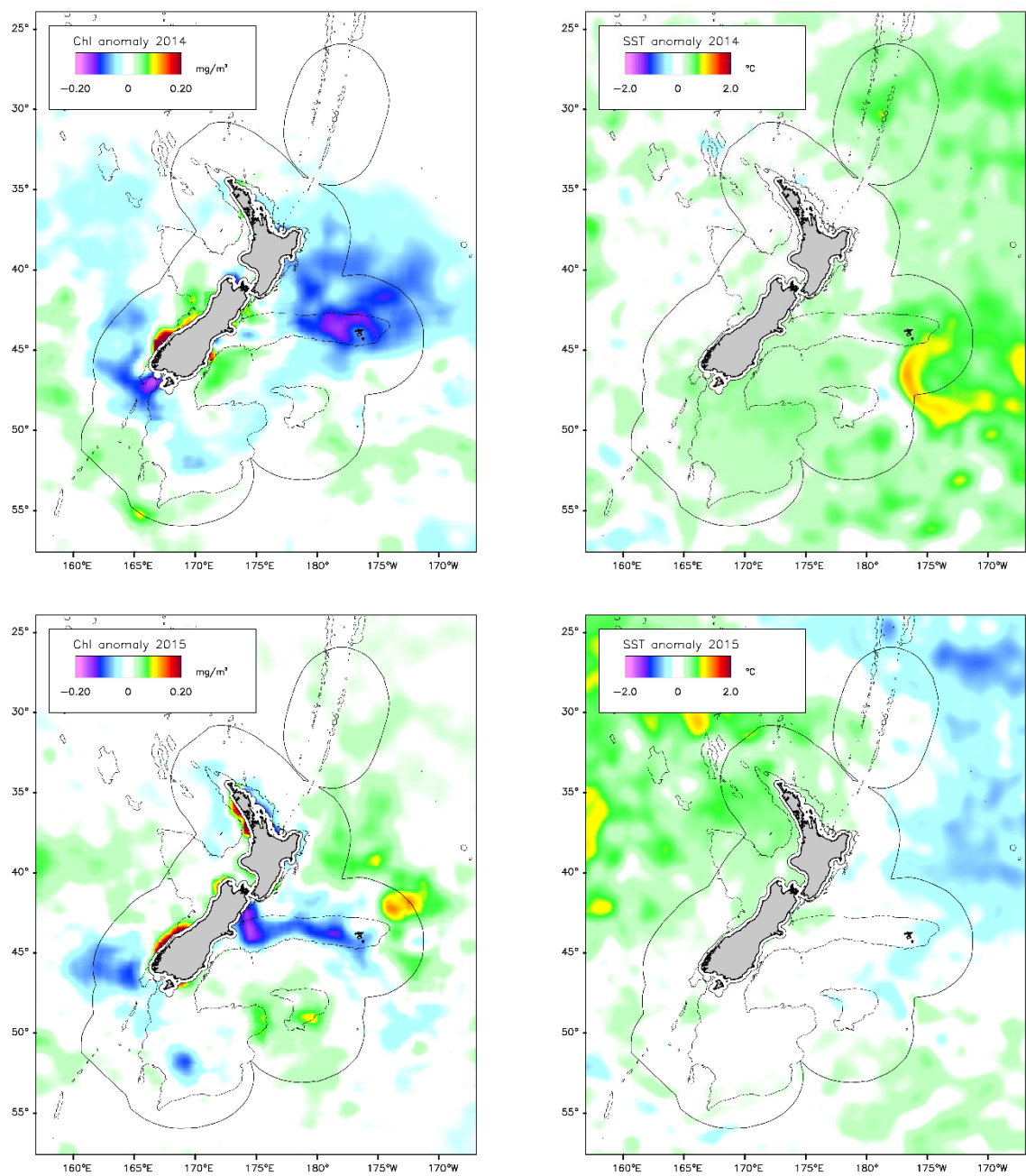


Figure 3-3: Oceanic: Annual mean chl-a and sea-surface temperature (SST) annual anomalies by year. (Continued and concluded)

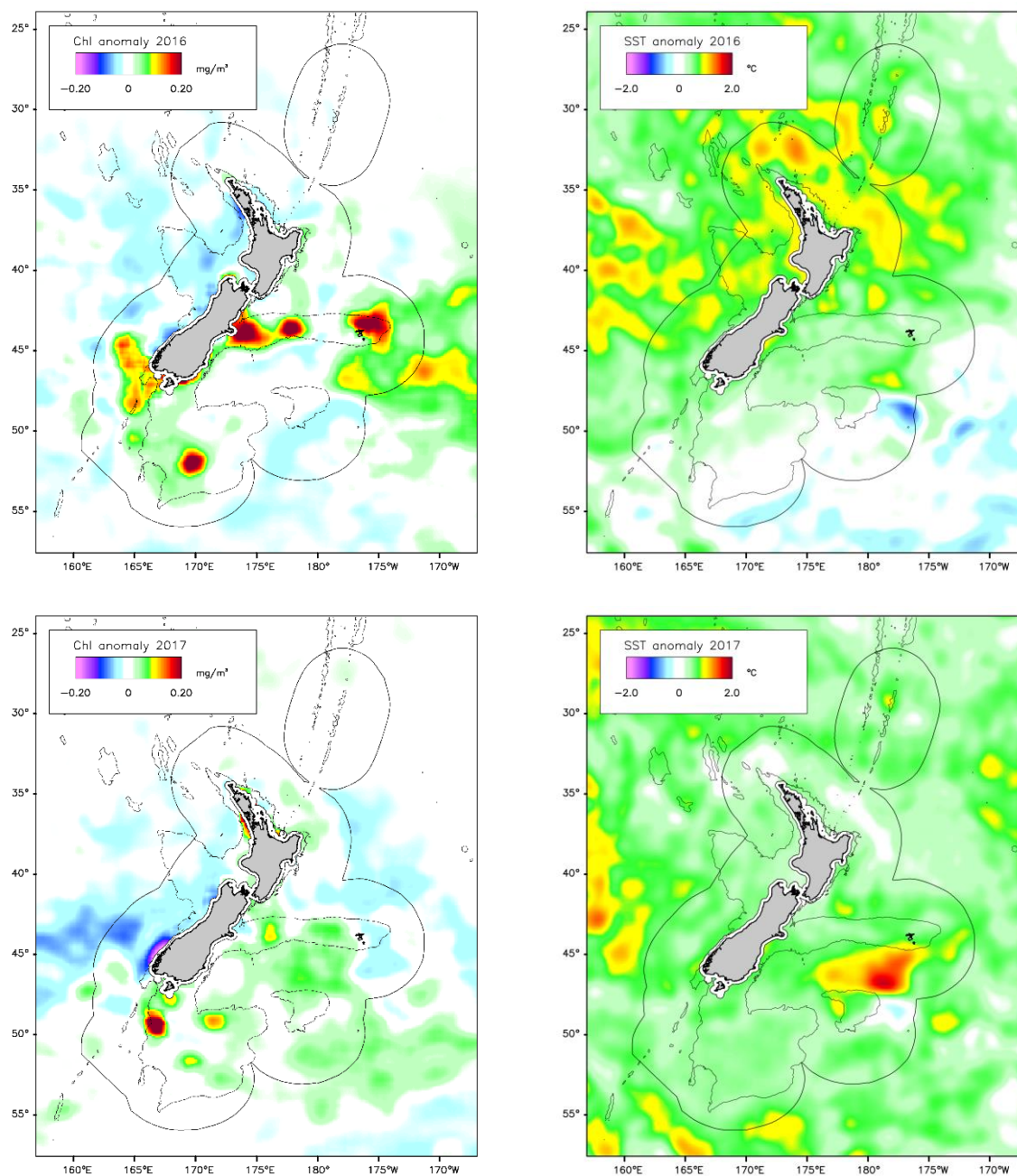


Figure 3-3: Oceanic: Annual mean chl-a and sea-surface temperature (SST) annual anomalies by year. (Continued and concluded)

3.1.3 Oceanic: Monthly time series

Monthly-mean values of chl-a in the EEZ and four oceanic regions are shown in Figure 3-4. Monthly anomalies for chl-a (monthly mean value minus the climatological or long-term monthly mean) are shown in Figure 3-5. Monthly sea-surface temperature (SST) anomalies are shown in Figure 3-6.

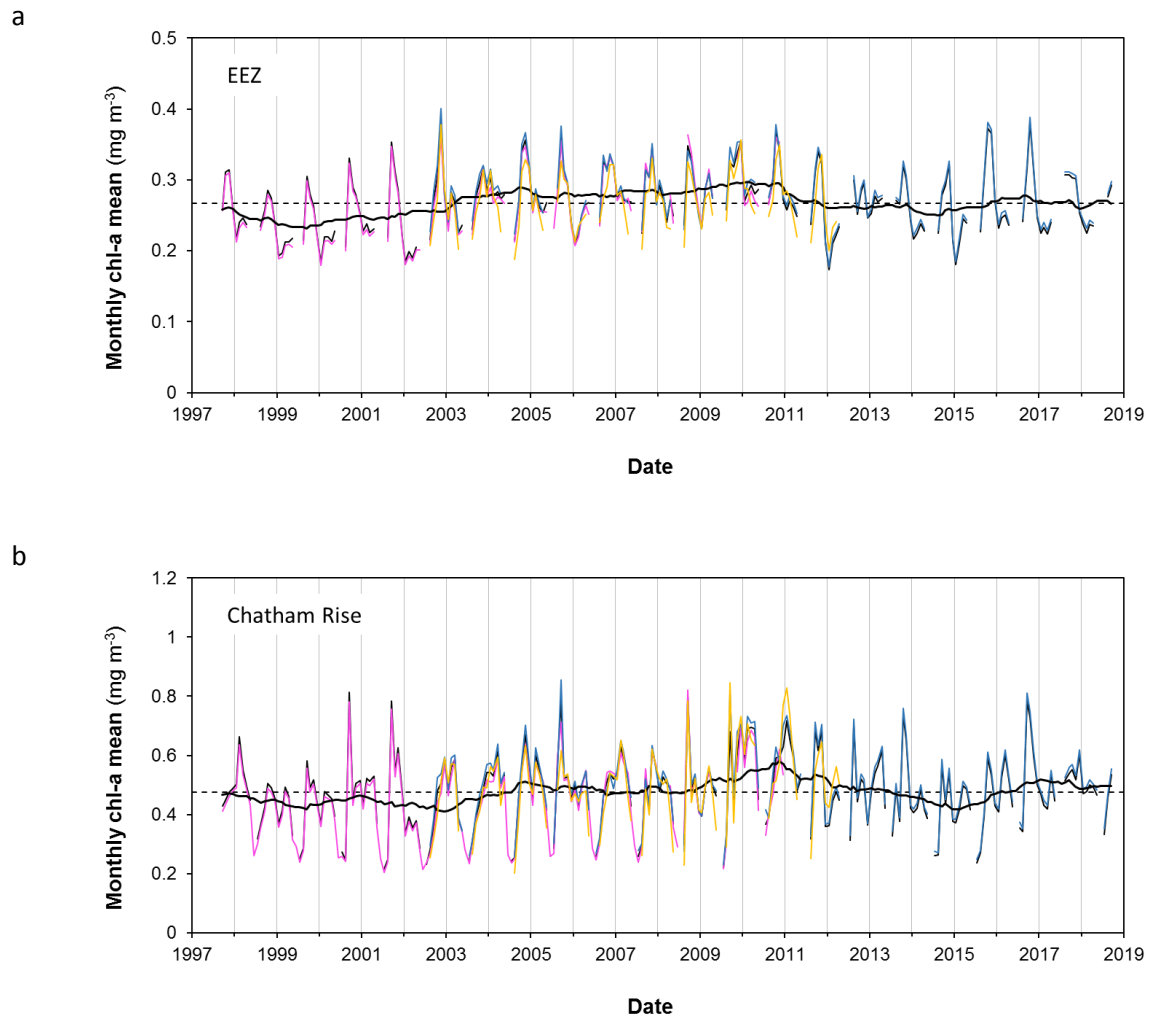
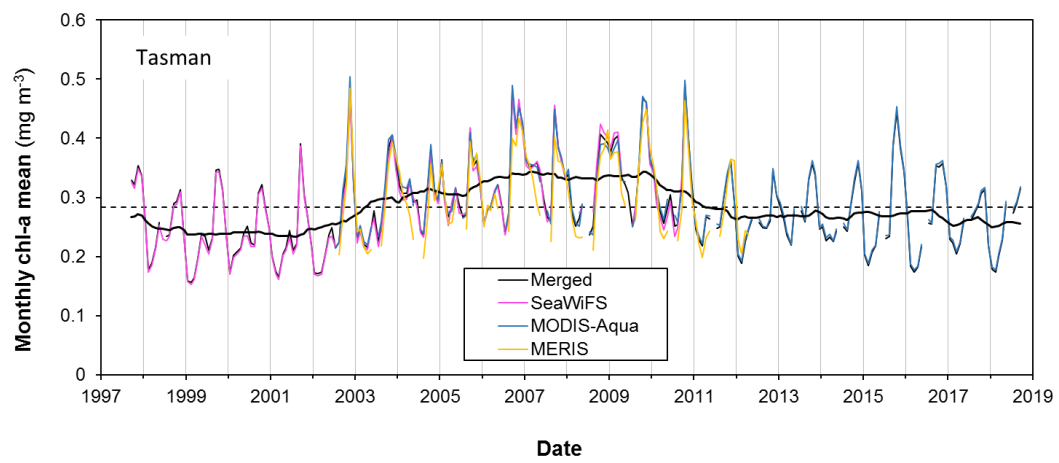
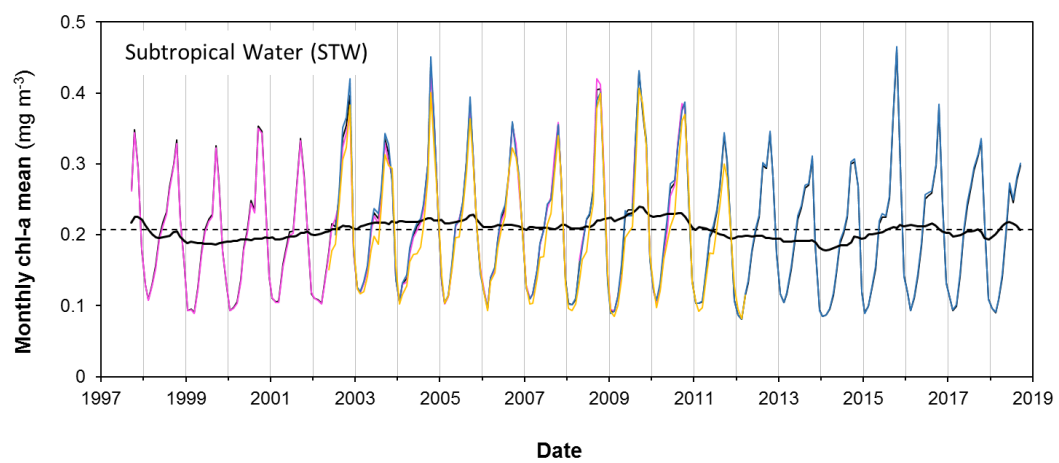


Figure 3-4: Oceanic: Monthly mean chl-a concentrations between 1997 and 2018 for descriptive New Zealand regions. The regions (Figure 2-3) are: **a:** EEZ; **b:** Chatham Rise; **c:** Tasman Sea; **d:** Subtropical Water (STW); **e:** Subantarctic Water (SAW). The monthly data shown are the merged dataset (thin black lines), SeaWiFS (pink), MODIS-Aqua (blue) and MERIS (orange). Monthly data are not shown where there was less than 80% data coverage for a given month in the region. The thick black line is the merged dataset smoothed with a 4-year running mean. The vertical grey lines divide different years. The dashed horizontal lines show the long-term means. Note the panels have different scales on the y-axis.

c



d



e

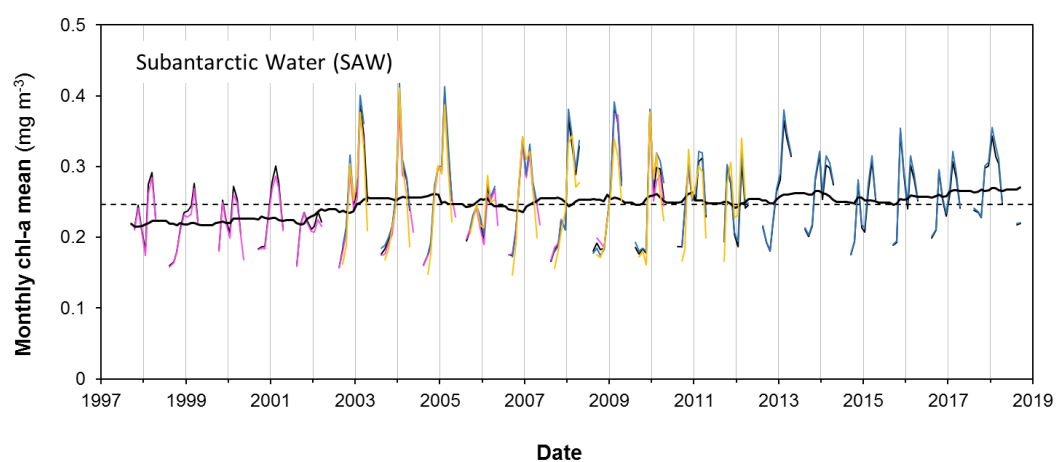


Figure 3-4: Oceanic: Monthly mean chl-a concentrations between 1997 and 2018 for descriptive New Zealand regions. (Continued and concluded)

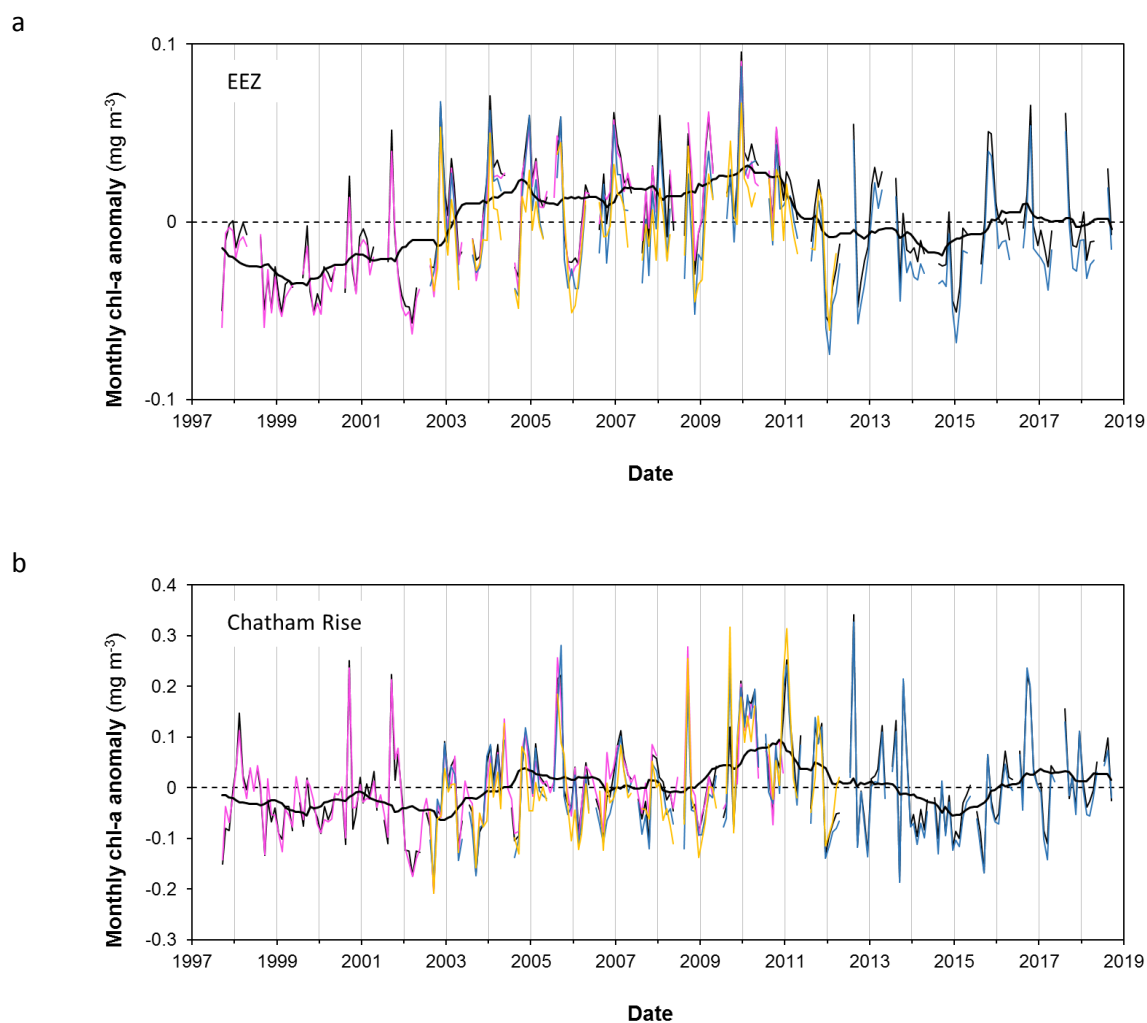


Figure 3-5: Oceanic: Monthly chl-a anomalies between 1997 and 2018 for descriptive New Zealand regions. The regions (Figure 2-3) are: **a:** EEZ; **b:** Chatham Rise; **c:** Tasman Sea; **d:** Subtropical Water (STW); **e:** Subantarctic Water (SAW). The monthly anomalies shown are the merged dataset (thin black lines), SeaWiFS (pink), MODIS-Aqua (blue) and MERIS (orange). Monthly data are not shown where there was less than 80% data coverage for a given month in the region. The thick black line is the merged dataset smoothed with a 4-year running mean. The vertical grey lines divide different years. The dashed horizontal lines show zero anomaly. Note the panels have different scales on the y-axis.

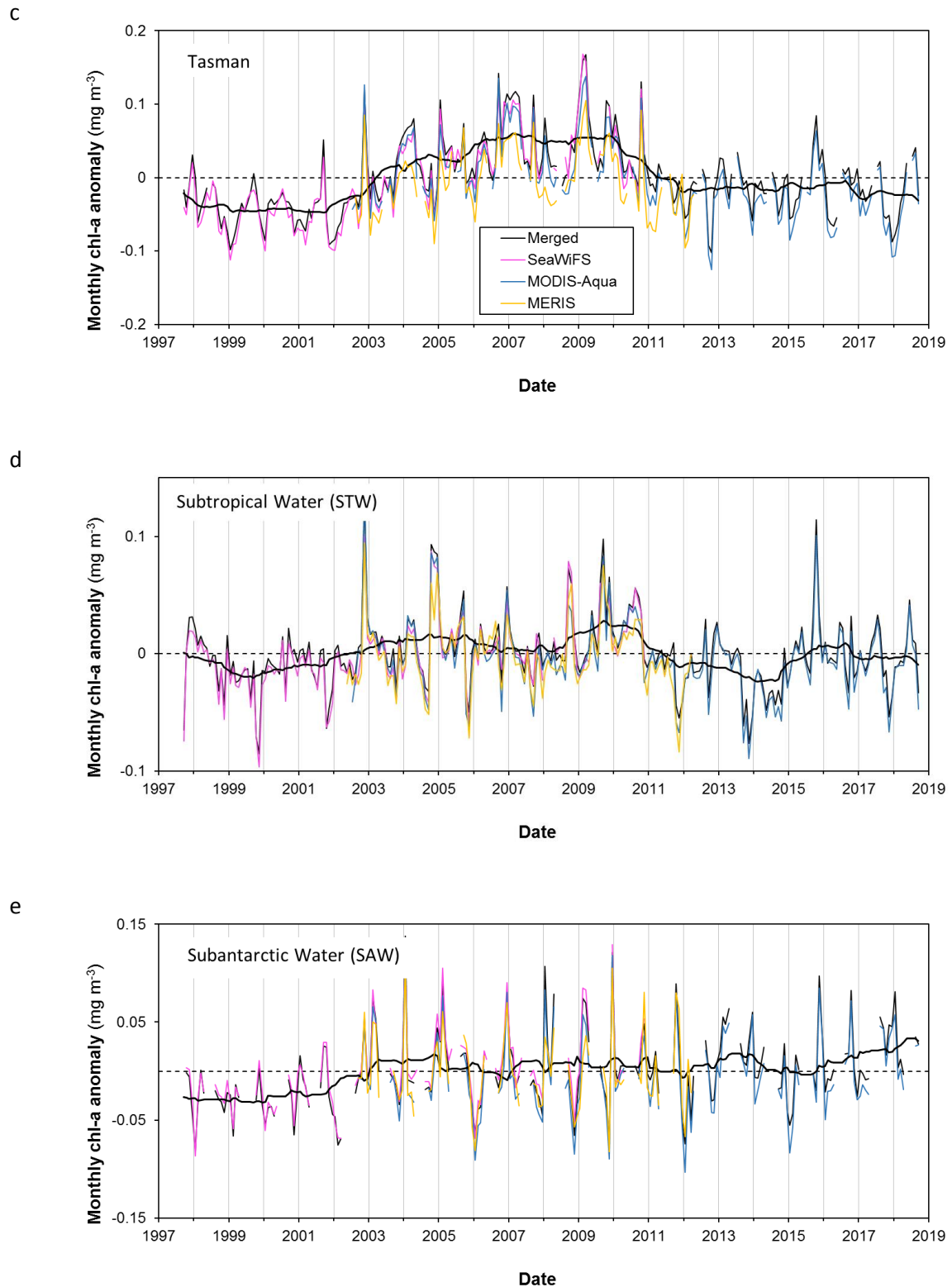


Figure 3-5: Oceanic: Monthly chl-a anomalies between 1997 and 2018 for descriptive New Zealand regions. (Continued and concluded)

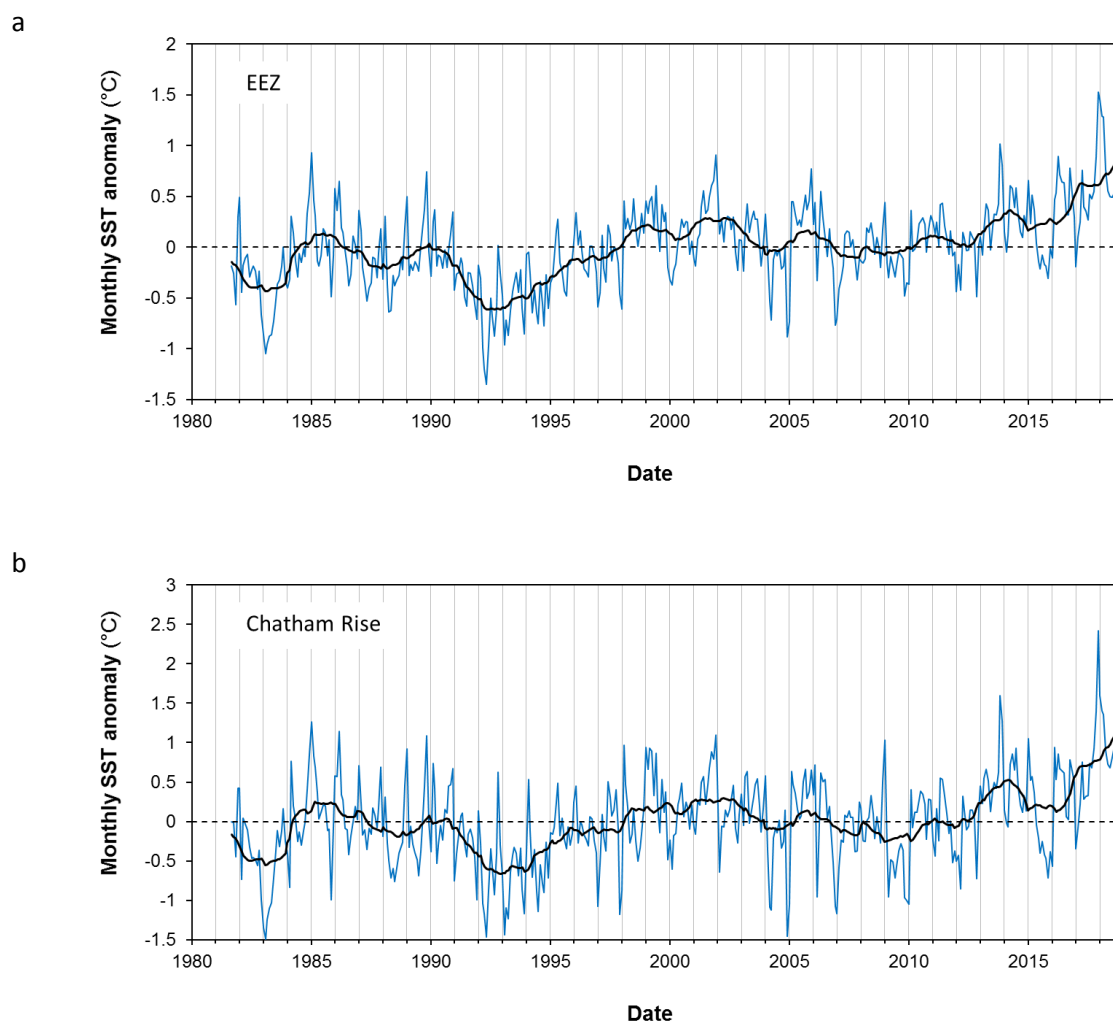
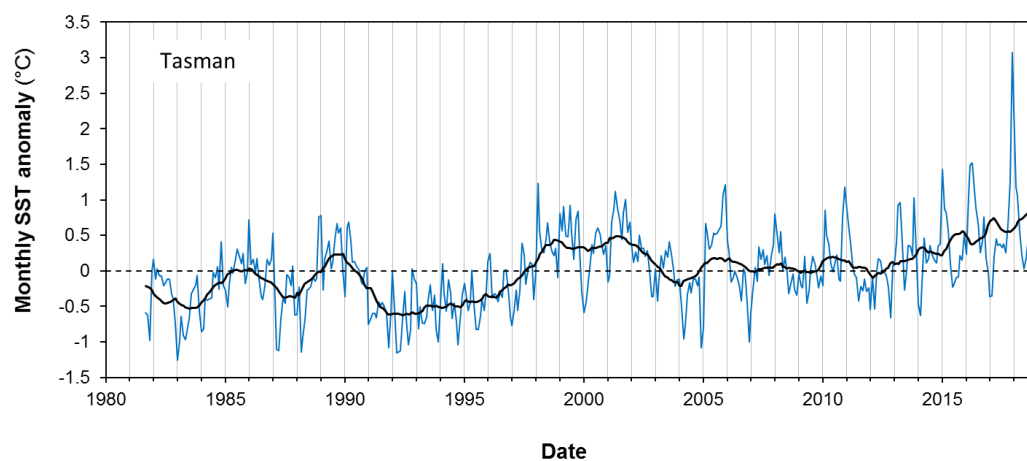
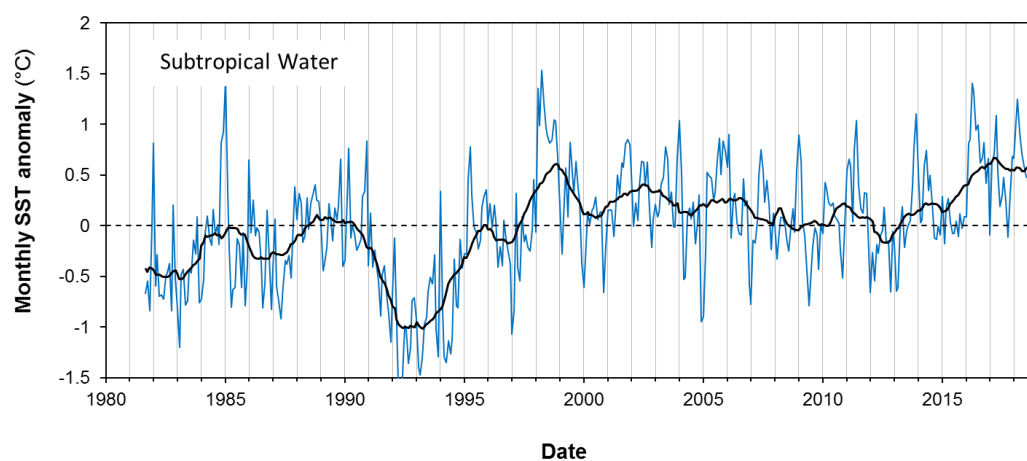


Figure 3-6: Oceanic: Monthly SST anomalies between 1981 and 2018 for descriptive New Zealand regions. The regions (Figure 2-3) are: **a:** EEZ; **b:** Chatham Rise; **c:** Tasman Sea; **d:** Subtropical Water (STW); **e:** Subantarctic Water (SAW). The thick black line is the merged dataset smoothed with a 4-year running mean. The vertical grey lines divide different years. The dashed horizontal lines show zero anomaly. Note the panels have different scales on the y-axis. In comparing with Figure 3-5, note that the x-axes are different (from 1980 here).

c



d



e

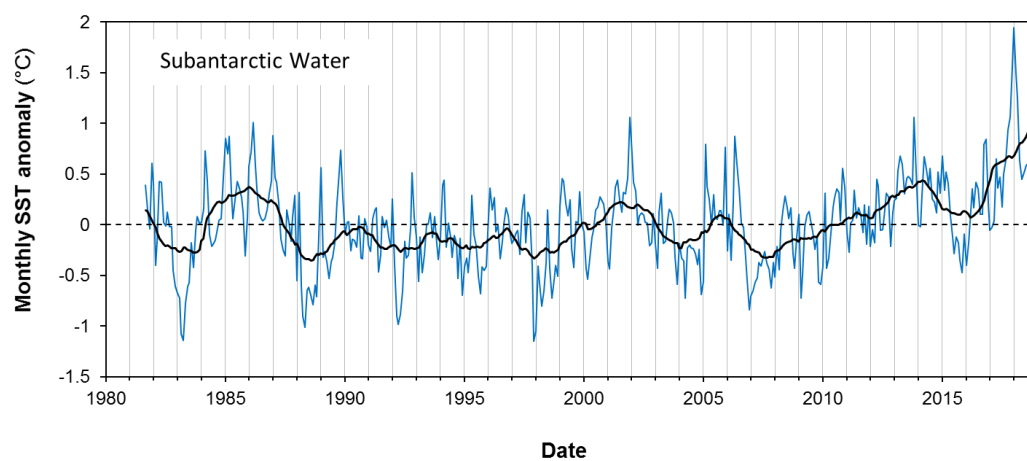


Figure 3-6: Oceanic: Monthly SST anomalies between 1981 and 2018 (Continued and concluded)

3.1.4 Oceanic: Spatial trend analysis

Temporal trends in monthly SST anomalies (Figure 3-7) show that most of the ocean round New Zealand has warmed significantly between 1981 and 2018 (significant positive trends in SST anomalies in most areas). Average warming rates are given as “°C per decade” which is the global standard for reporting such trends in SST. The highest rate of warming in the New Zealand EEZ was 0.38°C per decade (on average between 1981 and 2018). Warming rates were highest in the Subtropical Water and the Tasman Sea and lowest in Subantarctic Water. For the New Zealand EEZ as a whole, the area-weighted mean rate of surface warming was 0.15°C per decade on average between 1981 and 2018. Trends in SST in all descriptive regions were all positive and all significant (Table 3-1). See Section 4.3 for a comparison of these warming rates with the global average.

Some ocean areas around New Zealand have experienced significant positive trends in chl-a (likely indicative of increased ocean productivity), especially the Subtropical Front southwest and southeast of New Zealand and over Chatham Rise (Figure 3-8). The rates of increase in chl-a were up to 2% per year in these areas on average. Significant negative trends in chl-a anomalies (likely indicative of decreasing ocean productivity) were found in two areas: (1) Subtropical Water to the east of New Zealand (outside the EEZ); and (2) around Northland and the northeast New Zealand continental slope (continental slope offshore of the Hauraki Gulf, eastern Coromandel and Bay of Plenty). The average magnitude of rates of decrease in chl-a in these areas were 1–2% per year. These trends in chl-a were not generally sufficient to give significant trends at the larger spatial scales of the descriptive regions of EEZ (Table 3-1).

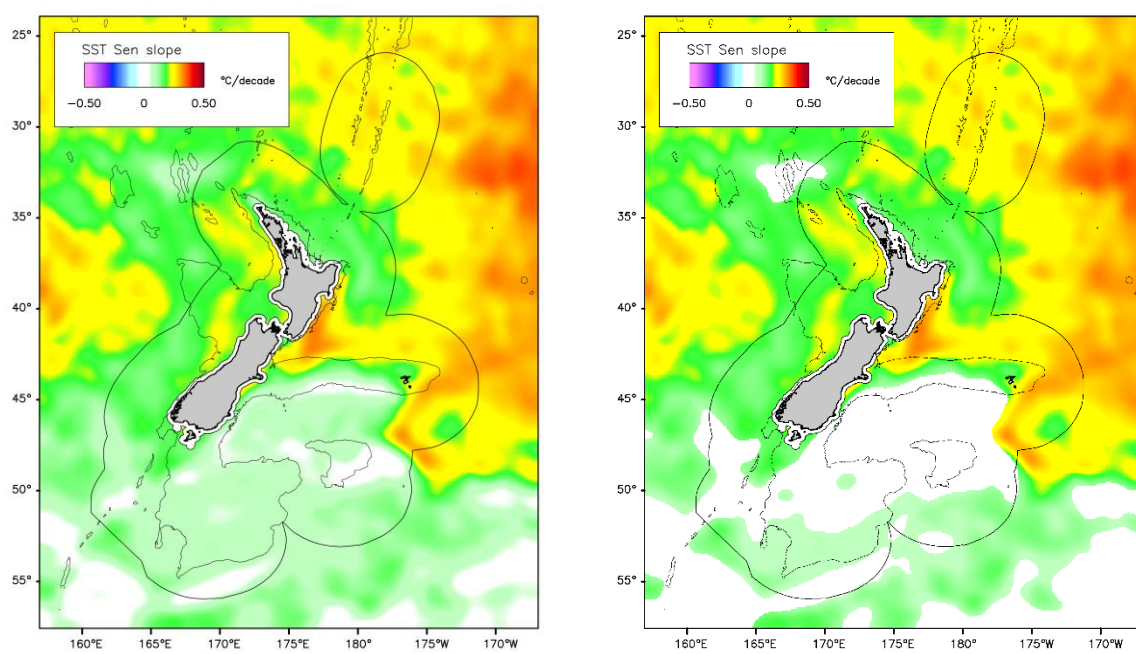


Figure 3-7: Oceanic: Spatial trends in monthly anomalies of SST from AVHRR (1981-2018). Sen-slope trends in sea-surface temperature (SST) are shown as °C per decade. **Left:** All trends. **Right:** Significant trends only (95% confidence level; Mann-Kendall analysis corrected for auto-correlation), with non-significant trends shown white. No data or no analysis is shown grey in both panels. SST data were from the AVHRR satellite data (1981-2018).

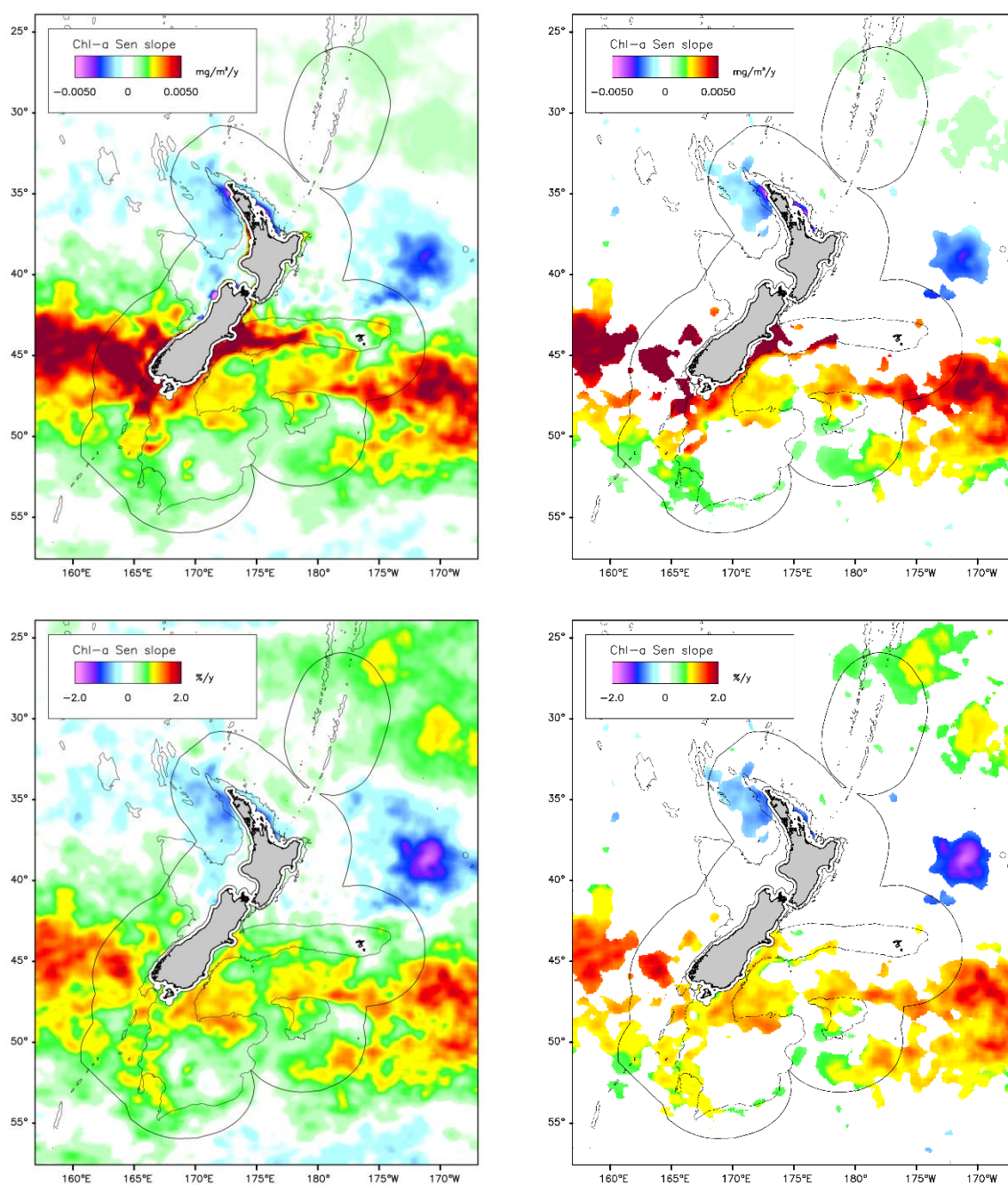


Figure 3-8: Oceanic: Spatial trends in monthly anomalies of surface chl-a (1997-2018). **Top:** Sen-slope trends in absolute chl-a values per year (mgChl-a m^{-3} per year). **Bottom:** Sen-slope trends as a proportion of the median value (bottom, % per year). **Left panels:** All trends. **Right panels:** Significant trends only (95% confidence level; Mann-Kendall analysis corrected for auto-correlation), with non-significant trends shown white. No data or no analysis is shown grey in both panels. Data from the merged SeaWiFS-MODIS-Aqua dataset (1997-2018).

Table 3-1: Trend analysis for oceanic chl-a and sea surface temperature (SST). The Mann Kendall test is applied to monthly anomalies in the EEZ and descriptive region. The periods of analysis are different for the two variables: SST (1981–2018); chl-a (1997–2018). See text for more details. ¹ Note that the “Sen slope/median” test is not applied for SST because the scale offset is arbitrary. Significance is shown: *** p<0.001; ** p<0.01; * p<0.05

Descriptive region	Z	p	Sen slope	Median	Slope/median	Significance
Sea surface temperature						
(1981–2018)			°C decade ⁻¹	°C	%	
EEZ	3.92	9E-05	0.15	12.8	Not applied ¹	***
Chatham	2.96	3E-03	0.15	12.4	Not applied ¹	**
Tasman	3.49	5E-04	0.19	15.4	Not applied ¹	***
Subtropical Water	3.61	3E-04	0.20	18.0	Not applied ¹	***
Subantarctic Water	1.96	0.05	0.09	8.9	Not applied ¹	*
Chlorophyll-a concentration						
(1997–2018)			mg m ⁻³ y ⁻¹	mg m ⁻³	%	
EEZ	-0.46	0.65	-0.00020	0.23	-0.09	
Chatham	0.51	0.61	0.00080	0.41	0.20	
Tasman	-2.42	0.02	-0.00210	0.24	-0.87	*
Subtropical Water	-1.61	0.11	-0.00067	0.17	-0.40	
Subantarctic Water	1.57	0.12	0.00095	0.23	0.42	

3.1.5 Oceanic: Spatial correlation analysis

Correlation analysis between chl-a and SST anomalies can help understand the underlying drivers of these oceanographic properties (Feng & Zhu, 2012; Kumar et al., 2016). In the New Zealand region, correlations between monthly anomalies of chl-a and SST for each pixel between 1997 and 2018 (Figure 3-9) were found to be negative in Subtropical Water and the Tasman Sea, and positive in Subantarctic Water. In Subtropical Water and the Tasman Sea, this means that when the surface water is warmer than normal, surface chl-a (and likely ocean productivity) tends to be lower than normal. In Subantarctic Water the reverse is true: when the surface water is warmer than normal, ocean productivity tends to be increased. These relationships follow expectations based on the oceanographic factors affecting primary productivity round New Zealand (see Section 4.3.2).

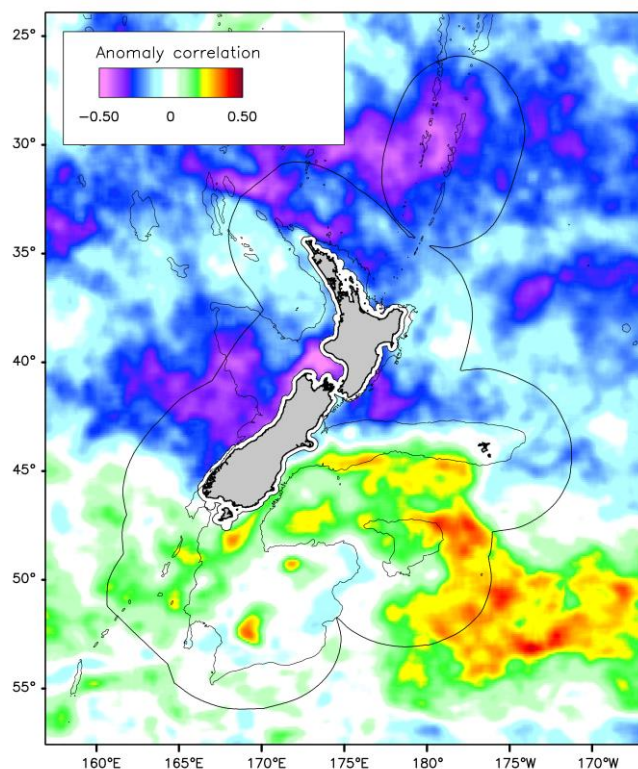


Figure 3-9: Oceanic: the linear Pearson correlation coefficient between monthly anomalies of chl-a and SST (1997–2018). The period of analysis is between 1997 and 2018, and the data are smoothed.

3.1.6 Ocean SST comparison with previous work

Although the satellite sensors used in this study are the same as those used in previous “State of the Environment” reporting in New Zealand (MfE & Statistics NZ 2015; 2016), the processing and spatial resolution are different. The AVHRR satellite SST data used in previous reporting (MfE & Statistics NZ 2015; 2016) was from the dataset received and processed locally at NIWA following the methodology of Uddstrom & Oien (1999). Differences from the OISST product include cloud detection and clearing approaches, spatial resolution compositing, temperature-estimation algorithms and temporal aggregation. We also note that the oceanic descriptive regions ‘Subtropical Water’ and ‘Subantarctic Water’ for SST in previous reporting (MfE & Statistics NZ 2015; 2016) differ from those used for chl-a (Pinkerton, 2015; 2016; 2018). Using data remapped onto three consistent oceanic regions, a comparison was made between the two versions of the SST data (Figure 3-10). This comparison shows broad agreement but significant differences. The overall agreement in SST anomalies between the two datasets over the three descriptive regions was $R^2=0.61$. Individually, the values were $R^2=0.85$ (Tasman), $R^2=0.76$ (Subtropical), and $R^2=0.41$ (Subantarctic). Particularly notable was the difference between the mean Subantarctic SST: 10.0°C (MfE & Statistics NZ 2016) versus 9.3°C (OISST, this study). The difference is likely to be a result of the processing methodology (including cloud clearing) and the optimum interpolation analysis method (OISST) compared to averaging (Uddstrom & Oien, 1999). It is not known which product should be preferred for state of the

Environment reporting and we recommend that further intercomparison of the products be carried out in the future, including potentially, comparison with in situ measurements across the New Zealand coastal and ocean domains.

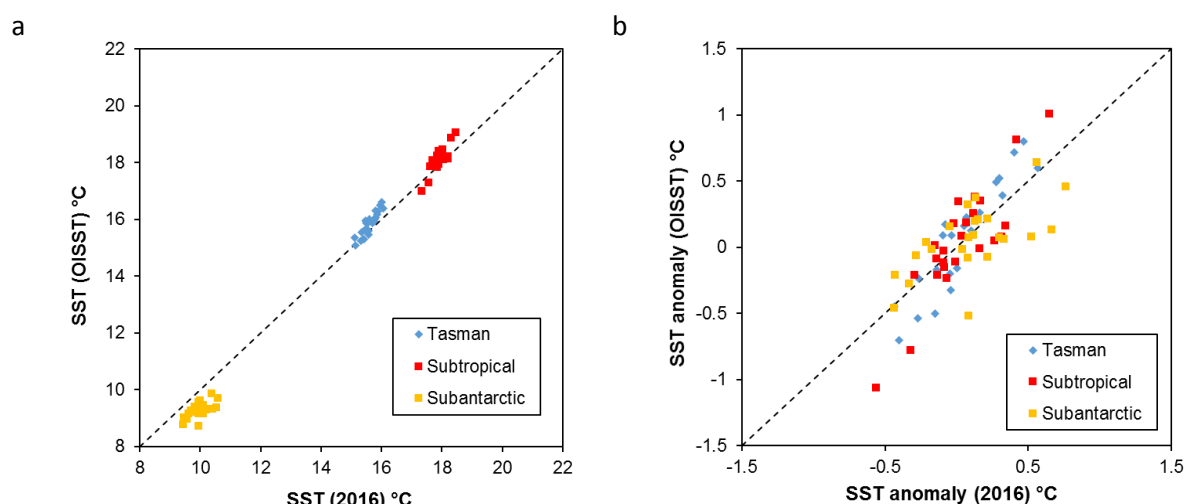


Figure 3-10: Comparison between OISST (Optimum Interpolation Sea Surface Temperature, SST) at 1/4° resolution with the results from NIWA 1 km SST product (Uddstrom & Oien, 1999) as used in 2016 State of the Environment reporting. a: Annual mean SST; b: Annual SST anomalies (relative to mean SST 1993-2012) for three (consistent) oceanic descriptive regions, 1993-2016.

3.2 Coastal analyses

3.2.1 Long-term mean chl-a and SST

The long-term average chl-a and SST for the New Zealand coastal region are shown in Figure 3-11. Water temperature around the coast is primarily related to latitude and water currents. For example, the Southland Current pushes cold water round the bottom of South Island and northwards past Dunedin; warm water from the East Auckland Current can be seen to affect the Bay of Plenty. Coastal productivity (and coastal chl-a concentrations) depend on the combination of oceanic conditions (cross-shelf intrusions) and local coastal effects including upwelling and the effects of land run-off (Pinkerton et al., 2005, 2006).

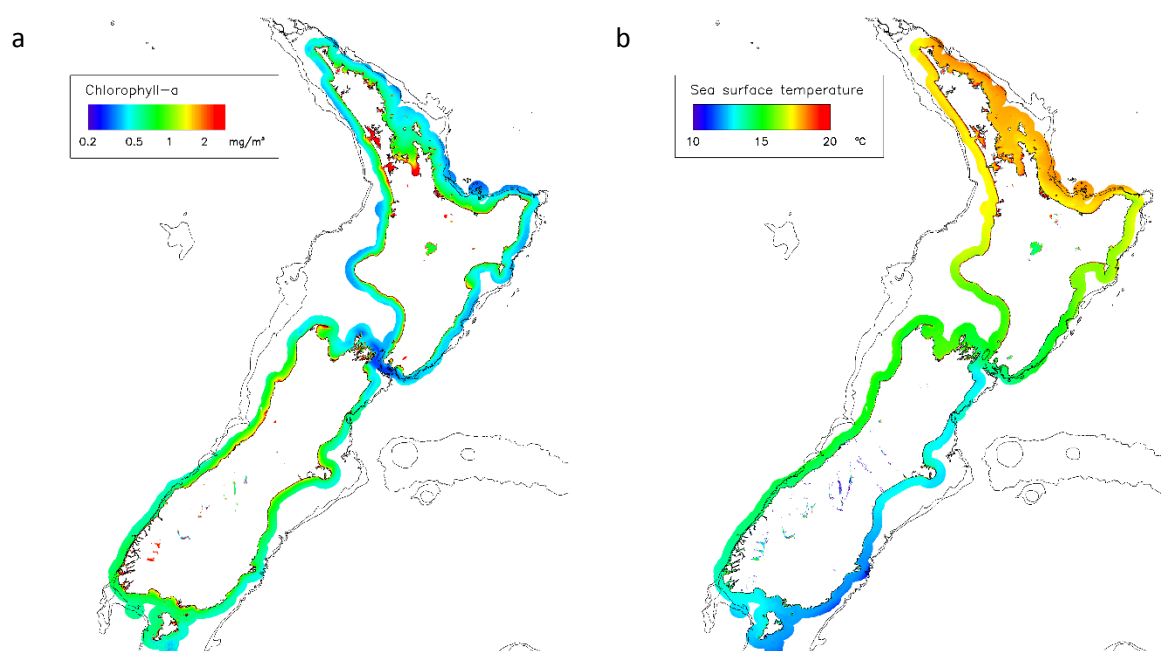


Figure 3-11: Coastal: Long-term mean a: chl-a and b: sea-surface temperature for the New Zealand territorial seas. The 250 m and 500 m depth contours are also shown.

3.2.2 Coastal SST: Monthly time series and trend analyses

Time-series of the monthly anomalies for the descriptive regions (figure 2.4) are shown in Figure 3-12, and trend analyses are shown in Table 3-2. We found significant positive trends in SST (warming) at better than 5% confidence level in all coastal regions between 1981 and 2018, with magnitudes between 0.12 and 0.28°C per decade (mean 0.20°C per decade). Many of the coastal regions show similar patterns: a period of cooling between 1990–1994 was followed by rapid temperature rise 1994–2000, and then evidence of gradual warming 2010–2018.

Table 3-2: Coastal region trend analysis for sea surface temperature (SST). The Mann Kendall test with correction for autocorrelation was applied to monthly anomalies in the coastal regions. The period of analysis is 1981–2018. Note that the “Sen slope/median” test is not applied for SST because the temperature scale offset is arbitrary. Significance is shown: *** p<0.001; ** p<0.01; * p<0.05

Area	Z	p	Sen slope (°C/decade)	Median (°C)	Significance
Northland	2.16	3E-02	0.13	17.4	*
Auckland_east	2.37	2E-02	0.14	17.4	*
Auckland_west	3.69	2E-04	0.23	16.9	***
Waikato_east	2.66	8E-03	0.16	17.4	**
Waikato_west	3.18	1E-03	0.21	16.6	**
Bay_of_Plenty	2.04	4E-02	0.12	17.2	*
Gisborne	3.50	5E-04	0.23	16.3	***
Manawatu-Wanganui_east	3.45	6E-04	0.28	14.9	***
Manawatu-Wanganui_west	2.93	3E-03	0.22	14.9	**
Hawkes_Bay	3.50	5E-04	0.26	15.8	***
Taranaki	2.82	5E-03	0.20	15.7	**
Wellington	3.07	2E-03	0.19	14.2	**
West_Coast	2.56	1E-02	0.19	14.4	*
Marlborough	2.68	7E-03	0.17	14.3	**
Canterbury	4.68	3E-06	0.24	12.6	***
Tasman	2.85	4E-03	0.19	14.9	**
Otago	3.28	1E-03	0.19	11.3	**
Southland	2.75	6E-03	0.19	12.3	**
Nelson	3.66	3E-04	0.22	15.4	***

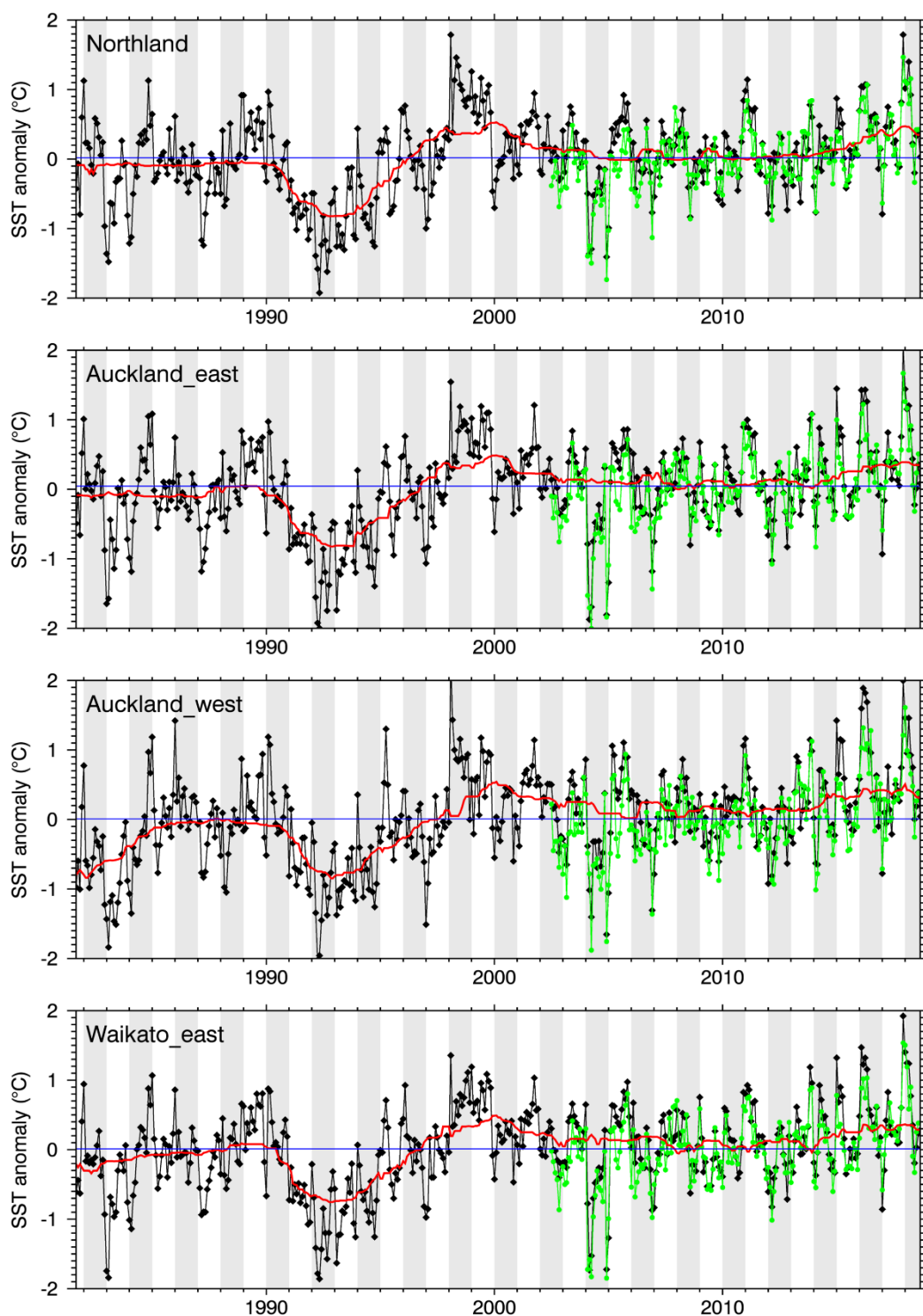


Figure 3-12: Coastal sea-surface temperature (SST) anomalies by month for coastal descriptive regions. OISST data are shown black, with a 4-year smoothed trend is shown red, and the mean value is shown blue. Green data (from 2002) are from MODIS-Aqua for comparison.

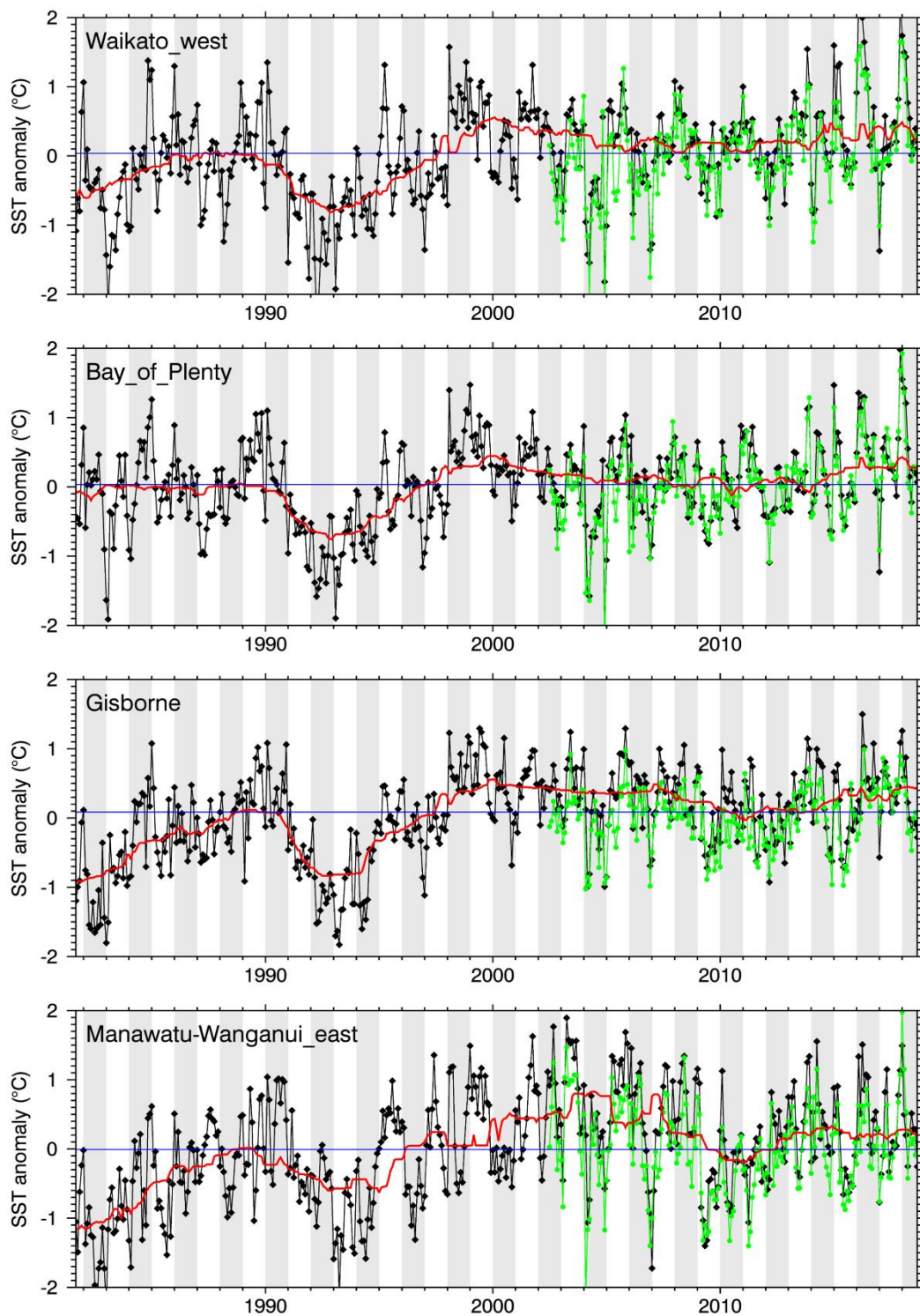


Figure 3-12: Coastal sea-surface temperature (SST) anomalies by month for coastal descriptive regions. Continued.

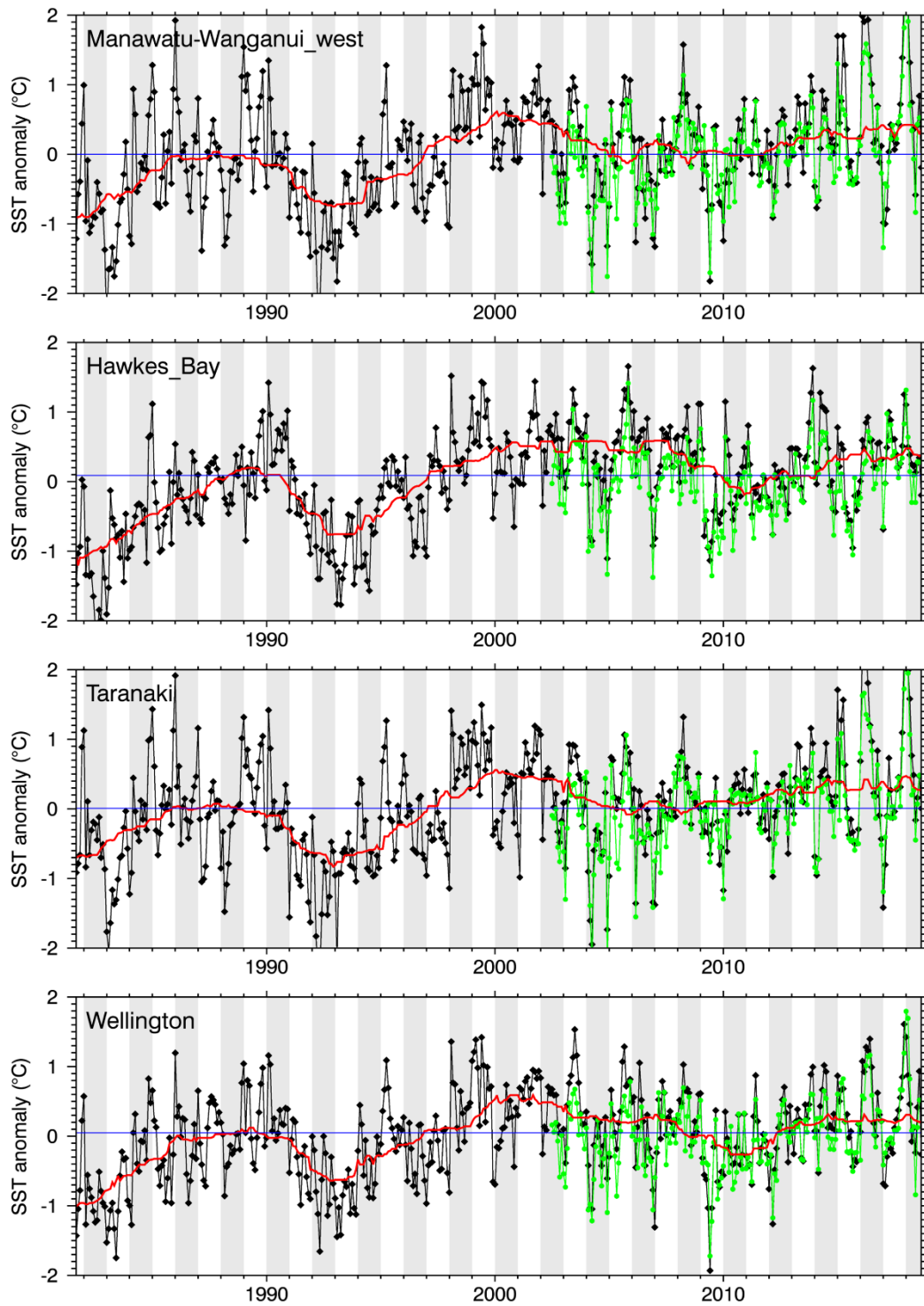


Figure 3-12: Coastal sea-surface temperature (SST) anomalies by month for coastal descriptive regions. Continued.

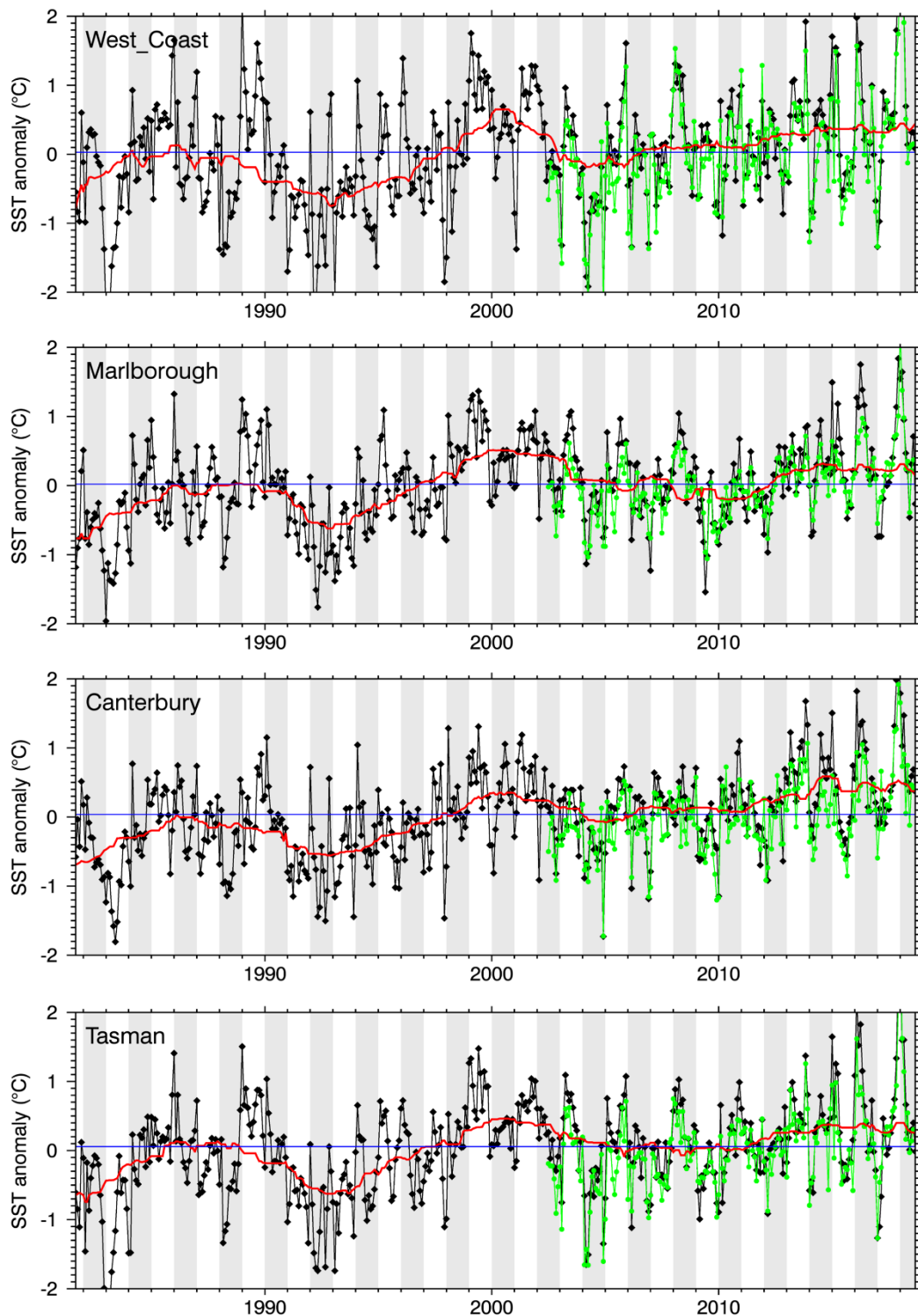
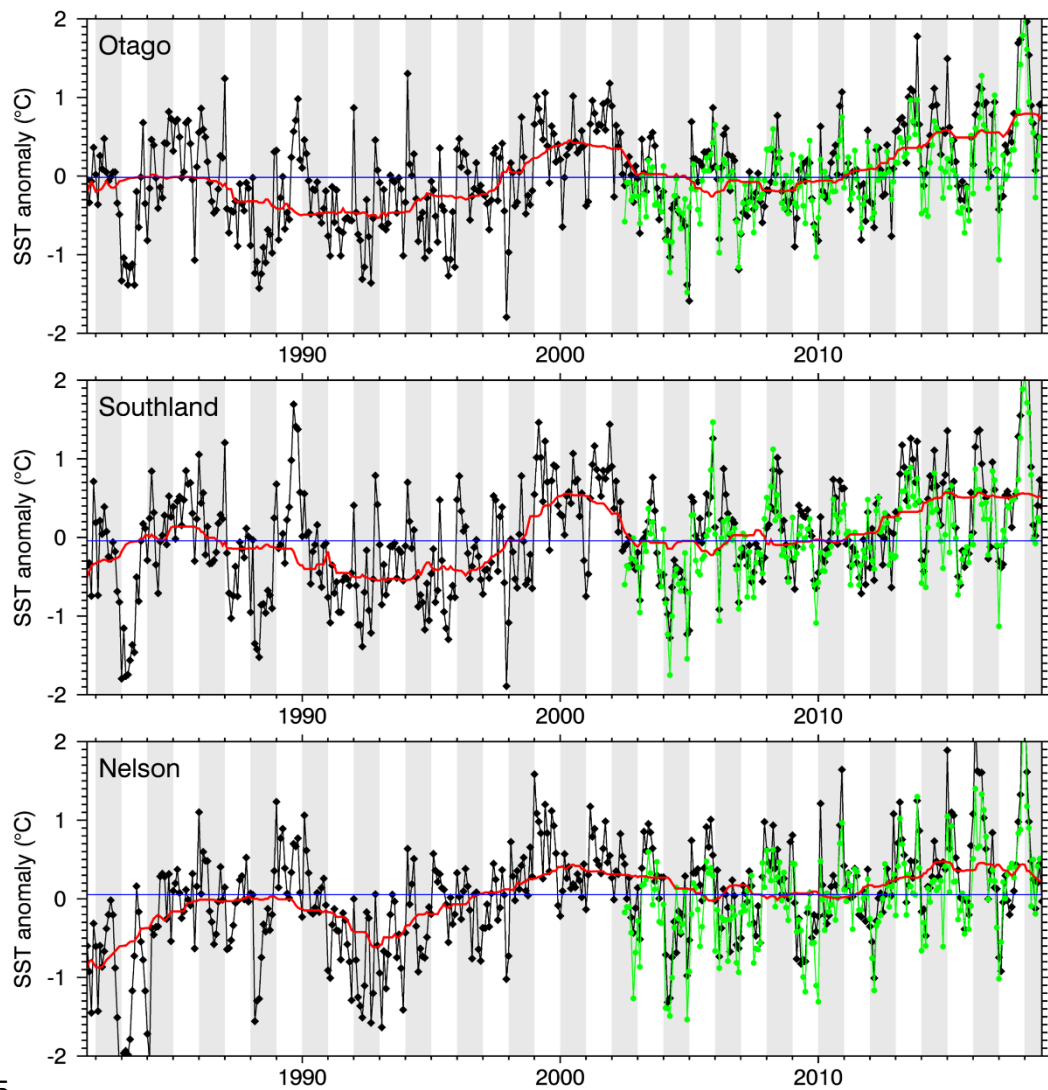


Figure 3-12: Coastal sea-surface temperature (SST) anomalies by month for coastal descriptive regions. Continued.



85

Figure 3-12: Coastal sea-surface temperature (SST) anomalies by month for coastal descriptive regions. Continued and concluded.

3.2.3 Coastal chl: Monthly time series and trend analyses

Time-series of chlorophyll-a concentration monthly averages (Figure 3-13) and anomalies (Figure 3-14) for the descriptive regions (figure 2.4) were calculated. Trend analyses are shown in Table 3-3. No coastal areas were found to have significant trends in chl-a at the scale of the Regional Council areas.

Table 3-3: Trend analysis for coastal region chlorophyll-a concentration (chl-a). The Mann Kendall test is applied to monthly anomalies in the coastal regions. The period of analysis is 2002–2018. Significance is shown: *** $p < 0.001$; ** $p < 0.01$; * $p < 0.05$

Area	Z	p	Sen slope ($\text{mg m}^{-3} \text{y}^{-1}$)	Median (mg m^{-3})	Slope/ median ($\% \text{y}^{-1}$)	Sig- nificance
Northland	-1.49	0.14	-0.002	0.46	-0.45	
Auckland_east	-1.65	0.10	-0.004	0.47	-0.86	
Auckland_west	-0.06	0.95	0.000	0.63	-0.03	
Waikato_east	-1.20	0.23	-0.003	0.49	-0.54	
Waikato_west	0.84	0.40	0.002	0.48	0.43	
Bay_of_Plenty	-0.74	0.46	-0.001	0.45	-0.29	
Gisborne	-1.15	0.25	-0.002	0.40	-0.42	
Manawatu-Wanganui_east	-0.17	0.87	0.000	0.39	-0.09	
Manawatu- Wanganui_west	-0.39	0.70	-0.001	0.47	-0.24	
Hawkes_Bay	-0.65	0.52	-0.001	0.43	-0.31	
Taranaki	0.31	0.76	0.001	0.44	0.14	
Wellington	-0.34	0.74	0.000	0.38	-0.11	
West_Coast	-1.65	0.10	-0.006	0.68	-0.88	
Marlborough	-0.57	0.57	-0.001	0.40	-0.17	
Canterbury	0.60	0.55	0.002	0.56	0.29	
Tasman	-1.27	0.20	-0.004	0.52	-0.73	
Otago	-0.22	0.82	-0.001	0.47	-0.14	
Southland	-0.16	0.88	0.000	0.50	-0.09	
Nelson	-1.68	0.09	-0.005	0.45	-1.06	

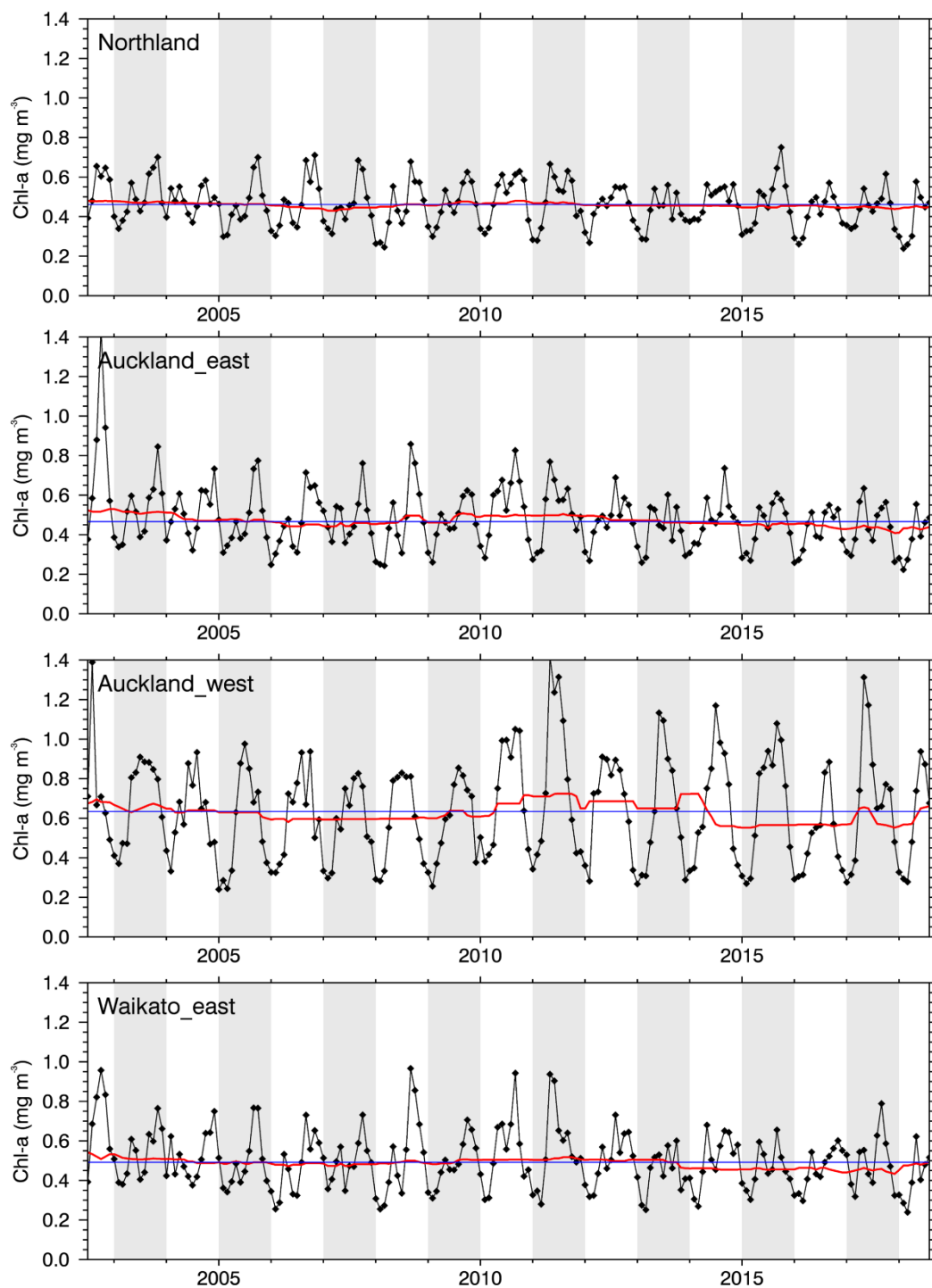


Figure 3-13: Coastal mean chlorophyll-a (chl-a) by month for coastal descriptive regions. The 4-year smoothed trend is shown red, and the long-term median value is shown blue.

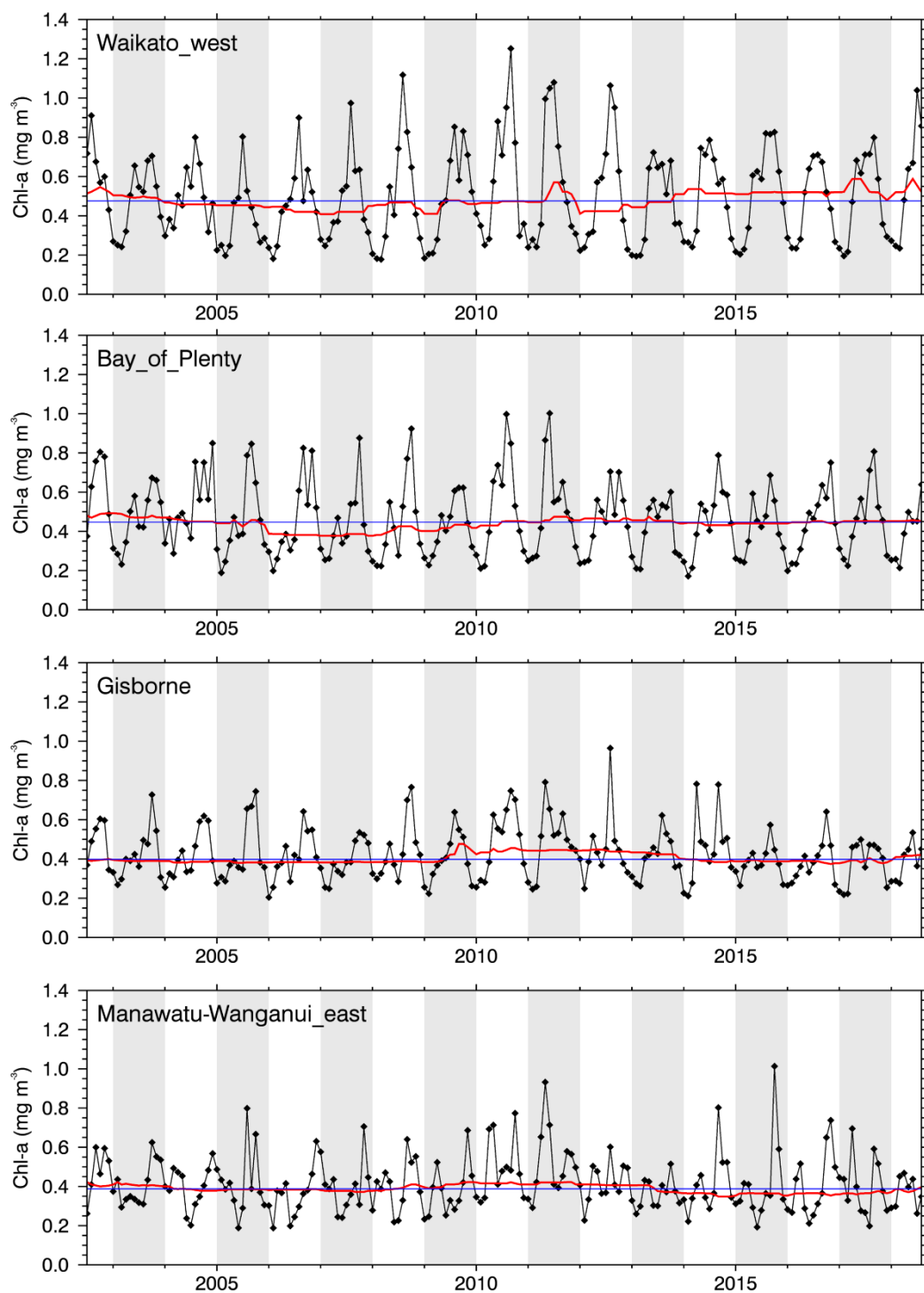


Figure 3-13: Coastal mean chlorophyll-a (chl-a) by month for coastal descriptive regions. Continued.

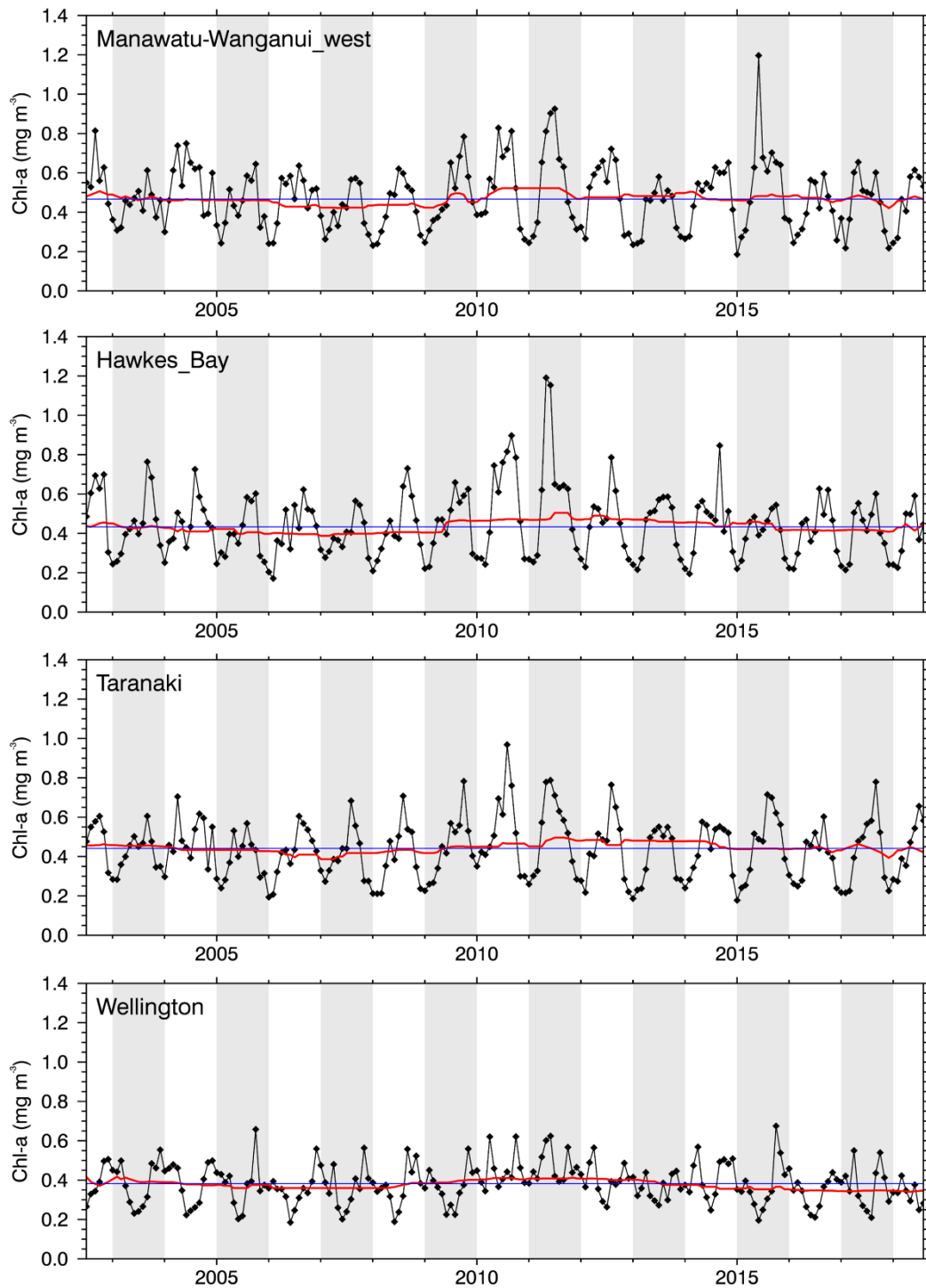


Figure 3-13: Coastal mean chlorophyll-a (chl-a) by month for coastal descriptive regions. Continued.

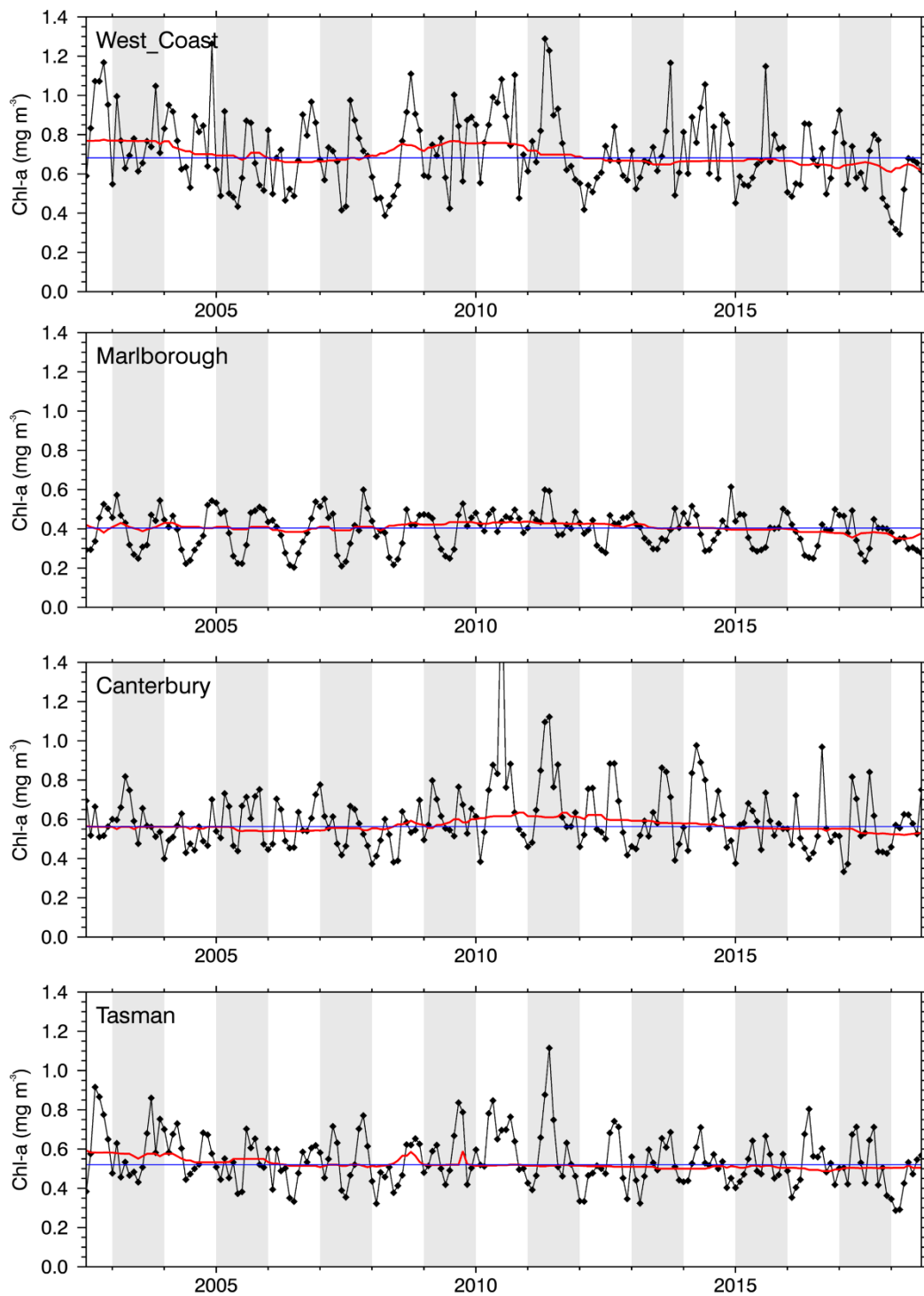


Figure 3-13: Coastal mean chlorophyll-a (chl-a) by month for coastal descriptive regions. Continued.

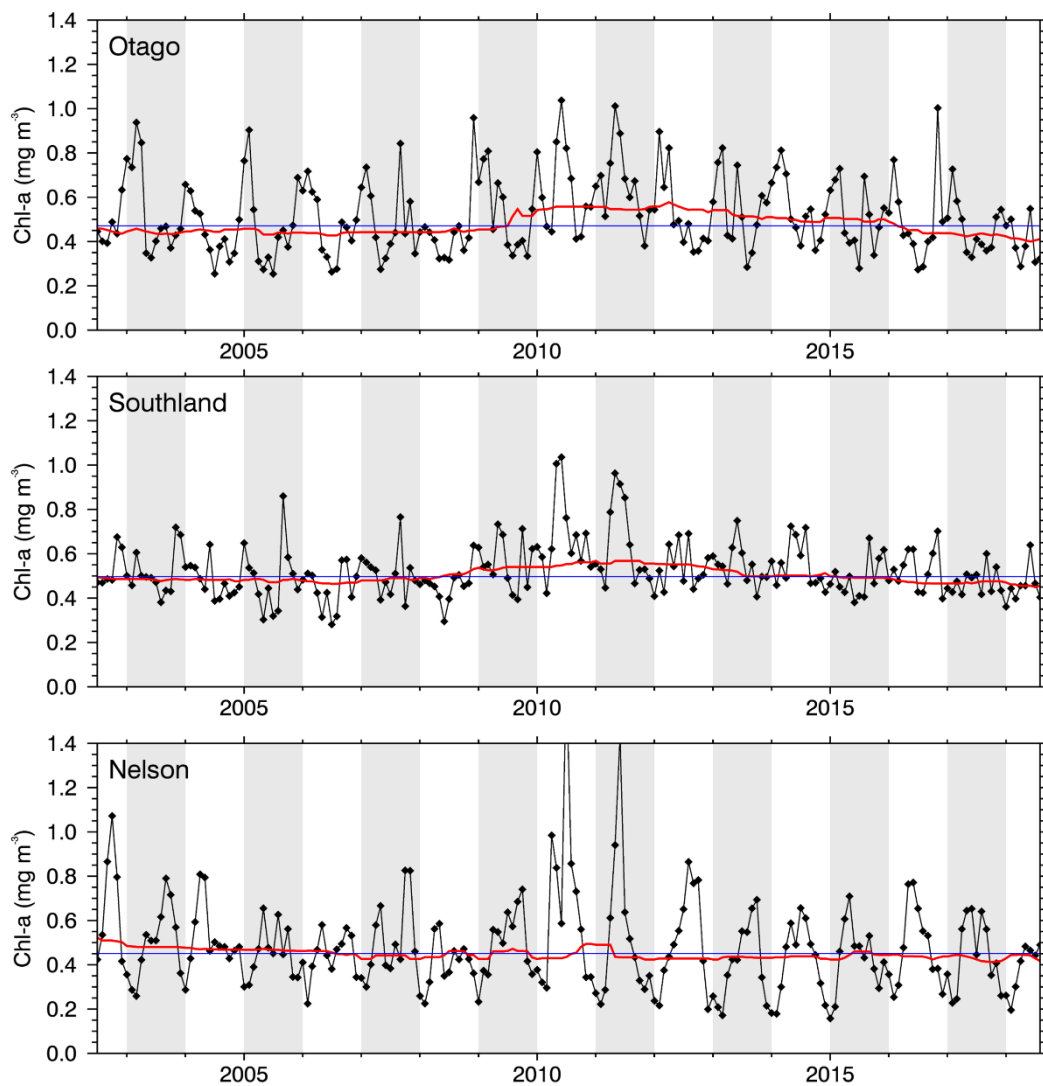


Figure 3-13: Coastal mean chlorophyll-a (chl-a) by month for coastal descriptive regions. Continued and concluded.

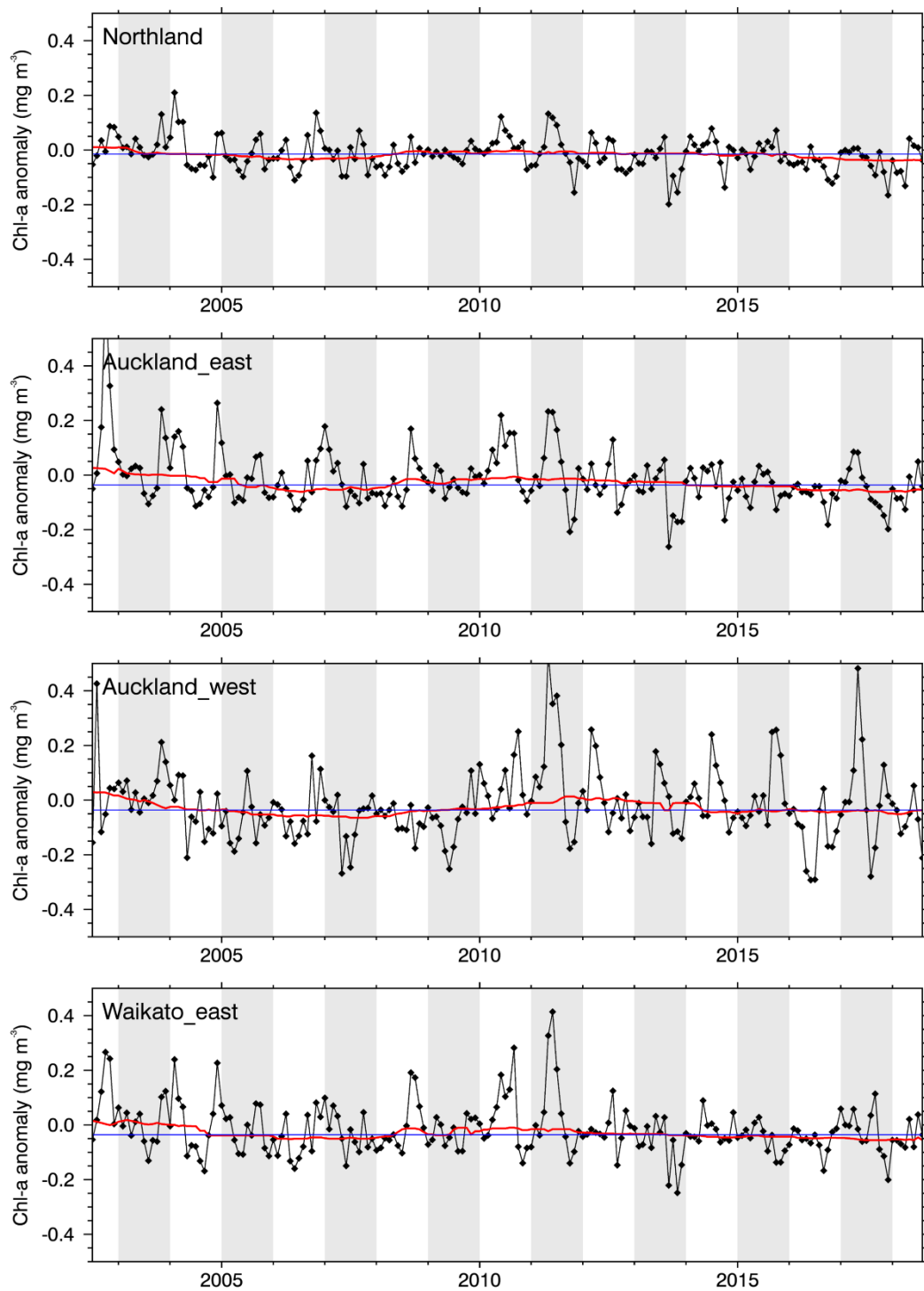


Figure 3-14: Coastal chlorophyll-a (chl-a) anomalies by month for coastal descriptive regions. The 4-year smoothed trend is shown red, and the long-term median value is shown blue.

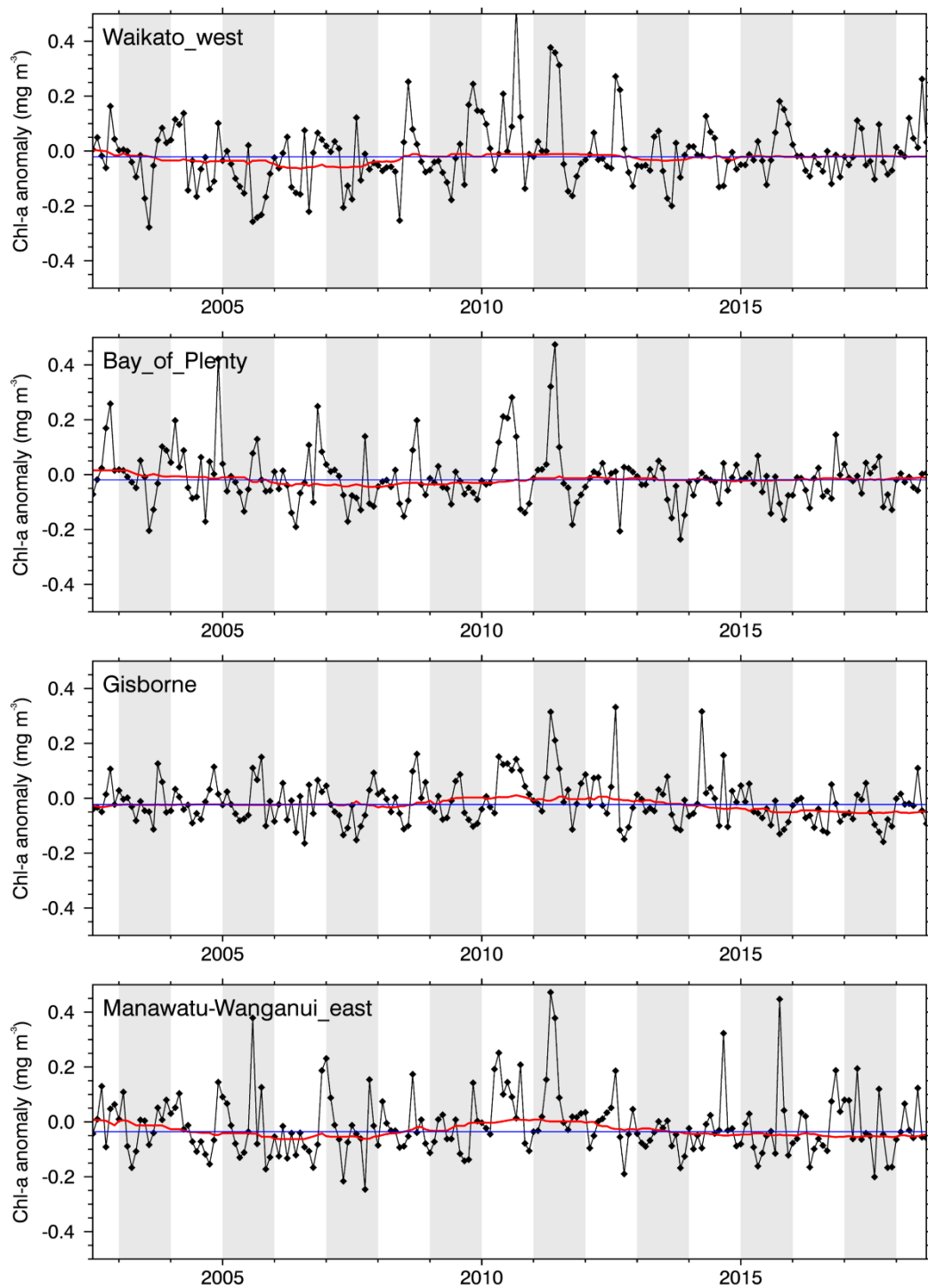


Figure 3-14: Coastal chlorophyll-a (chl-a) anomalies by month for coastal descriptive regions. Continued.

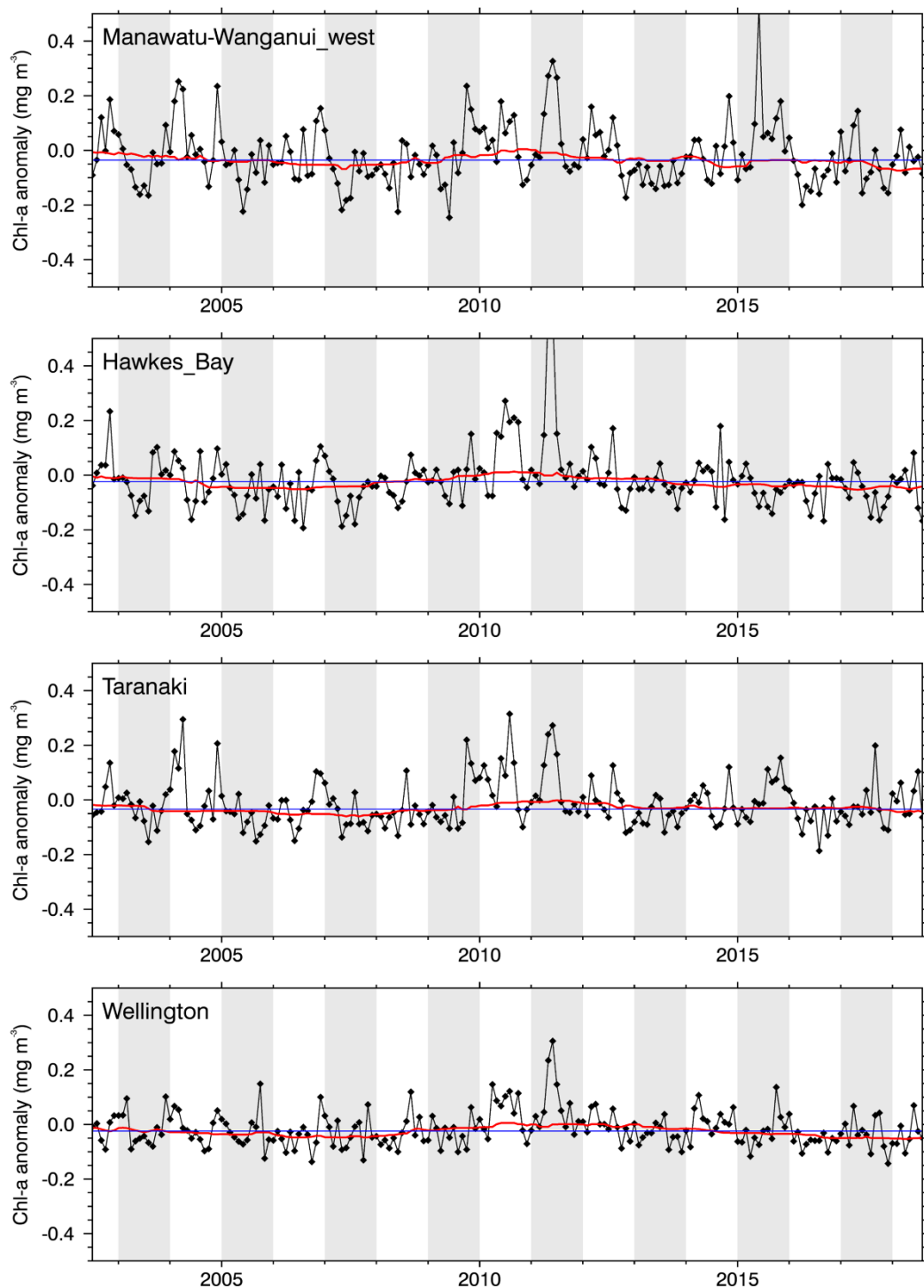


Figure 3-14: Coastal chlorophyll-a (chl-a) anomalies by month for coastal descriptive regions. Continued.

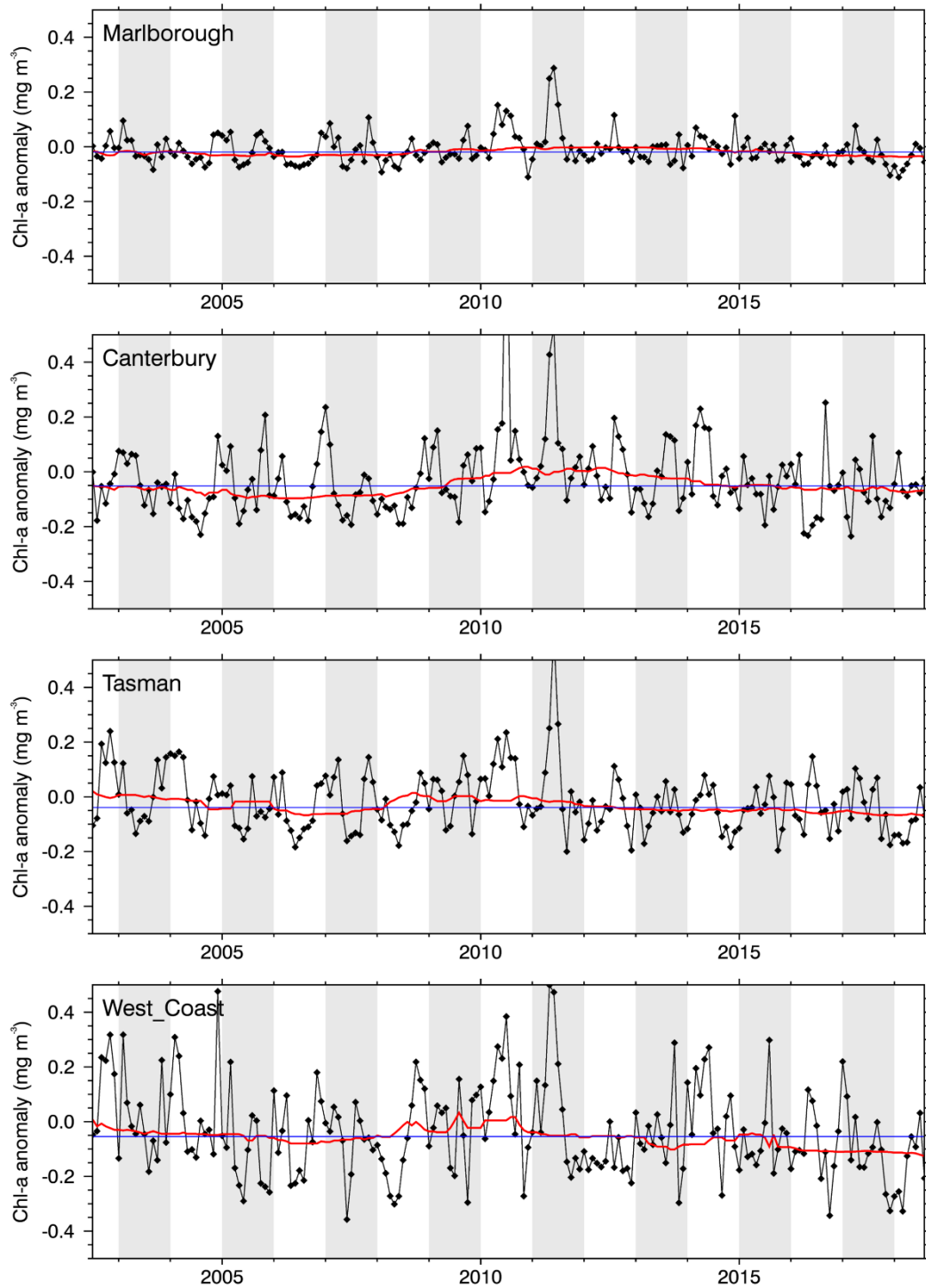


Figure 3-14: Coastal chlorophyll-a (chl-a) anomalies by month for coastal descriptive regions. Continued.

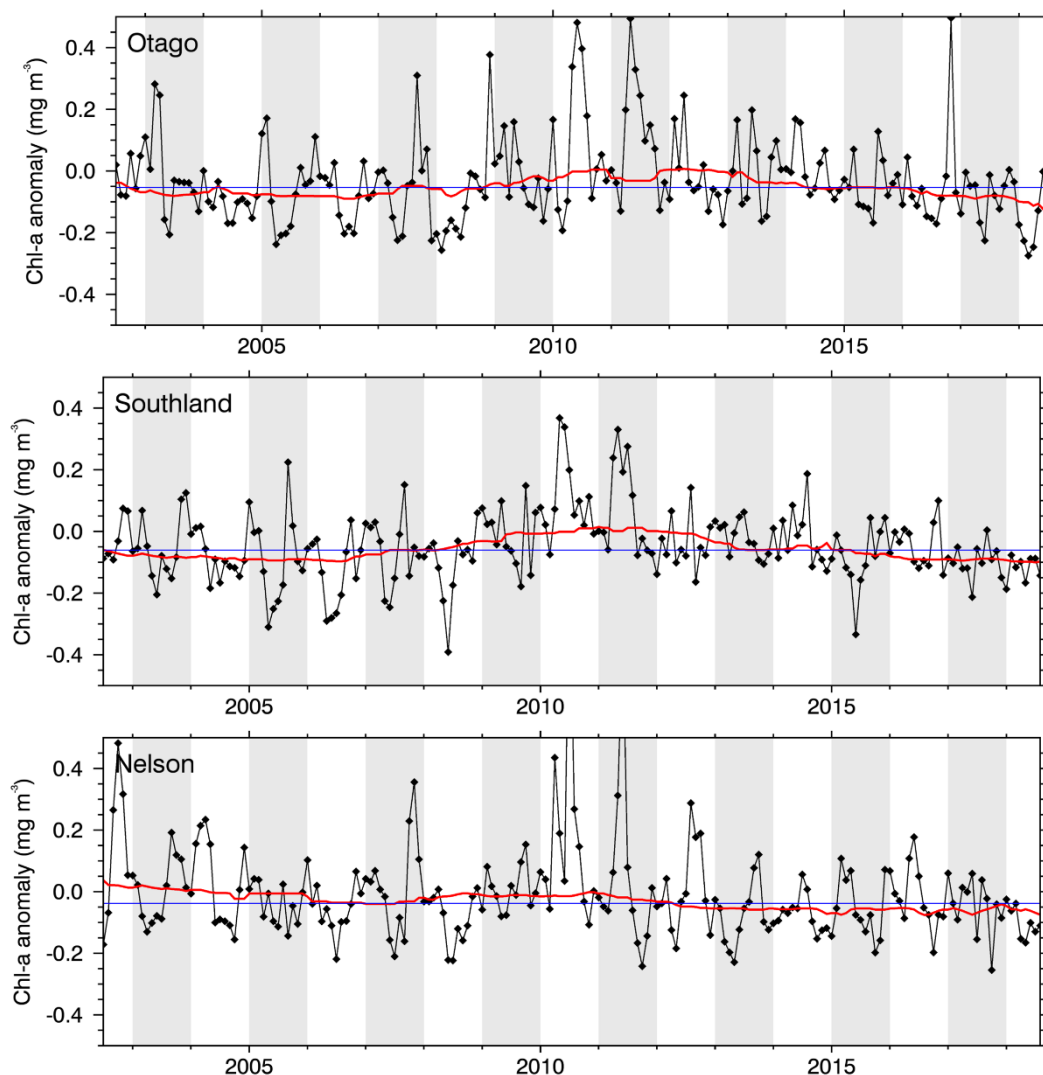


Figure 3-14: Coastal chlorophyll-a (chl-a) anomalies by month for coastal descriptive regions. Continued and concluded.

3.2.4 Coastal: Spatial trend analysis

Spatial trends in chl-a and SST were calculated for each pixel in the territorial seas based on the high-resolution (500 m) MODIS-Aqua data over the period 2002-2018 (Figure 3-15). Over this period, we found significant surface ocean warming through most of the New Zealand coastal zone, consistent with the regional analysis. For the period 2002-2018, the spatial analysis shows that trends in warming were strongest on the west coast of South Island and around Southland. In contrast with the longer-term (1981-2018) regional analysis, warming trends were not significant on the east coast of North Island between 2002-2018. This is explained by looking at the time series information shown in Figure 3-12. For the West Coast and Southland regions, pronounced warming is seen from about 2003 onwards, whereas for the Manawatu-Wanganui_east and Hawkes_Bay regions most of the warming occurred before 2005. These results lead to two observations. First, that the period of analysis is very important when considering trends, with longer periods of analysis, of course, being

more informative. Second, that patterns of warming in the New Zealand territorial seas are not uniform in space or time, being influenced significantly by changes to the large-scale offshore oceanographic setting.

In terms of coastal productivity (chl-a), the spatial analysis (Figure 3-16) shows areas with significant negative trends (likely indicative of decreasing productivity) between 2002-2018 along the north-east New Zealand shelf, especially offshore Hauraki Gulf, the east coast of Northland and, to a lesser extent, in parts of the Bay of Plenty. Evidence of decreasing coastal productivity was also found in Golden-Tasman Bays and along the west coast of South Island. Evidence of increasing coastal productivity (2002-2018) was found in the Firth of Thames (Hauraki Gulf), west coast of North Island (between Kaipara and New Plymouth), Hawke's Bay, north-east coast of South Island (around Kaikoura), off Oamaru, and around Stewart Island. None of these long-term changes in chl-a were sufficient to translate to significant trends at the regional level (Table 3-3).

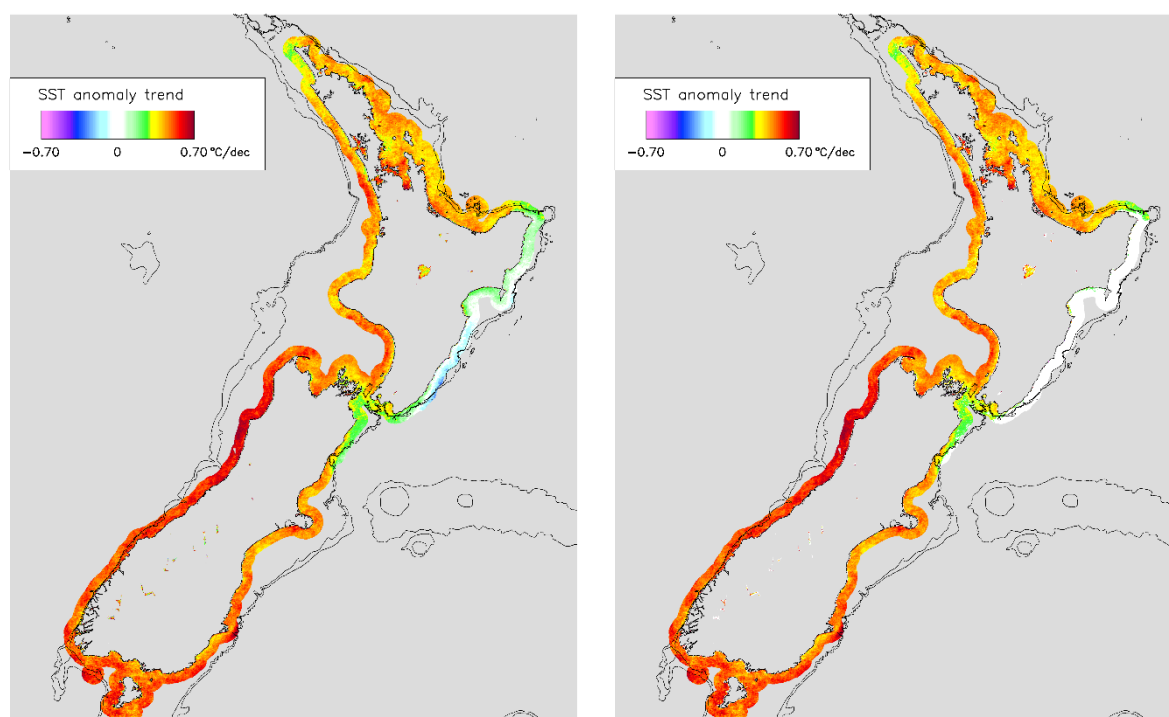


Figure 3-15: Coastal: Spatial trends in monthly anomalies of SST from MODIS-Aqua, 2002-2018. Sen-slope trends in sea-surface temperature (SST) are shown as °C per decade. **Left:** All trends. **Right:** Significant trends only (95% confidence level; Mann-Kendall analysis corrected for auto-correlation), with non-significant trends shown white. No data or no analysis is shown grey in both panels. High-resolution (500 m) data from MODIS-Aqua was used covering the 16-year period (2002-2018). Note the trends in SST differ from those shown in Table 3-2 and Figure 3-8 which are for the longer 37-year period (1981–2018).

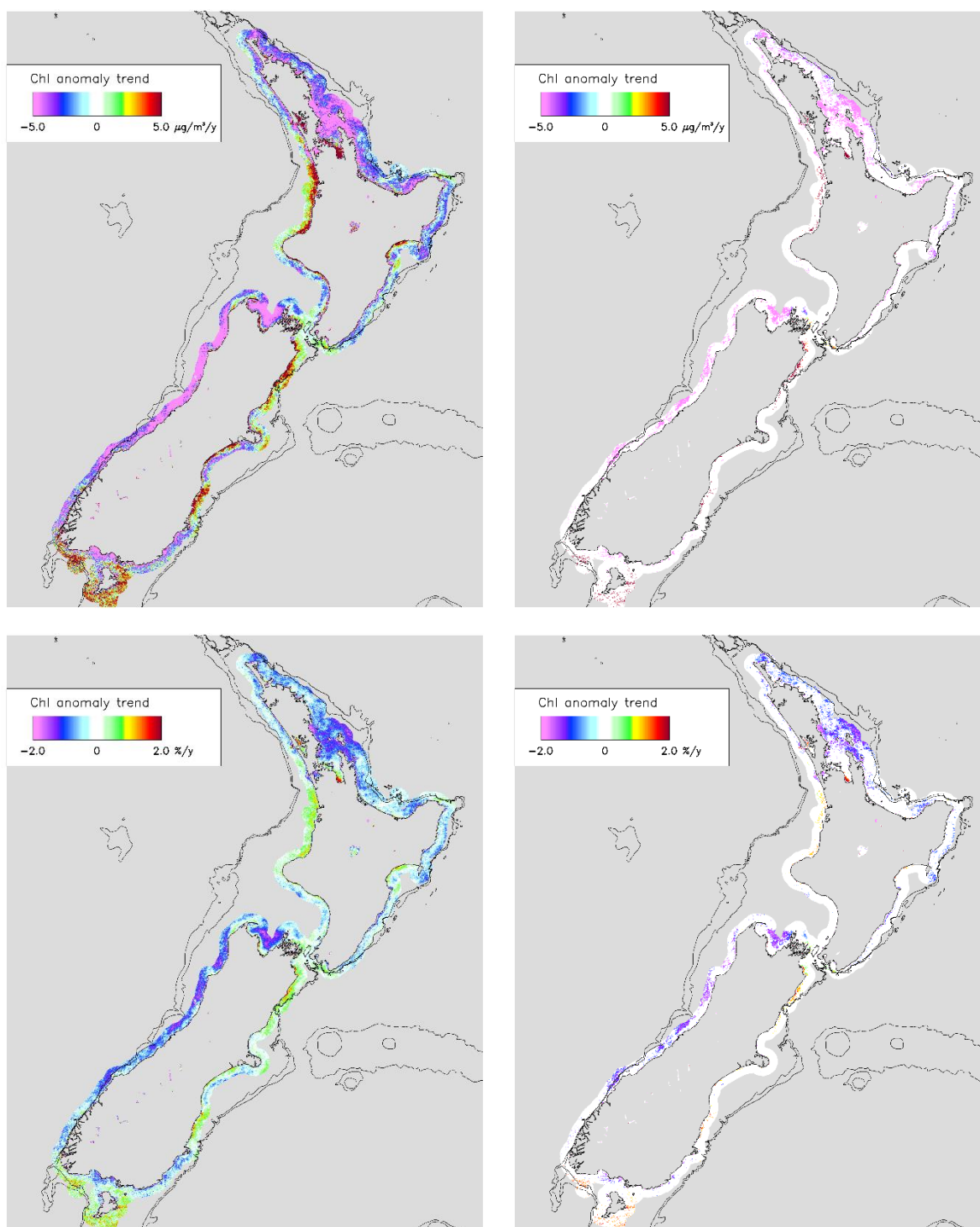


Figure 3-16: Coastal: Spatial trends in monthly anomalies of surface chl-a from MODIS-Aqua, 2002-2018. **Top:** Sen-slope trends in absolute chl-a values per year ($\mu\text{gChl-a m}^{-3}$ per year). **Bottom:** Sen-slope trends as a proportion of the median value (bottom, % per year). **Left panels:** All trends. **Right panels:** Significant trends only (95% confidence level; Mann-Kendall analysis corrected for auto-correlation), with non-significant trends shown white. No data or no analysis is shown grey in both panels. High-resolution (500 m) data from MODIS-Aqua was used covering the 16-year period (2002-2018).

3.2.5 Coastal: Spatial correlation analysis

Spatial correlation analysis between chl-a and SST anomalies through the territorial seas can help understand the underlying drivers of change. Correlations between monthly anomalies of chl-a and SST for each pixel 2002-2018 (Figure 3-17) were found to be predominantly negative, i.e. coastal warming led to lower coastal primary productivity. This relationship was strongest off the New Zealand north-east shelf, and the north and west coasts of South Island. Smaller, more localised and enclosed inshore areas show the opposite relationship (coastal warming correlated with increasing productivity): Kaipara Harbour, Manukau Harbour, inner Hauraki Gulf (including Firth of Thames, Tamaki Strait), Tauranga Harbour, off Raglan, Marlborough Sounds, inner Golden and Tasman Bays, South Canterbury Bight. These positive relationships between SST and chl-a anomalies, and the increasing coastal productivity close inshore in these areas in general, are likely to result from land-use changes rather than from larger-scale offshore oceanographic changes.

A positive relationship between SST and chl-a anomalies was also seen over a large offshore area south of Stewart Island and stretching west past Solander Island. These changes are likely to result from oceanographic changes, where warming of Subantarctic Water leads to high oceanic primary productivity, consistent with the oceanic analysis.

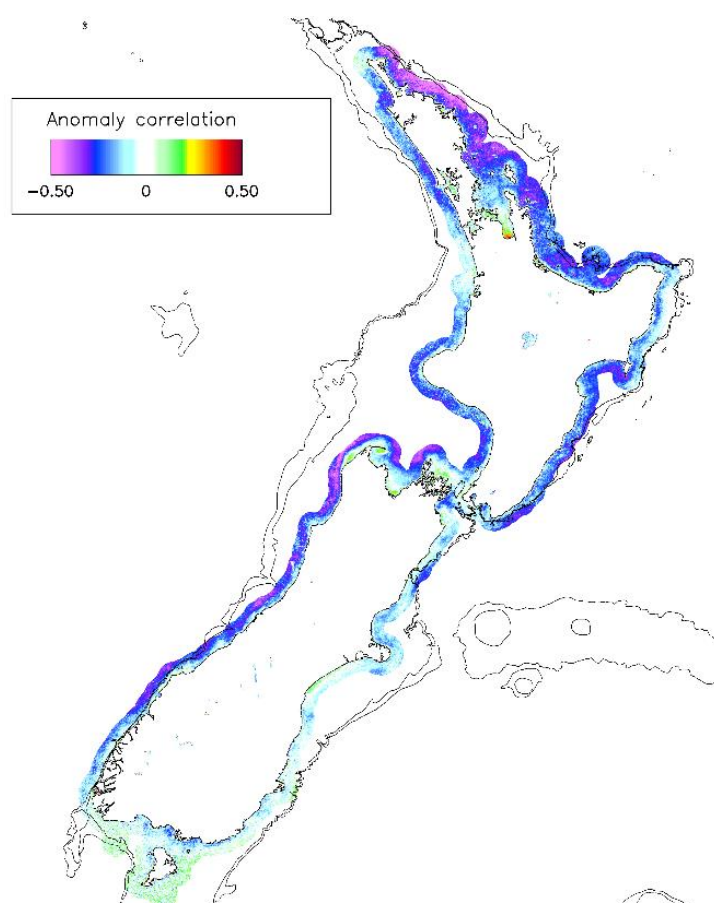
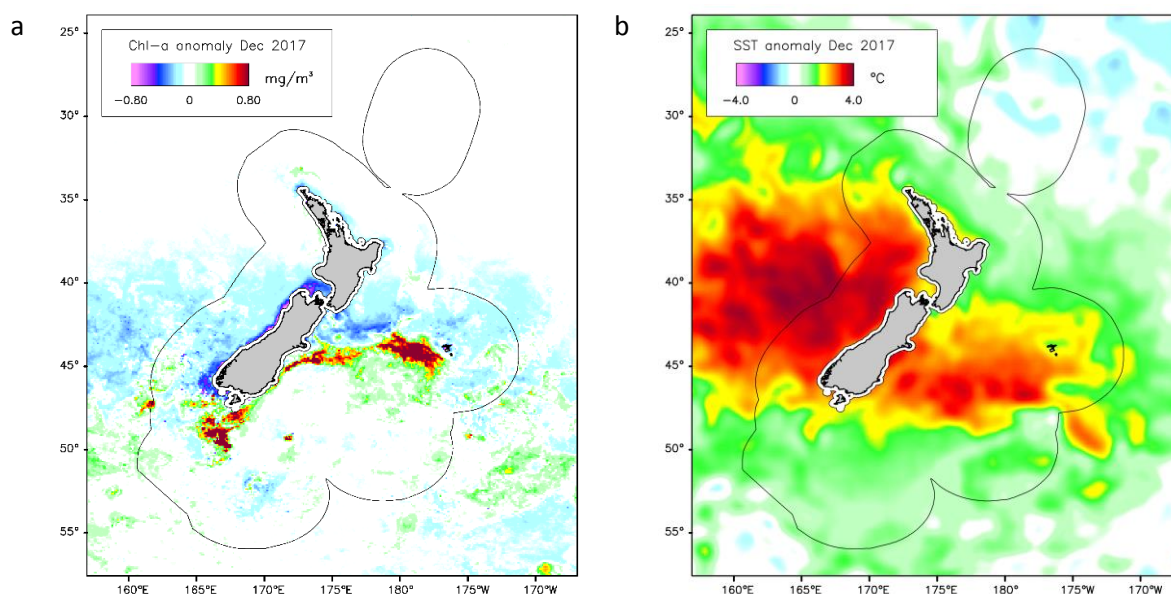


Figure 3-17: Coastal: the linear Pearson correlation coefficient (R) between monthly anomalies of chl-a and SST from MODIS-Aqua (2002–2018). The period of analysis is between 1997 and 2018. Only data in the

territorial seas (to 12 nautical miles offshore) were analysed. The 250 m and 500 m depth contours are also shown.

3.3 New Zealand's 2017 “marine heat wave”

A high anomaly in SST (Figure 3-6) in December 2017 to January 2018 was unprecedented in the satellite SST record (since 1981). This event received a lot of attention in the media where it was called the “marine heat wave” (e.g. New Zealand Herald, 2018). The ocean warming seems to have been due to an extended period of very low winds which led to warming of the surface ocean but which did not extend very far through the water column (NIWA, unpublished data). Because this seems such an unusual event, we include the images of the SST and chl-a anomalies for these months (Figure 3-18) to show its spatial extent. Parts of the Tasman Sea region were up to 4°C warmer than normal in December 2017, with the Tasman Sea region anomaly about 3°C in December 2017. The area of Subantarctic Water south of the Chatham Rise was also much warmer than normal. Chl-a concentrations were not substantially affected throughout these large areas, but there were strong negative anomalies in chl-a along the whole west coast of the South Island (especially around Westport and south of Fiordland) and South Taranaki Bight, indicative of much lower than normal ocean productivity in these areas. This low productivity may also be due to low winds, which may have reduced the amount of wind-driven upwelling along the west coast. In contrast, chl-a was elevated substantially south of the Snares Islands (south of Stewart Island) and over the Chatham Rise. In the coastal data (Figure 3-18c,d) based on a much shorter period of data (2002–2018), anomalies were more pronounced in January 2018 than in December 2017 and characterised by negative anomalies in chl-a (likely lower productivity) along the west coast of South Island and to the west of Stewart Island.



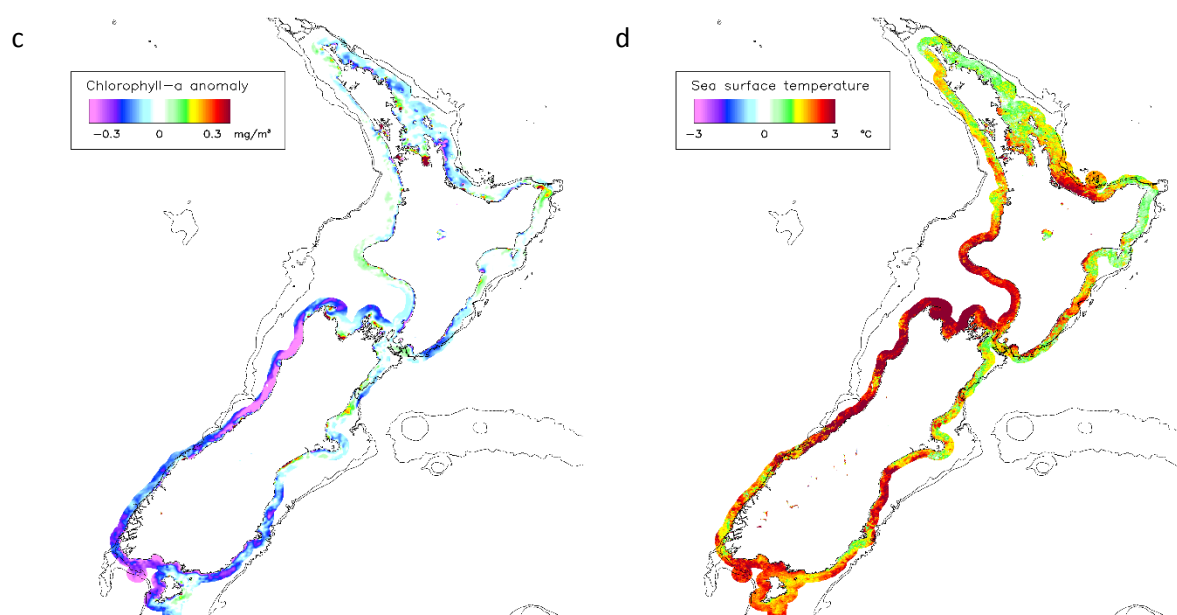


Figure 3-18: Monthly anomalies in chl-a and SST for December 2017 (oceanic) and January 2018 (coastal). a: Oceanic scale chl-a anomaly (relative to baseline 1997–2018); b: oceanic scale SST anomaly (relative to baseline 1981–2018); c: Coastal scale chl-a anomaly (relative to baseline 2002–2018); d: Coastal scale SST anomaly (relative to baseline 2002–2018). The New Zealand EEZ is also shown in a and b, and the 250 m and 500 m depth contours in c and d.

4 Discussion and conclusions

4.1 Chlorophyll-a and primary productivity

The concentration of chl-a is not the same thing as ocean primary productivity, although it is related to it. Net primary productivity (NPP) is the vertically-integrated rate of growth of phytoplankton after allowing for respiration (units of $\text{mg carbon m}^{-2} \text{d}^{-1}$). NPP is the amount of organic material potentially available to higher trophic levels (consumers). Generally, the majority of NPP occurs by the growth of phytoplankton in the mixed-layer⁵, though phytoplankton can grow at the base of the mixed-layer forming sub-surface phytoplankton maxima (Campbell et al., 2002; Aiken et al., 2004). Light, temperature, nutrient concentrations and algal functional group are the major factors controlling phytoplankton biomass and NPP in the ocean (Platt, 1986).

There are many different methods of estimating NPP from satellite data (e.g. Platt & Sathyendranath, 1993; Antoine & Morel 1996a,b; Behrenfeld & Falkowski, 1997b; Behrenfeld et al. 2005; Westberry et al. 2008). None of these methods includes NPP in sub-surface maxima, consistent with the assumption that this contribution is minor compared to NPP in the mixed-layer (Campbell et al., 2002; Behrenfeld et al. 2005; Westberry et al. 2008). The concentration of chl-a typically accounts for the majority (~70%) of the variability in satellite estimates of NPP but, in reality, phytoplankton physiology is probably responsible for much (or even most) of the variability in NPP, but phytoplankton physiological variations are poorly measured remotely (Behrenfeld & Falkowski, 1997b).

Estimates of NPP by different methods differ considerably (Campbell et al., 2002) and it is not known whether any available satellite-based estimates of NPP bracket the true value in the New Zealand

⁵ The “mixed layer” is the surface-most part of the ocean, with a depth of between about 50 and 200 m, where the water is mixed by wind and wave stirring.

region (Schwarz et al., 2008). In the context of monitoring for change in marine productivity, the simpler and better understood proxy of chl-a is often preferred over satellite-based estimates of NPP (Aiken et al., 2004; Pinkerton et al., 2015; O'Reilly & Sherman, 2016) and this approach is taken here. It is reasonable to expect that, for the purposes of exploring long-term trends and variability in ocean productivity round New Zealand, changes in chl-a observed by satellite are indicative of changes in ocean productivity (NPP).

4.2 Accuracy of satellite estimates of chl-a

The ability of satellite sensors to measure chl-a is limited by cloud cover, solar elevation, variations in sensor calibration, and uncertainties associated with the processing of satellite data (atmospheric correction and in water algorithms). These uncertainties are considered below.

4.2.1 Cloud cover and solar elevation

In the New Zealand region, only about 10–30% of chl-a images are cloud-free, depending on location and season (NIWA, unpublished data). Ocean colour data availability in New Zealand Subantarctic Water during winter is also limited by solar elevation, i.e. the sun is so low in the sky when the satellite is overhead that there is not enough light leaving the water to allow a reliable measurement of ocean colour. These data gaps were accommodated by excluding periods where less than 80% of data in a given region were available in a month. This approach biases the annual average chl-a (Figure 3-2) and annual chl-a anomalies (Figure 3-3), especially in the Subantarctic region. However, the bias in our monthly analysis caused by having no data in some winter months is likely to small (see Section 2.5.3). Nevertheless, we recommend that optimal interpolation methods (related to objective analysis) should be investigated in the future as a way to reduce these biases in the chl-a analysis.

4.2.2 Radiometric sensor degradation

Considerable international effort is focussed on tracking the degradation of radiometric (i.e. “ocean colour”) sensors over time (Brewin et al., 2014). The technical and scientific process of design, pre-launch characterisation, on-going tracking of sensor change, and validation of inter-sensor consistency are carried out by a number of space agencies and involve periodic reprocessing of the entire ocean colour archive as more is learned about sensors and as new processing methods become available (e.g. McClain et al., 2004; Franz et al., 2005; Meister et al., 2012, 2013). The international technical and scientific effort work on ocean colour observation aims to address the explicit needs of United Nations Framework Convention on Climate Change (UNFCCC) for long term, consistent measurements⁶. This concerted international effort makes it highly likely that, on a global scale, SeaWiFS, MODIS-Aqua and MERIS time series of ocean colour data are consistent over time - both within a given mission and between different sensors – and that they are “fit for purpose” in the sense of detecting and quantifying long-terms trends in chl-a round New Zealand.

4.2.3 Oceanic: Uncertainties in processing methods

Measurements of chl-a from ocean colour satellites are inherently less accurate than from laboratory analysis of water samples; the target accuracy for modern satellite measurements of chl-a in the open ocean is $\pm 35\%$ (Hooker et al., 1992) compared to laboratory accuracy of a few percent. There is a random (short-term) and a systematic (long-term) component to the uncertainty in measuring chl-a using satellite methods, and it is the systematic uncertainty that is particularly relevant to the

⁶ http://www.esa-oceancolour-cci.org/?q=webfm_send/397

detection and monitoring of trends in chl-a from satellite observation (Dierssen, 2010). The relative magnitudes of the random and systematic uncertainties in satellite measurements of chl-a in the New Zealand region are not well known (Murphy et al., 2001). In general, in the ocean domain, the random component is likely to be only a small part of the total uncertainty, and is reduced further by using averages of a relatively large amount of satellite data (monthly composites, spatial averages). We consider it highly likely that changes in patterns and concentrations of chl-a in the oceanic area presented in this study indicate genuine changes in the New Zealand ocean environment.

4.2.4 Coastal: Uncertainties in processing methods

Measuring chl-a concentrations in turbid coastal waters from satellites is scientifically and technically challenging (Pinkerton et al., 2005; Pinkerton, 2015). Consequently, satellite estimates of chl-a in the coastal zone are understood to have relatively high uncertainties (perhaps $\pm 50\%$). Much of this uncertainty will be systematic (i.e. acting over large space and time scales) rather than being random from pixel-to-pixel. It remains difficult to quantify the level of uncertainty in the satellite measurements of coastal chl-a (IOCCG, 2000; Pinkerton et al., 2018), with the normal way of assessing the accuracy being to compare in situ measurements of chl-a with satellite measurements taken in the same area at approximately the same time. When this was carried out for the New Zealand territorial seas (Table 2-2, Figure 2-1), the agreement between in situ and satellite estimates of chl-a was similar to that found in coastal areas elsewhere (e.g. Pinkerton et al. 2003; Darecki & Stramski, 2004; Chang & Gould, 2006), with $R^2=0.23$ on log-log scales.

The mismatch between in situ and satellite measurements potentially has many causes (IOCCG, 2000; Pinkerton et al. 2003). (1) The distribution of chl-a through the water column is often not uniform so that differences can be caused by taking a water sample from a different depth than the satellite observes. Typically, the satellite signal depends on chl-a averaged over the top ~ 10 m whereas a bottle sample will just represent one depth. (2) There are fundamental differences in the spatial and temporal scales of observation by satellites and moorings (Pinkerton et al. 2003; Gall & Zeldis, 2011). In highly tidal environments such as estuaries, a difference in sampling time of a few minutes can make a large difference to the comparison. To retain enough match-up samples for a statistically valid analysis, a wide time difference is usually allowed. (3) Variability in the inherent optical properties of phytoplankton and co-occurring sediment and CDOM affect the performance of satellite processing algorithms (Garver & Siegel, 1997; IOCCG, 2000; Lee et al. 2002; Lohrenz et al. 2003). (4) Additional uncertainties are due to inaccuracies in the remote sensing of water-leaving radiance, for example due to imperfect atmospheric correction or surface wave effects (Pinkerton et al. 2003).

The consequence of the mismatch in the spatial scale of sampling between satellites and in situ samples, the large differences in times of measurements, and the dynamic nature of the coastal environment, is that the “match-up” comparison method is a very limited way of assessing satellite data quality in highly dynamic coastal environments. This remains an active area of research in New Zealand and around the world and data quality will improve in the future. In the meantime, the processing and analysis used here follow best scientific practice worldwide, and we believe represents the best available data for tracking changes to the productivity of New Zealand territorial waters to date.

4.3 Oceanic variations in chl-a and SST

4.3.1 Oceanic summary

For the New Zealand **EEZ** as a whole, monthly chl-a anomalies were negative (below average) around the start and end of the period (1997–2003 and 2012–2018) and positive (above average) in the middle (2003–2012). The monthly chl-a anomalies had a root-mean-square (RMS) value 11.3% of the overall chl-a mean value. The mean absolute value (the average size, neglecting whether it was positive or negative) of the monthly chl-a anomaly was 9.3% of the overall chl-a mean value. The patterns of anomalies at the EEZ scale seen in this latest analysis were consistent with those in Pinkerton (2016).

The largest monthly chl-a anomalies were in the **Chatham Rise** region (up to about $\pm 0.2 \text{ mg m}^{-3}$). The mean absolute value of chl-a anomalies for the Chatham Rise region was 14.5% of the overall mean value (RMS 18.9%) which was the highest for any region in this analysis. The Chatham Rise area has the highest offshore productivity in the New Zealand EEZ (mean chl-a concentrations of 0.47 mg m^{-3}) because of mixing of different water masses in the overlying Subtropical Front. Elevated productivity in Chatham Rise region supports valuable deepwater fisheries including hoki, hake and ling. Differences in the timing of the spring and autumn blooms of phytoplankton is likely to have contributed to higher chl-a anomalies observed in this region. The satellite data for the Chatham Rise region show negative anomalies in chl-a around the start and end of the period (1997–2003 and 2012–2016) and positive (above average) in the middle and last year (2003–2012, 2017). The decreasing trend in chl-a in the Chatham Rise region between October 2010 and February 2016 reported in Pinkerton (2016) ceased around February 2015 in this new analysis, and values were above average in 2018.

The patterns of long-term variation in the chl-a anomaly in the **Tasman Sea** were the clearest in any of the regions and very consistent with those reported in previous analyses (Pinkerton, 2015; Pinkerton, 2016). There were negative anomalies around the start and end of the period (1997–2003 and 2012–2018) and positive anomalies in the middle (2003–2012). The mean value of absolute chl-a anomalies for the Tasman region was 13.6% of the mean (RMS 17.8%). Positive anomalies around 2007–2010 were due to especially large anomalies in chl-a in the western Subtropical Front (offshore of Fiordland in the Tasman Sea). The satellite data show especially low productivity on the west coast of the South Island in late 2017.

The seasonal pattern of chl-a in **Subtropical Water** (STW region) was pronounced, with monthly mean chl-a values of $\sim 0.35 \text{ mg m}^{-3}$ in the spring and $\sim 0.1 \text{ mg m}^{-3}$ in autumn. The longer-term variation in chl-a superimposed over this seasonal cycle was quite weak; mean absolute chl-a anomalies for the Subtropical region were 9.9% of the mean (RMS 14.2%). The patterns of variation in chl-a seen in the STW region were very similar to those reported previously (Pinkerton, 2015; Pinkerton, 2016). There were negative anomalies around the start and end of the period (1997–2003 and 2012–2018) and positive in the middle (2003–2012). Chl-a concentrations in Subtropical Water in November 2002 and October 2015 were particularly elevated (by more than 50% of the mean).

The satellite record of chl-a anomalies in **Subantarctic Water** (south of New Zealand) was incomplete because low solar elevations in this region invalidate satellite measurements of ocean colour in the winter. Consistent with previous analyses (Pinkerton, 2015; Pinkerton, 2016), the satellite data show evidence of an upwards trend in chl-a between 1997 and 2018 superimposed on the general pattern

seen in other regions (lower values 1997-2003, and higher values 2003-2012). Mean absolute chl-a anomalies for the Subantarctic Water region were 11.5% of the mean (RMS 15.5%).

Pixel-by-pixel analysis: Trend analysis on a pixel-by-pixel basis using the Sen-slope is a powerful way of exploring changes in ocean properties around New Zealand. Temporal trends in monthly anomalies of SST (Figure 3-8) show that the oceans round New Zealand have generally all warmed significantly between 1981 and 2018, with the highest rate of warming of 0.38 °C per decade occurring in Subtropical Water and the Tasman Sea.

For the New Zealand EEZ as a whole, the area-weighted mean rate of surface warming was 0.15°C per decade on average between 1981 and 2018, and was 0.11°C per decade between 1981 and 2015 (i.e. excluding the last two years of the time series). Globally, between 1981 and 2015, the global SST trend was 0.12°C per decade (NOAA, 2016; analysis including data after 2015 is not available at present). This means that between 1981 and 2015, the ocean in the New Zealand EEZ has warmed at close to the same rate as the global average (Figure 4-1).

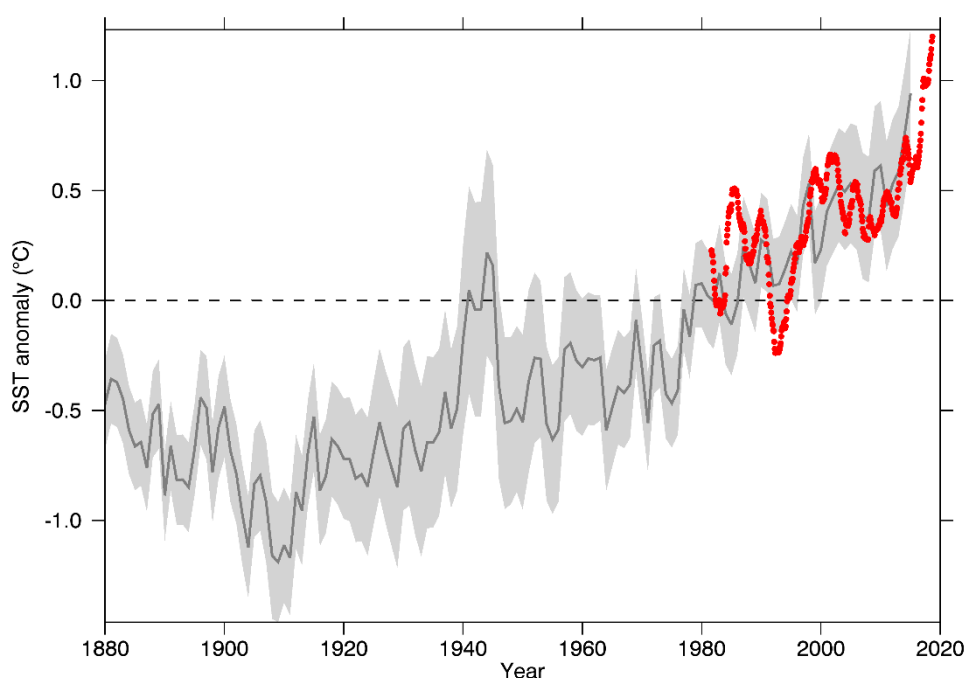


Figure 4-1: Anomalies in sea-surface temperature (SST): global average and New Zealand EEZ. Grey: global average SST anomalies from the NOAA extended reconstructed sea surface temperature (ERSST.v4; NOAA, 2016) showing median and upper/lower 95% confidence intervals. The global SST baseline (zero anomaly) is the mean SST between 1971 and 2000. Red: New Zealand EEZ monthly anomalies from AVHRR satellite data, smoothed as described in the text. Because the global data are referenced to the 1971-2000 mean, and New Zealand data are not available for that time period, the New Zealand EEZ anomalies have been adjusted to have the same mean as the global anomalies in the overlapping period (1981–2015).

Similar “pixel-by-pixel” analysis of trends in chl-a anomalies show that some ocean areas around New Zealand are likely to have experienced increases in ocean productivity of up to 2% per year between 1997 and 2018, especially the Subtropical Front (southwest and southeast of New Zealand and over

the Chatham Rise). Decreasing trends in ocean productivity of 1–2% per year were found in Subtropical Water around Northland, the northeast New Zealand shelf slope, and to the east of New Zealand (outside the EEZ). The magnitudes of these long-term trends in chl-a were small compared to the interannual variability in chl-a. This means that while the mean conditions of chl-a are not yet moving outside the natural envelope of variability, if these trends continue in the future, in some areas round New Zealand, future extremes in chl-a will be outside current variability. Longer period of observation of chl-a will improve our ability to determine whether these changes are statistically significant.

4.3.2 Causes of changes in oceanic chl-a

In order to improve our ability to interpret changes in chl-a, we carried out a comparison of SST and chl-a anomalies as has been performed elsewhere in the world (e.g. Feng & Zhu, 2012; Kumar et al., 2016). The rate of growth of phytoplankton is affected by the availability of macronutrients (such as nitrate, phosphate, silicate), micronutrients (such as iron) and sufficient amounts of light (Eppley, 1972). All these factors are affected by the structure of the water column, and, in particular by the depth of mixing near the sea-surface (Behrenfeld & Falkowski, 1997a). Water column structure is affected by oceanographic and climate forcing such as solar heating of the upper ocean and wind-speed at the sea-surface (Uddstrom & Oien, 1999; Sutton, 2001). Increases in SST tend to be indicative of increased vertical stratification in the water column (i.e. the strength of the thermocline). Increased vertical stratification potentially has two effects on phytoplankton growth. First, increased stratification inhibits the mixing of nutrients (like nitrate, phosphate and silicate) into the surface mixed-layer which can reduce phytoplankton growth. Second, in contrast, a shallower mixed layer may lead to phytoplankton experiencing higher light intensities and potentially higher growth rates (higher primary productivity).

Spatial patterns of trends in SST and chl-a anomalies (Figure 3-8) together with the correlations between these anomalies (Figure 3-9) were consistent with our understanding of factors controlling primary production in these waters (Murphy et al., 2001). Phytoplankton growth in Subtropical Water around New Zealand and the Tasman Sea is believed to be primarily limited by nutrient availability, so we would expect (and see) a negative correlation between SST and chl-a (warm anomalies tend to reduce primary production) in these areas. In Subantarctic Water, primary production is believed to be limited mainly by factors other than macro-nutrient availability, such as incident light intensity, and micro-nutrients such as bio-available iron. Consistent with this understanding, we found generally positive correlations between SST and chl-a (warm anomalies tended elevate ocean productivity) in Subantarctic Water.

The largest and most significant trends in chl-a anomalies over the entire 1997–2018 time series were found in the Subtropical Front (positive trends), and around Northland and the northeast New Zealand continental slope (negative trends). In these regions, trends in SST anomalies were not particularly high and neither were there strong correlations between chl-a anomalies and SST anomalies. Understanding the reasons for the high chl-a anomalies and high chl-a trends in these frontal and shelf-slope areas will require further work that is beyond the scope of the present study (see Section 4.5).

Overall, the changes in SST and chl-a presented here are suggestive of two types of large-scale climate-environmental forcing in the New Zealand EEZ between 1997 and 2018. First, negative SST and chl-a anomalies (and likely decreases in ocean primary productivity) through most of the EEZ over the period September 1997 to 2003, were followed by positive anomalies in the middle of the

time series (2004–2012), and then back to negative anomalies from 2012–2018. This general pattern held for Chatham Rise, Tasman region, and Subtropical Water. Second, there was evidence of relatively-rapid warming of surface water through most of the New Zealand region since 2012 which is continuing as of April 2018. In Subantarctic Water, this recent period of warming has led to chl-a remaining higher than normal and continuing to increase in the period 2012–2018. There was also a very large and unprecedented (in the satellite data record) warming event in December 2017 especially in the Tasman Sea. This December 2017 warm event was associated with localised, record negative anomalies in chl-a along the west coast of the South Island and strong positive anomalies in chl-a over the Chatham Rise and near the Snares Islands.

4.4 Coastal variations in chl-a and SST

4.4.1 Coastal summary

We used the lower resolution satellite SST data to investigate trends surface water temperature in territorial waters because this gave us the longest period of data (1981 to 2018). Based on this 37-year time series of observations, we found evidence of long-term warming throughout New Zealand territorial waters, with average rates of warming between +1.2 and +2.8°C per decade (mean of +2.0°C per decade). Many coastal regions show a period of cooling between 1990–1994, a rapid temperature rise 1994–2000, and then evidence of gradual warming between 2010 and the present day. The changes in SST in the coastal regions (territorial seas) very closely followed those in the neighbouring offshore areas (Figure 2-2), though the coarse spatial resolution of the OISST data prevented us from looking very close to the shore over the full period (1981–2018) where small-scale effects (e.g. of land run-off) would have been more important.

The period of observation of chl-a in territorial waters is much shorter (16 years, 2002–2018) because the presence and technical performance of the early satellite sensors was limiting. Over the period considered, we found no significant trends in coastal chl-a when summarised at the Regional Council scale though some trends at a pixel level were significant. This lower level of statistical significance does not indicate that no trends are present or that the changes are not ecologically important. Rather, we note that the period of observation of chl-a is short compared to the underlying patterns of change and this reduces our ability to identify statistically-significant long-term trends. As the length of observation increases we will be better able to determine the statistical significance of these long-term trends.

The areas with the greatest negative (decreasing) trends in coastal chl-a formed two groups: (1) around Northland and the north-east shelf offshore of Auckland and the Coromandel; (2) around the top and west coast of South Island (Tasman, Nelson, West coast). In these areas, there was evidence of decreasing ocean chl-a with average rates of change of chl-a between 2002 and 2018 of 0.5–0.7 % per year. Evidence of increasing coastal productivity (2002–2018) was found in the Firth of Thames (Hauraki Gulf), west coast of North Island (between Kaipara and New Plymouth), Hawke's Bay, north-east coast of South Island (around Kaikoura), off Oamaru, and around Stewart Island.

4.4.2 Causes of changes in coastal chl-a

The reasons for changes in coastal chl-a have not been established empirically and here we offer only preliminary interpretation. In the area of negative trends in chl-a around the north-east shelf, the changes were consistent with trends in chl-a offshore, suggesting the coastal changes were being driven largely from large-scale oceanographic change. In contrast, we found no significant trends in chl-a anomalies at the oceanic scale offshore of the second area with negative trends in chl-a, off the

top and west of South Island. This suggests that smaller-scale factors and coastal processes may have been responsible for the observed trends in coastal chl-a around the north and west of South Island.

Small “pockets” of increasing coastal chl-a over the 16 year period 2002-2018 were found in the Firth of Thames (Hauraki Gulf), west coast of North Island (between Kaipara and New Plymouth), in Hawke’s Bay, along the north-east coast of South Island (between Blenheim and Kaikoura), off Oamaru, and around Stewart Island. Due to the differences between inshore and offshore changes in chl-a in these areas, it is possible that these localised increases are due to changes in land-use or riverine run-off. Further research in these areas would be needed to test this suggestion.

4.5 Recommendations

We provide recommendations from this study below.

1. We recommend that satellite trend analyses of ocean chl-a and SST be updated every 3–4 years. The next re-analysis of chl-a should include the NASA sensor VIIRS⁷ (Visible Infrared Imaging Radiometer Suite) as MODIS-Aqua is likely to become non-functional soon. A three-way merging analysis (SeaWiFS, MODIS-Aqua, VIIRS) will be needed for the New Zealand region to produce a consistent long-term satellite data set of chl-a.
2. We recommend that satellite observations of SST and chl-a continue be analysed together to provide a better understanding of drivers of changes to ocean productivity. An improved understanding of the drivers of changes in ocean productivity will be useful to decision makers and the New Zealand public than simply a description of changes to date as it will improve our ability to anticipate future changes. Further analysis of satellite observations of SST and chl-a at *seasonal* (rather than monthly) scales may help to explain why trends in chl-a are largest in the Subtropical Front even though trends in SST are not generally significant there. For example, there may be particularly strong trends in SST in the austral spring period when rates of primary productivity in the Subtropical Front are highest. It would also be useful to also analyse other available oceanographic data to help understand changes in chl-a, such as:
 - 2.1 Incident light intensity at the sea-surface (photosynthetically active radiation, PAR):
Daily estimates of incident light intensity at the sea surface (irrespective of cloud cover) are available from ocean colour satellite sensors. Preliminary analysis (data not shown) indicates that there are no large-scale, long-term trends in incident light intensity in the New Zealand region, but this should be further examined.
 - 2.2 Water column structure (mixed layer depth, MLD): The thickness of the upper mixed layer of the ocean links the warming of the surface to nutrient supply and light availability to phytoplankton. Information on MLD in the New Zealand region is available from hindcast data-assimilating numerical ocean models (e.g. BlueLink, Schiller et al. 2008; Oke et al. 2008) or from profiling drifters (e.g. Argo floats, Chiswell & Sutton, 2015).
3. A larger spatial domain of oceanic analysis (for example covering the whole Tasman Sea across to Australia and extending further into the southwest Pacific Ocean) would likely be

⁷ <https://npp.gsfc.nasa.gov/viirs.html>

useful to characterise long-term large-scale variations in oceanography, and understand the connections between SST in the New Zealand region and global climate patterns.

4. We recommend that satellite observations of coastal SST should be combined with analysis of in situ measurements of coastal SST (as used in New Zealand environmental reporting) to test for consistency.
5. Future updates of this (and other environmental indicators) in New Zealand should consider whether a fixed reference period rather than the whole dataset should be used to calculate anomalies. Using a fixed reference period has the advantage that historical anomalies do not change when new information is added to the time series. Disadvantages to using a fixed reference period include the fact that the size of anomalies (and less so the trends) depend on the particular reference period chosen, which is somewhat subjective. Choosing a reference period is not straightforward because it is preferable to use the same reference period for different measurements (e.g. SST and chl-a) but the lengths of observation are different.
6. It would be useful to consider whether the area of the Subtropical Front west of New Zealand should be considered a separate descriptive oceanic area in its own right for future environmental reporting of SST and chl-a. At present, this area is included in the “Tasman Sea” oceanic area, but the oceanography and trends in this region are different from those in the larger Tasman Sea.
7. In general, oceanic descriptive areas should be examined across the New Zealand environmental reporting system to see if greater insight can be achieved using consistent regions (e.g. between SST, chl-a and extreme waves; Gorman, 2018).
8. Satellite remote sensing can provide information on water quality (e.g. turbidity, suspended sediment, light attenuation) at moderate spatial resolution (500 m) for the coastal zone. We recommend that New Zealand environmental reporting includes these complementary coastal indicators based on satellite data for the New Zealand territorial seas as they become available.
9. Longer-term work that is beyond the scope of “state of the environment” reporting but relevant to it should continue. Much of this research is underway based on NIWA Coasts & Oceans Programme 4 (SSIF funded). This includes:
 - 9.1 The cause of differences in SST values and anomalies between the “global standard” OISST (Reynolds et al., 2002), “New Zealand SST” (Uddstrom & Oien, 1999) and MODIS-Aqua SST should be determined. Comparison of satellite measurements of SST with in situ measurements (from coastal stations and research vessels) may be useful in helping to recommend the appropriate data to use for New Zealand environmental reporting in the future. At present, it is not possible to recommend using one SST dataset over another.
 - 9.2 Research to determine if separate functional groups of phytoplankton in the New Zealand ocean can be distinguished from ocean colour observations. Such a capability would give more information on the ecological significance of changes in ocean phytoplankton, and more insight into drivers of these changes.

- 9.3 Validation and development of net primary production (NPP) algorithms for satellites should continue. If and when research has established an effective, well-characterised and robust approach to estimating NPP for the New Zealand ocean, this should replace (or at least augment) the indicator based on chl-a.
- 9.4 The importance of sub-surface phytoplankton to the water column averaged phytoplankton biomass (and primary production) should be further examined.
- 9.5 An improved methodology is needed for validation (ground-truthing) of coastal chl-a estimates. In the meantime, continuing the coastal water quality sampling and coupled analysis with satellite data will be of some use in characterising the satellite uncertainties.

5 Acknowledgements

This project was funded by the Ministry for the Environment (MfE projects 20991, 20056 and 092201; NIWA projects MFE15302, MfE16304, MfE18301, MFE19304), and was based on research in NIWA Coasts & Oceans Programme 4 (“Structure and function of marine ecosystems”). We thank Pierre Tellier (MfE), David Harris (Statistics New Zealand) and Stephen Chiswell (NIWA) for comments on a draft of this work that helped improve it. SeaWiFS data were used courtesy of NASA Goddard Space Flight Center and OrbImage Inc (USA). MODIS data were used courtesy of NASA Goddard Space Flight Center, MODIS project. MERIS data are used courtesy of the European Space Agency (ESA). Data were accessed via the NASA Ocean Biology Distributed Active Archive Center (OB.DAAC). AVHRR are used courtesy of NOAA (USA). We acknowledge Bruce Dudley (NIWA), MfE project 18501 and Regional Councils of New Zealand for in situ water quality monitoring data.

6 Glossary of abbreviations and terms

Algorithm	A mathematical recipe for combining data.
Annual anomaly	How different one year is from the average.
Atmospheric correction	The process of estimating ocean colour from the signal received by a radiometric sensor at the top of the atmosphere. This involves estimating and removing the signal which comes from the scattering of light in the atmosphere.
AVHRR	Advanced Very High Resolution Radiometer (USA)
CDOM	Coloured dissolved organic matter
Chlorophyll-a / chl-a	The ubiquitous pigment in marine phytoplankton.
EEZ	Exclusive Economic Zone
GSM	Garver-Siegel-Maritorena
MERIS	Medium Resolution Imaging Spectro-radiometer (European Space Agency).
MLD	Mixed layer depth
MODIS	Moderate Resolution Imaging Spectro-radiometer (NASA). There are two MODIS sensors, Terra and Aqua.
Monthly anomaly	How different one month is from the average (e.g. the difference between January 2000 and an average January).
MUMM	Scientific Service Management Unit of the Mathematical Model of the North Sea
NASA	National Aeronautics and Space Administration of the USA
NOAA	National Oceanic and Atmospheric Administration of the USA
NPP	Net primary productivity (rates of growth of phytoplankton)
NZTM	New Zealand Transverse Mercator Eastings and Northings
PAR	Photosynthetically active radiation (light between 400 and 700 nm)
QAA	Quasi-Analytical Algorithm
Radiometric	Pertaining to the measurement of the intensity of light.
SeaWiFS	Sea-viewing Wide Field-of-view Sensor (OrbImage/NASA)
SSIF	Strategic Science Investment Fund
VIIRS	Visible Infrared Imaging Radiometer Suite (VIIRS) (USA)

7 References

- Aiken, J.; Moore, G.F.; Holligan, P.M. (2004). Remote sensing of oceanic biology in relation to global climate change. *Journal of Phycology*, 28(5): 579-590.
- Antoine, D.; Morel, A. (1996a). Oceanic primary production 1: Adaptation of a spectral light-photosynthesis model in view of application to satellite chlorophyll observations. *Global Biogeochemical Cycles*, 10: 43-55.
- Antoine, D.; Morel, A. (1996b). Oceanic primary production 2: Estimation of global scale from satellite (Coastal Zone Color Scanner) chlorophyll. *Global Biogeochemical Cycles*, 10: 57-69.
- Babin, M.; Stramski, D.; Ferrari, G.M.; Claustre, H.; Bricaud, A.; Obolensky, G.; Hoepffner, N. (2003). Variations in the light absorption coefficients of phytoplankton, nonalgal particles, and dissolved organic matter in coastal waters around Europe. *Journal of Geophysical Research*, 108(C7), 1-20.
- Banse, K.; English, D.C. (1997). Near-surface phytoplankton pigment from the Coastal Zone Color Scanner in the Subantarctic region southeast of New Zealand. *Marine Ecological Progress Series*, 156: 51-66.
- Barnes, R.A.; Eplee, R.E.; Schmidt, M.; Patt, F.S.; McClain, C.R. Calibration of SeaWiFS. (2001). 1: Direct techniques. *Applied Optics*, 40: 6682-6700.
- Behrenfeld, M.J.; Boss, E.; Siegel, D.A.; Shea, D.M. (2005). Carbon-based ocean productivity and phytoplankton physiology from space. *Global Biogeochemical Cycles*, 19(1): GB1006.
- Behrenfeld, M.J.; Falkowski, P.G. (1997a). A consumer's guide to phytoplankton primary productivity models. *Limnology and Oceanography*, 42: 1479-1491.
- Behrenfeld, M.J.; Falkowski, P.G. (1997b). Photosynthetic rates derived from satellite-based chlorophyll concentration. *Limnology and Oceanography*, 42: 1-20.
- Bissett, W.P.; Patch, J.S.; Carder, K.L.; Lee, Z.P. (1997). Pigment packaging and Chl a-specific absorption in high-light oceanic waters. *Limnology and Oceanography*, 42(5), 961-968.
- Boyd, P.; LaRoche, J.; Gall, M.; Frew, R.; McKay, R.M.L. (1999). The role of iron, light and silicate in controlling algal biomass in sub-Antarctic water SE of New Zealand. *Journal of Geophysical Research*, 104(C6): 13395-13408.
- Brewin, R.J.W.; Mélin, F.; Sathyendranath, S.; Steinmetz, F.; Chuprin, A.; Grant, M. (2014). On the temporal consistency of chlorophyll products derived from three ocean-colour sensors. *ISPRS Journal of Photogrammetry and Remote Sensing*, 97: 171-184.
- Bricaud, A.; Babin, M.; Morel, A.; Claustre, H. (1995). Variability in the chlorophyll-specific absorption coefficients of natural phytoplankton: analysis and parametrisation. *Journal of Geophysical Research*, 100: 13321-13332.
- Campbell, J.; with 22 co-authors (2002). Comparison of algorithms for estimating ocean primary production from surface chlorophyll, temperature, and irradiance. *Global Biogeochemical Cycles*, 16(3): 9.1-9.15.

- Chiswell, S.M.; Sutton, P.J.H. (2015). Drifter- and float-derived mean circulation at the surface and 1000 m in the New Zealand region. *New Zealand Journal of Marine and Freshwater Research*, 49(2): 259-277.
- Dierssen, H.M. (2010). Perspectives on empirical approaches for ocean color remote sensing of chlorophyll in a changing climate. *Proceedings of the National Academy of Sciences of the United States of America*, 107(40): 17073–17078.
- Dudley, B.; Zeldis, J.; Burge, O. (2017). New Zealand Coastal Water Quality Assessment. NIWA report 2016093CH prepared for Ministry for the Environment. February 2017. Pp 84.
- Dudley, B.; Jones-Todd, C. (2018). New Zealand Coastal Water Quality Assessment Update. NIWA report 2018096CH for Ministry for the Environment, May 2018. Pp 34.
- Eplee, R.E.; Robinson, W.D.; Bailey, S.W.; Clark, D.K.; Werdell, P.J.; Wang, M.; Barnes, R.A.; McClain, C.R. Calibration of SeaWiFS (2001). 2: Vicarious techniques. *Applied Optics*, 40: 6701-6718.
- Eppley, R.W. (1972). Temperature and phytoplankton growth in the sea. *Fishery Bulletin*, 70(4): 1063-1085.
- Feng, J.F.; L. Zhu (2012). Changing trends and relationship between global ocean chlorophyll and sea surface temperature. *Procedia Environmental Sciences*, 13: 626-631.
- Franz, B.A.; Werdell, P.J.; Meister, G.; Bailey, S.W.; Eplee, R.E.; Feldman, G.C.; Kwiatkowska, E.; McClain, C.R.; Patt, F.S.; Thomas, D. (2005). The continuity of ocean color measurements from SeaWiFS to MODIS. *Proceedings SPIE*, 5882: 588-20W.
- Franz, B.A.; Werdell, P.J.; Meister, G.; Kwiatkowska, E.J.; Bailey, S.W.; Ahmad, Z.; McClain, C.R. (2006). MODIS land bands for ocean remote sensing applications. *Proc Ocean Optics XVIII*, Montreal, Canada, 9-13 October 2006.
- Friedland, K.D.; Stock, C.; Drinkwater, K.F.; Link, J.S.; Leaf, R.T.; Shank, B.V.; Rose, J.M.; Pilskaln, C.H.; Fogarty, M.J. (2012). Pathways between primary production and fisheries yields of Large Marine Ecosystems. *PLoS One*, 7(1): e28945.
doi:10.1371/journal.pone.0028945
- Garver, S.A.; D.A. Siegel (1997). Inherent optical property inversion of ocean color spectra and its biogeochemical interpretation: I. Time series from the Sargasso Sea. *Journal of Geophysical Research*, 102: 18,607-18,625.
- Gordon, H.R. (1997). Atmospheric correction of ocean colour imagery in the Earth Observing system era. *Journal of Geophysical Research*, 102, 17081-17106.
- Gordon, H.R.; Brown, J.W.; Brown, O.B.; Evans, R.H.; Clark, D.K. (1983). Nimbus-7 CZCS: reduction of its radiometric sensitivity with time. *Applied Optics*, 22(24): 3929-3931.
- Gordon, H.R.; Brown, O.B.; Evans, R.H.; Brown, J.W.; Smith, R.C.; Baker, K.S.; Clark, D.K. (1988). A semianalytic radiance model of ocean colour. *Journal of Geophysical Research*, 93(D9): 10909-10924.

- Gorman, R. (2018). Extreme wave indices for New Zealand coastal and oceanic waters. Updated to 2017. NIWA report for MFE19201, November 2018. Pp 43.
- Hamed, K.H.; Rao, A.R. (1998). A modified Mann-Kendall trend test for autocorrelated data. *Journal of Hydrology*, 204(1-4): 182–96. doi:10.1016/s0022-1694(97)00125-x.
- Hipel, K.W.; McLeod, A.I. (1994). *Time Series Modelling of Water Resources and Environmental Systems*. Elsevier, Amsterdam.
- Hooker, S.B.; Esaias, W.E.; Feldman, G.C.; Gregg, W.W.; McClain, C.R. (1992). An overview of SeaWiFS and ocean colour. NASA Technical Memorandum 194566 (SeaWiFS Technical Report Series) Volume 1, NASA Goddard Space Flight Center, Maryland, USA. 24 p.
- IOCCG (2000). Remote Sensing of Ocean Colour in Coastal, and Other Optically-Complex, Waters. In: Sathyendranath S (ed) Reports of the International Ocean-Colour Coordinating Group, No. 3, IOCCG, Dartmouth, Canada.
- IOCCG, (2008). Why Ocean Colour? The Societal Benefits of Ocean Colour Technology, eds Platt T, et al. Reports of the International Ocean-Colour Coordinating Group, No. 7 (IOCCG, Dartmouth, NS, Canada), 83–102.
- Kendall, M.G. (1975). *Rank Correlation Methods*. Griffin, London, UK.
- Kirk, J.T.O. (2011). *Light and photosynthesis in aquatic ecosystems*. Cambridge University Press, Cambridge. Pp 649.
- Kumar, G.S.; S. Prakash; M. Ravichandran; A.C. Narayana (2016). Trends and relationship between chlorophyll-a and sea surface temperature in the central equatorial Indian Ocean. *Remote Sensing Letters*, 7: 1093-1101.
- Lavender, S.J.; Pinkerton, M.H.; Moore, G.F.; Aiken, J.; Blondeau-Patissier, D. (2005). Modification to the atmospheric correction of SeaWiFS ocean colour images over turbid waters. *Continental Shelf Research*, 25(4): 539-555.
- Lee, Z.P.; Carder, K.L.; Arnone, R.A. (2002). Deriving inherent optical properties from water color: A multi- band quasi-analytical algorithm for optically deep waters, *Applied Optics*, 41: 5755- 5772.
- Lee, Z.P.; Lubac, B.; Werdell, J.; Arnone, R. (2009). An Update of the Quasi-Analytical Algorithm (QAA_v5). Open file online at: http://www.ioccg.org/groups/Software_OCA/QAA_v5.pdf, 9 pp., 2009.
- Mann, H.B. (1945). Nonparametric tests against trend. *Econometrica*, 13: 245-259.
- McClain, C.R.; Feldman, G.C.; Hooker, S.B. (2004). An overview of the SeaWiFS project and strategies for producing a climate research quality global ocean bio-optical time series. *Deep-Sea Research II*, 51(1–3): 5–42.
- Meister, G.; Franz, B.; Eplee, G. (2013). Recent Calibration Issues with SNPP VIIRS and MODIS Aqua. Presentation at workshop “Satellite Instrument Pre- and Post-Launch Calibration II”, Frascati, Italy December 3rd, 2013.

- Meister, G.; Franz, B.A.; Kwiatkowska, E.J.; McClain, C.R. (2012). Corrections to the calibration of MODIS Aqua ocean color bands derived From SeaWiFS data. *IEEE Transactions on Geoscience and Remote Sensing*, 50(1): 310-319.
- Melin, F.; Zibordi, G.; Berthon, J-F.; Bailey, S.; Franz, B.; Voss, K.; Flora, S.; Grant, M. (2011). Assessment of MERIS reflectance data as processed with SeaDAS over the European seas, *Optics Express*, 19: 25,657-25,671.
- MfE & Statistics NZ (2015). New Zealand's Environmental Reporting Series: Environment Aotearoa 2015. Ministry for the Environment & Statistics New Zealand. Available from www.mfe.govt.nz and www.stats.govt.nz.
- MfE & Statistics NZ (2016). New Zealand's Environmental Reporting Series: Our marine environment 2016. Available from www.mfe.govt.nz and www.stats.govt.nz.
- Murphy, R.J.; Pinkerton, M.H.; Richardson, K.M.; Bradford-Grieve, J.; Boyd, P.W. (2001). Phytoplankton distributions around New Zealand derived from SeaWiFS remotely-sensed ocean colour data. *New Zealand Journal of Marine and Freshwater Research*, 35: 343-362, 2001.
- NASA Goddard Space Flight Center, Ocean Ecology Laboratory, Ocean Biology Processing Group. Moderate-resolution Imaging Spectroradiometer (MODIS) Aqua Ocean Color Data; 2014 Reprocessing. NASA OB. DAAC, Greenbelt, MD, USA. doi: 10.5067/AQUA/MODIS_OC.2014.0. Accessed on 01/12/2018
- NASA Goddard Space Flight Center; Ocean Ecology Laboratory; Ocean Biology Distributed Active Archive Center (2014a). Sea-viewing Wide Field-of-view Sensor (SeaWiFS) Ocean Colour Data, SeaWiFS R2014.0. NASA OB.DAAC. doi:10.5067/ORBVIEW-2/SEAWIFS_OC.2014.0. (Accessed February 2016).
- NASA Goddard Space Flight Center; Ocean Ecology Laboratory; Ocean Biology Processing Group (2014b). Moderate-resolution Imaging Spectroradiometer (MODIS) Aqua Ocean Colour Data MODIS-Aqua R2014.0. NASA OB.DAAC. doi: 10.5067/AQUA/MODIS_OC.2014.0. (Accessed February 2016).
- NASA Goddard Space Flight Center; Ocean Ecology Laboratory; Ocean Biology Processing Group (2014c). Medium Resolution Imaging Spectrometer (MERIS) Ocean Colour Data MERIS R2012.1. NASA OB.DAAC. doi: 10.5067/ENVISAT/MERIS/L2/OC/2014. (Accessed February 2016).
- NASA Goddard Space Flight Center; Ocean Ecology Laboratory; Ocean Biology Processing Group (2018a). SeaWiFS Ocean Color Reprocessing 2018.0 <https://oceancolor.gsfc.nasa.gov/reprocessing/r2018/seawifs/> (Accessed May 2018).
- NASA Goddard Space Flight Center; Ocean Ecology Laboratory; Ocean Biology Processing Group (2018b). MODIS/Aqua Ocean Color Reprocessing 2018.0 <https://oceancolor.gsfc.nasa.gov/reprocessing/r2018/aqua/> (Accessed May 2018).
- New Zealand Herald (2018). Why our sea scorched: NZ's incredible marine heatwave, 8 April 2018. Available online (June 2018): www.nzherald.co.nz/nz/news/article.cfm?c_id=1&objectid=12028417

- NOAA (National Oceanic and Atmospheric Administration) (2016). Extended reconstructed sea surface temperature (ERSST.v4). National Centers for Environmental Information. Accessed March 2016. www.ncdc.noaa.gov/data-access/marineocean-data/extended-reconstructed-sea-surface-temperature-ersst.
- O'Reilly, J.E.; Sherman, K. (2016). Chapter 5.1: Primary productivity and trends. In IOC-UNESCO and UNEP (2016). Large Marine Ecosystems: Status and Trends. United Nations Environment Programme, Nairobi, Pp 91-99.
- O'Reilly, J.E.; Maritorena, S.; Mitchell, G.; Siegel, D.A.; Carder, K.L.; Garver, S.A.; Kahru, M.; McClain, C.R. (1998). Ocean colour algorithms for SeaWiFS. *Journal of Geophysical Research*, 103(C11), 24: 937-24,953.
- Ody, A.; Doxaran, D.; Vanhellemont, Q.; Nechad, B.; Novoa, S.; Many, G.; Bourrin, F.; Verney, R.; Pairaud, I.; Gentili, B. (2016). Potential of high spatial and temporal ocean color satellite data to study the dynamics of suspended particles in a micro-tidal river plume. *Remote Sensing*, 8:245; doi:10.3390/rs8030245.
- Oke, P.R.; Brassington, G.B.; Griffin, D.A.; Schiller, A. (2008). The Bluelink Ocean Data Assimilation System (BODAS). *Ocean Modelling*, 20:, 46-70, doi:10.1016/j.ocemod.2007.11.002.
- Parsons, T.R.; Takahashi, M.; Hargrave, B. (1977). *Biological Oceanographic Processes*, 2nd edition. Pergamon Press, Oxford, UK.
- Pinkerton, M.H. (2015). Ocean colour satellite observations of phytoplankton in the New Zealand EEZ, 1997–2014. NIWA report MfE15302-WLG2015-9. Prepared for Ministry for the Environment, January 2015. Pp 59.
- Pinkerton, M.H. (2016). Ocean colour satellite observations of phytoplankton in the New Zealand EEZ, 1997–2016. NIWA report WLG2016-19. Prepared for Ministry for the Environment, March 2016. Pp 43.
- Pinkerton, M.H. (2017) Satellite remote sensing of water quality and temperature in Manukau Harbour. NIWA report 2017092WN produced for Watercare Services Ltd, Pp 76.
- Pinkerton, M.H. (2018). Ocean colour satellite observations of phytoplankton in the New Zealand EEZ, 1997–2018. NIWA report MFE18301-2018180WN, Prepared for Ministry for the Environment, June 2018. Pp 56.
- Pinkerton, M.H.; Gall, M.; Wood, S.; Zeldis, J. (2018). Measuring the effects of bivalve mariculture on water quality in northern New Zealand using MODIS-Aqua satellite observations. *Aquaculture Environment Interactions*, In press.
- Pinkerton, M.H.; Moore, G.F.; Lavender, S.J.; Gall, M.P.; Oubelkheir, K.; Richardson, K.M.; Boyd, P.W.; Aiken, J. (2006). A method for estimating inherent optical properties of New Zealand continental shelf waters from satellite ocean colour measurements. *New Zealand Journal of Marine and Freshwater Research*, 40(2): 227-247.
- Pinkerton, M.H.; Richardson, K.M.; Boyd, P.W.; Gall, M.P.; Zeldis, J.; Oliver, M.D.; Murphy, R.J. (2005). Intercomparison of ocean colour band-ratio algorithms for chlorophyll

- concentration in the Subtropical Front east of New Zealand. *Remote Sensing of Environment*, 97: 382-402.
- Pinkerton, M.H.; Bell, R.; Chiswell, S.M.; Currie, K.; Mullan, A.B.; Rickard, G.; Stevens, C.; Sutton, P. (2015). Reporting on the state of the New Zealand marine environment: recommendations for ocean indicators as part of the Atmospheric and Ocean Climate Change Tier 1 Statistic. New Zealand Aquatic Environment and Biodiversity Report No. 151. ISBN - 978-0-908334-01-8 (online); ISSN -1179-6480 (online). Pp 89.
- Platt, T. (1986). Primary production of the ocean water column as a function of surface light intensity: algorithms for remote sensing. *Deep-Sea Research (A)*, 31: 1-11.
- Platt, T.; Sathyendranath, S. (1993). Estimators of primary production for interpretation of remotely sensed data on ocean color. *Journal of Geophysical Research*, 98: 14561-14567.
- Rast, M.; Bezy, J.-L. (1990). ESA's Medium Resolution Imaging Spectrometer: mission, system, and applications. *Proceedings SPIE 1298, Imaging Spectroscopy of the Terrestrial Environment*, 114. doi:10.1117/12.21342.
- Rast, M.; Bezy, J.L. (1999). The ESA Medium Resolution Imaging Spectrometer MERIS: A review of the instrument and its mission. *International Journal of Remote Sensing*, 20(9): 1681-1702.
- Reynolds, R.W.; Rayner, N.A.; Smith, T.M.; Stokes, D.C.; Wang, W. (2002). An improved in situ and satellite SST analysis for climate. *Journal of Climate*, 15: 1609-1625.
- Ruddick, K.G.; Ovidio, F.; Rijkeboer, M. (2000). Atmospheric correction of SeaWiFS imagery for turbid coastal and inland waters. *Applied Optics*, 39: 897-912.
- Scarsbrook, M. (2006). State and trends in the National Water Quality Network (1989-2005). NIWA Client Report HAM2006-131 to MfE.
- Schiller, A.; Oke, P.R.; Brassington, G.B.; Entel, M.; Fiedler, R.; Griffin, D.A.; Mansbridge, J. (2008). Eddy-resolving ocean circulation in the Asian-Australian region inferred from an ocean reanalysis effort. *Progress in Oceanography*, doi:10.1016/j.pocean.2008.01.003.
- Schwarz, J.N.; Gall, M.; Pinkerton, M.H.; Kennan, S. (2008). Primary production in the subtropical convergence zone: Comparison of in-situ measurement methods and remote estimates. *Proceedings of Ocean Optics XIX, Barga, Italy, 6-10 October 2008*.
- Sen, P.K. (1968). Estimates of the regression coefficient based on Kendall's tau. *Journal of the American Statistical Association*, 63: 1379-1389.
- Siegel, D.A.; Wang, M.; Maritorena, S.; Robinson, W. (2000). Atmospheric correction of satellite ocean color imagery: the black pixel assumption. *Applied Optics*, 39: 3582-3591.
- Sutton, P. (2001). Detailed structure of the Subtropical Front over Chatham Rise, east of New Zealand. *Journal of Geophysical Research*, 106 (C12): 31045-31056.
- Sutton, P.J.H.; Bowen, M.; Roemmich, D. (2005). Decadal temperature changes in the Tasman Sea. *New Zealand Journal of Marine and Freshwater Research*, 39: 1321-1329.

- Uddstrom, M.J.; Oien, N.A. (1999). On the use of high resolution satellite data to describe the spatial and temporal variability of sea surface temperatures in the New Zealand Region. *Journal of Geophysical Research (Oceans)*, 104(C9): 20729–20751.
- Wang, M.; Shi, W. (2007). The NIR-SWIR combined atmospheric correction approach for MODIS ocean color data processing. *Optics Express*, 15(24): 15722-15733.
- Westberry, T.; Behrenfeld, M.J.; Siegel, D.A.; Boss, E. (2008). Carbon-based primary productivity modeling with vertically resolved photo-acclimation. *Global Biogeochemical Cycles*, 22(2): GB2024.
- Yue, S.; Wang, C.Y. (2004). The Mann–Kendall test modified by effective sample size to detect trend in serially correlated hydrological series. *Water Resources Management*, 18: 201–218.

Appendix A Descriptive sub-regions

Table B-1: Co-ordinates defining descriptive regions.

Region	Co-ordinates of boundary	
	Latitude	Longitude
Chatham Rise	-42	174.3
	-45.5	170.8
	-45.5	185
	-42	185
Tasman Sea	-34.43	160.6
	-47.25	157.5
	-47.25	167.5
	-41.6	172.3
	-40.82	172.14
	-40.55	172.7
	-39.3	173.75
	-39.2	175
	-37.05	175
Subtropical Water (STW)	-34.43	172.8
	-29.82	172.87
	-34.43	172.87
	-37.05	175
	-38.67	176.44
	-42	174.3
	-42	185
Subantarctic Water (SAW)	-29.82	185
	-45.5	170.8
	-47.25	167.5
	-47.25	157.5
	-52.64	157.5
	-52.52	185
	-45.5	185